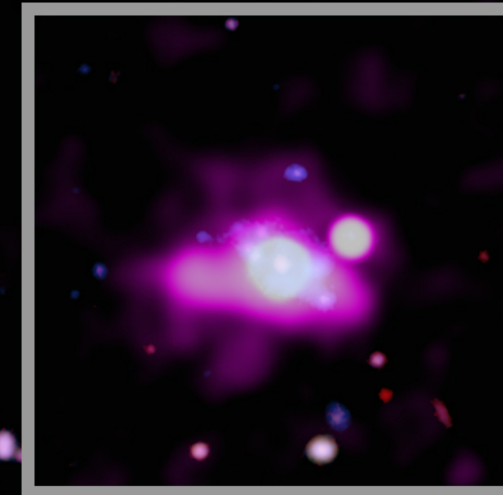
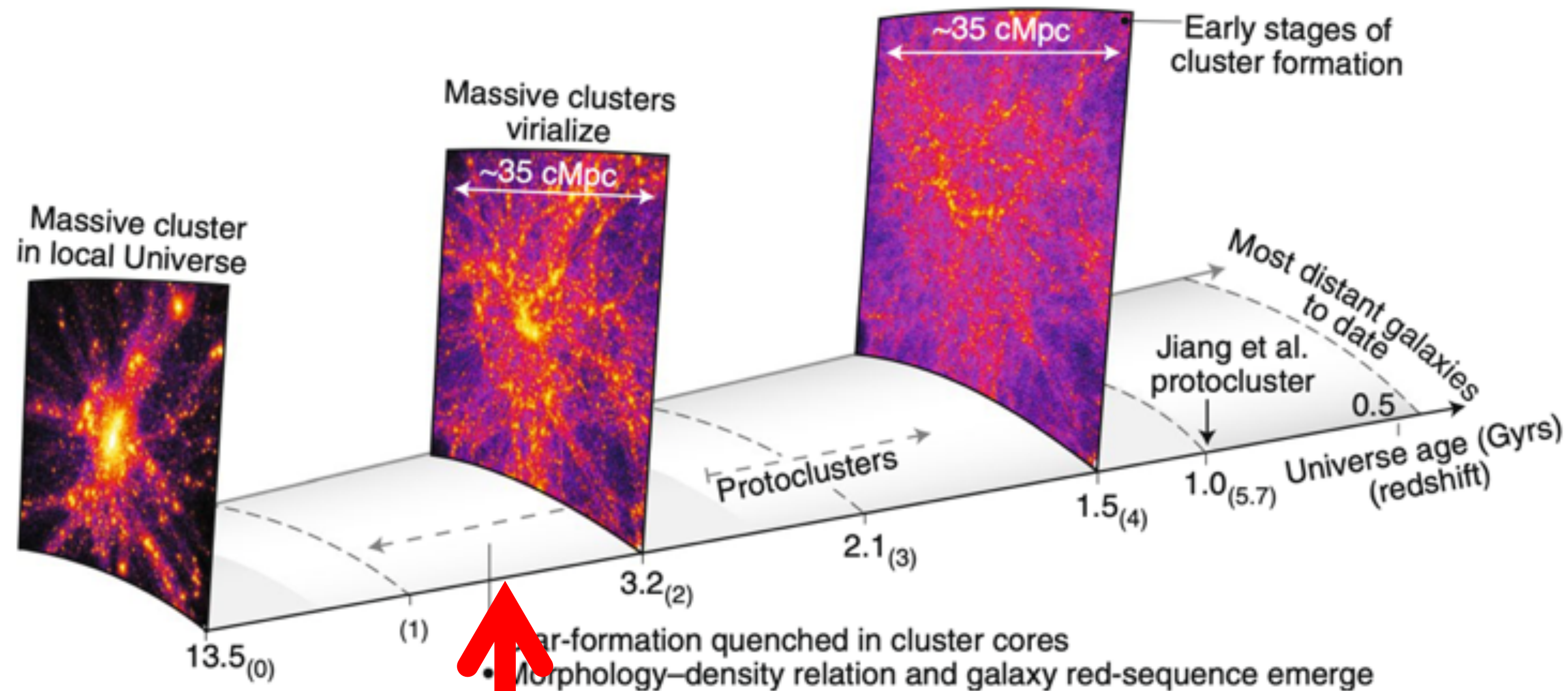


AGN enhancement and appearance of the ICM
in protoclusters of galaxies at $z > 2$
(What can we learn before the X-ray desert)

X-RAY & OPTICAL

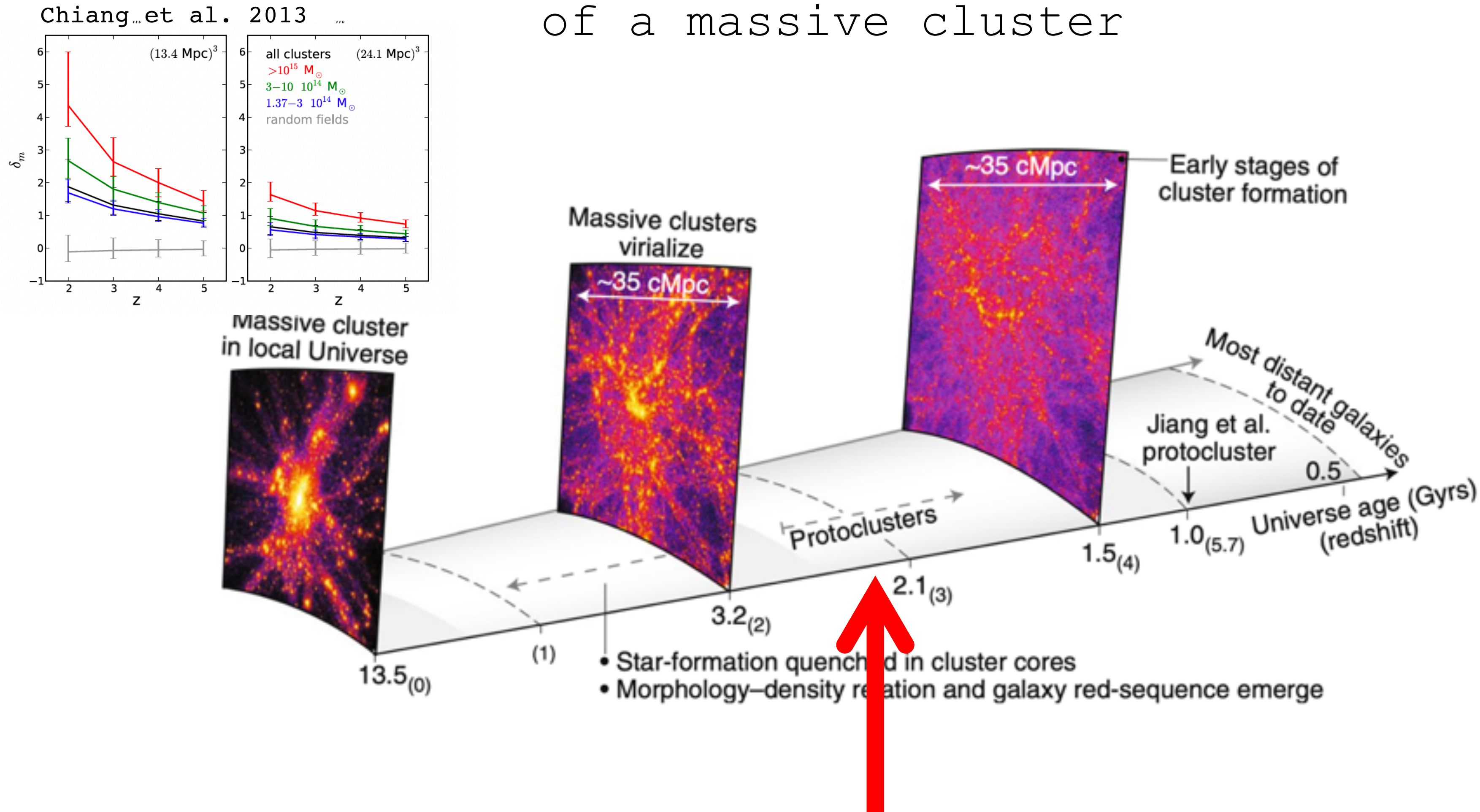


A schematic view of the cosmic evolution of a massive cluster



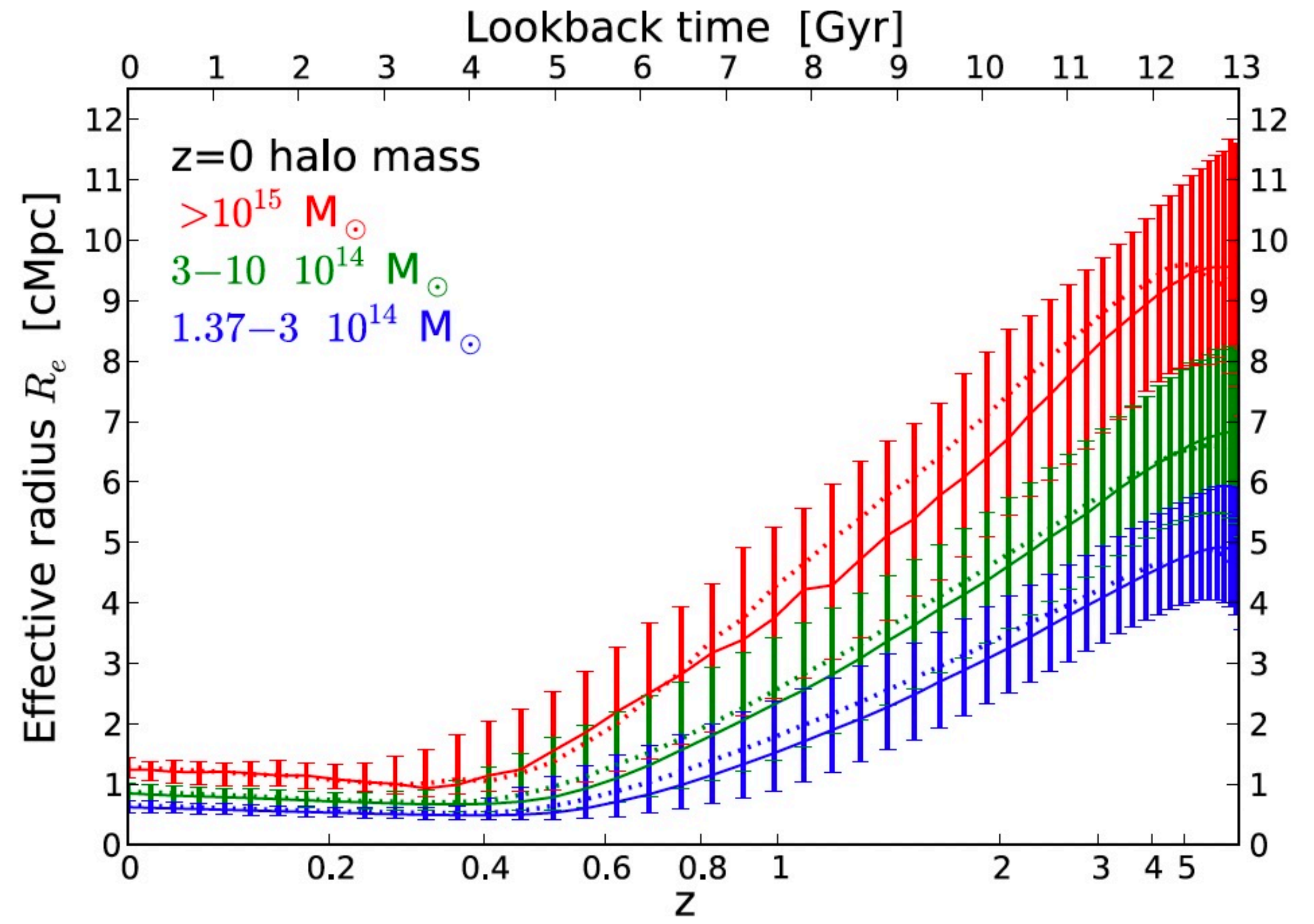
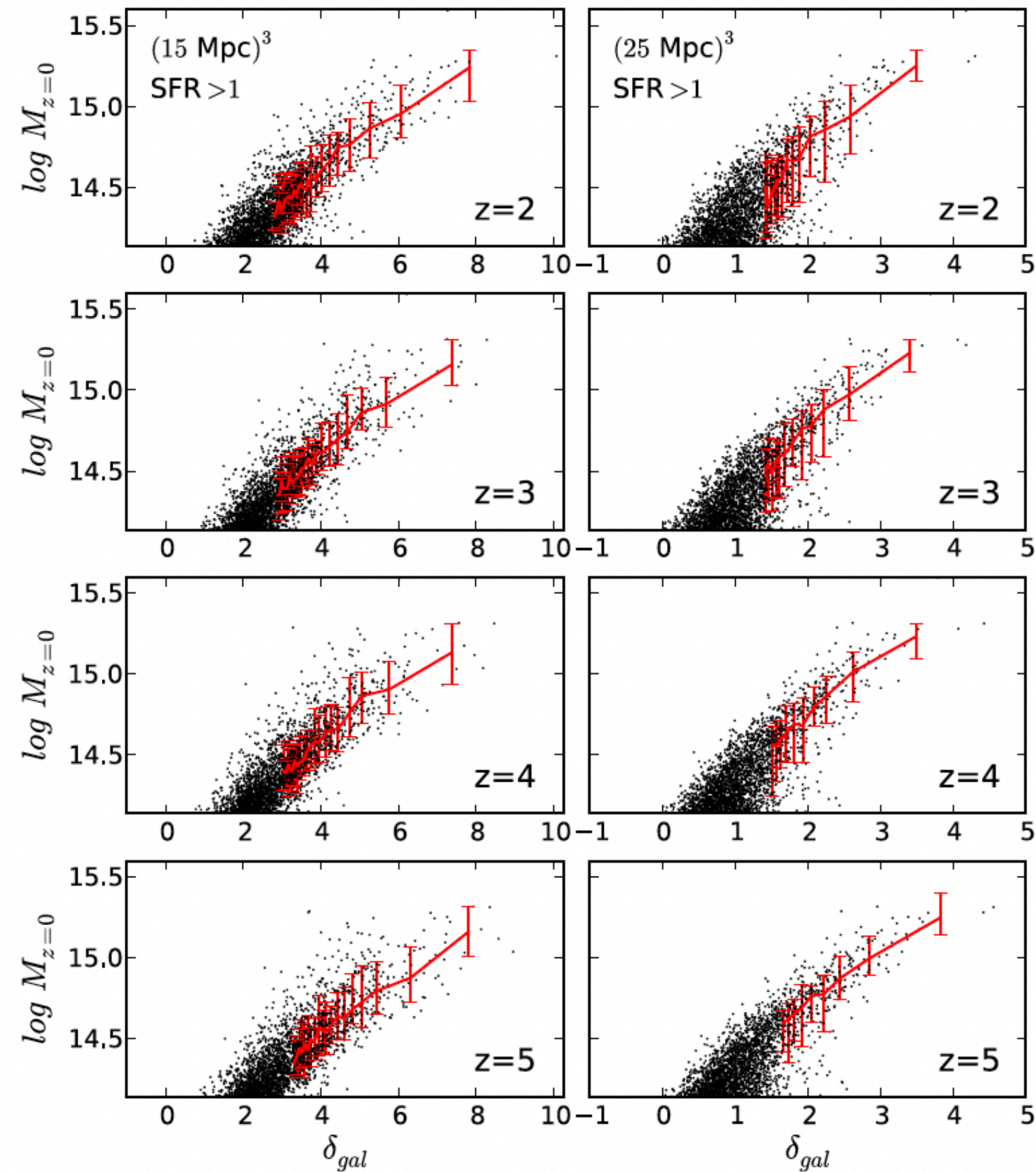
Rosati 2018

A schematic view of the cosmic evolution of a massive cluster



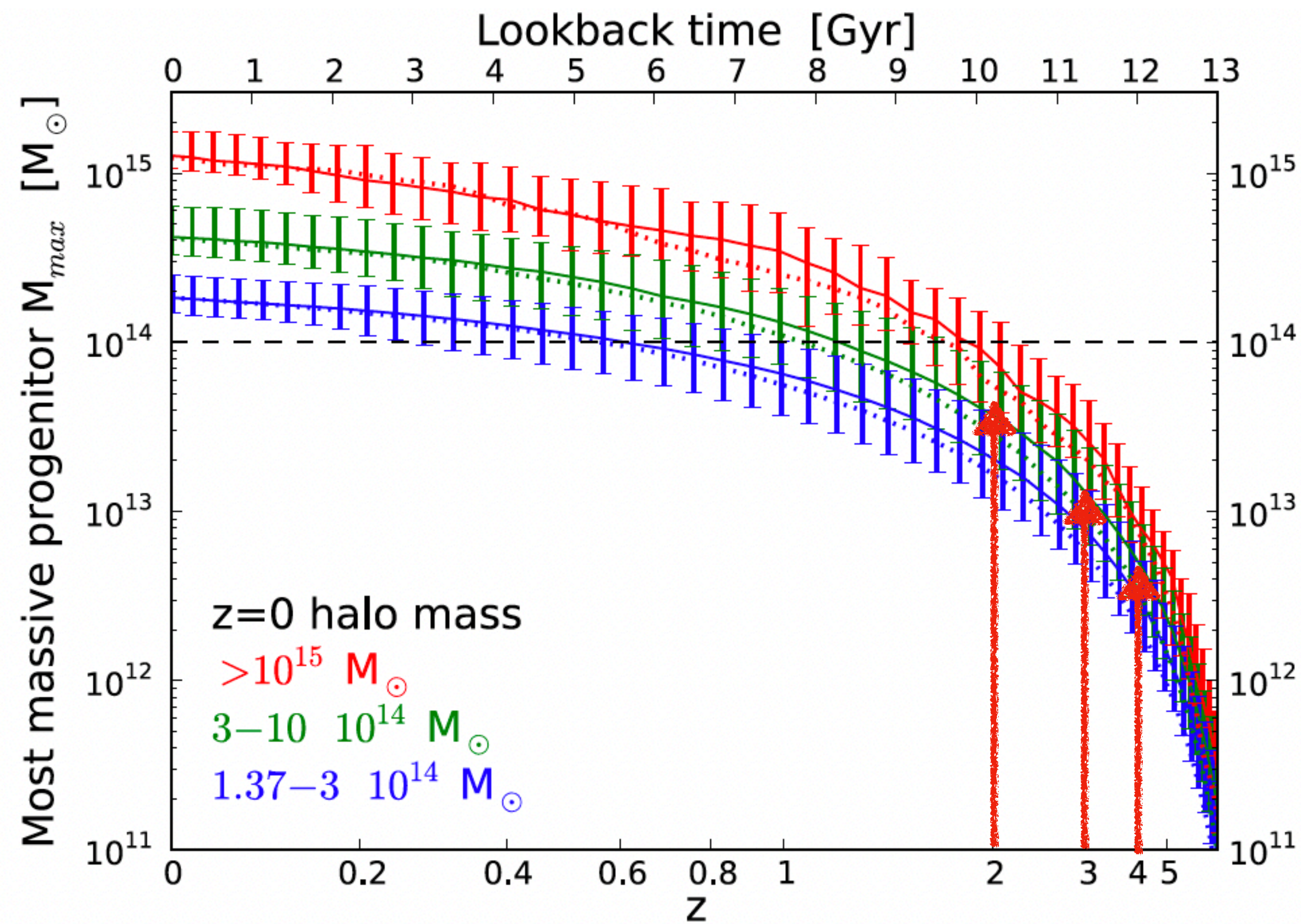
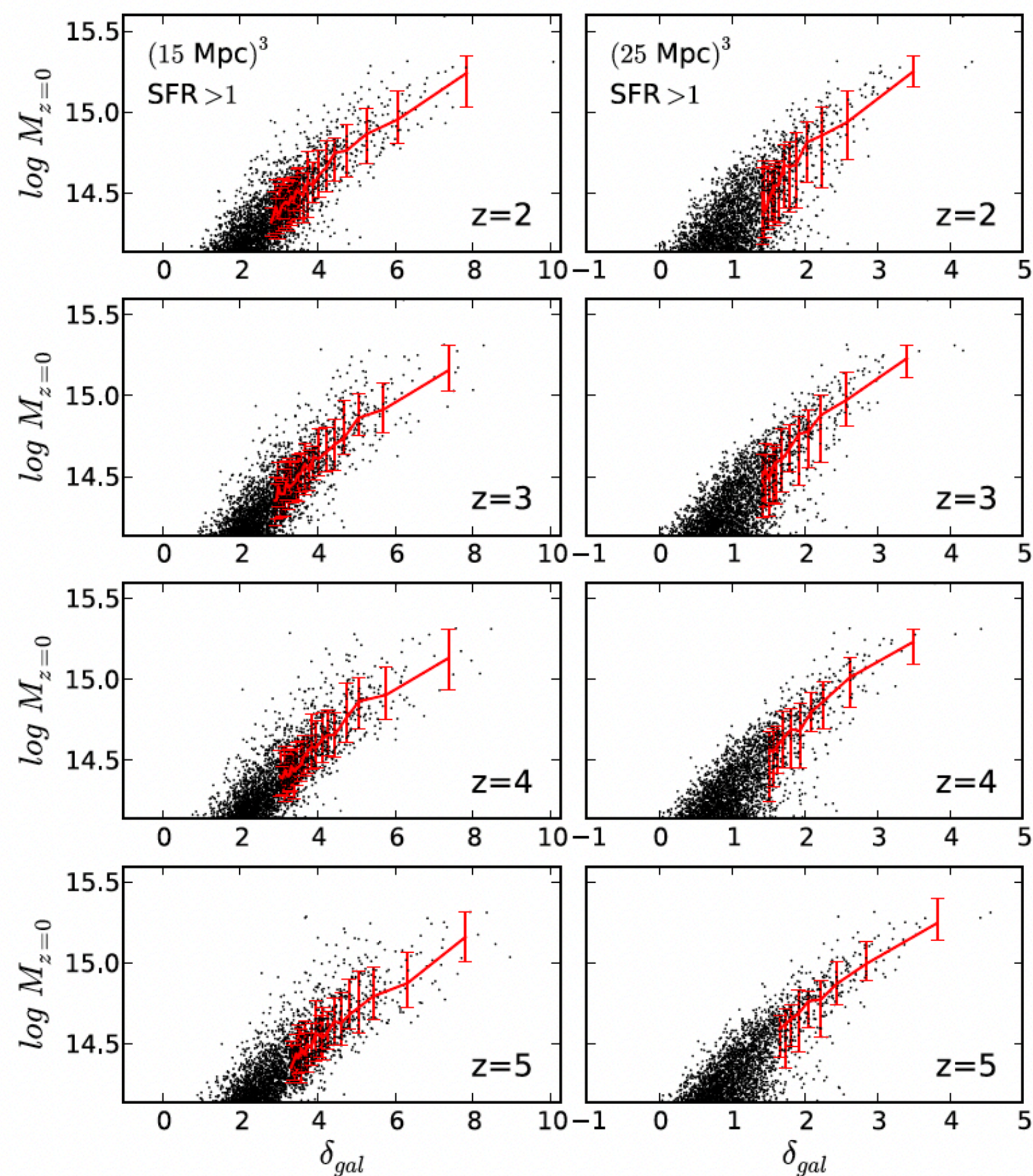
Rosati 2018

How to define and identify protoclusters



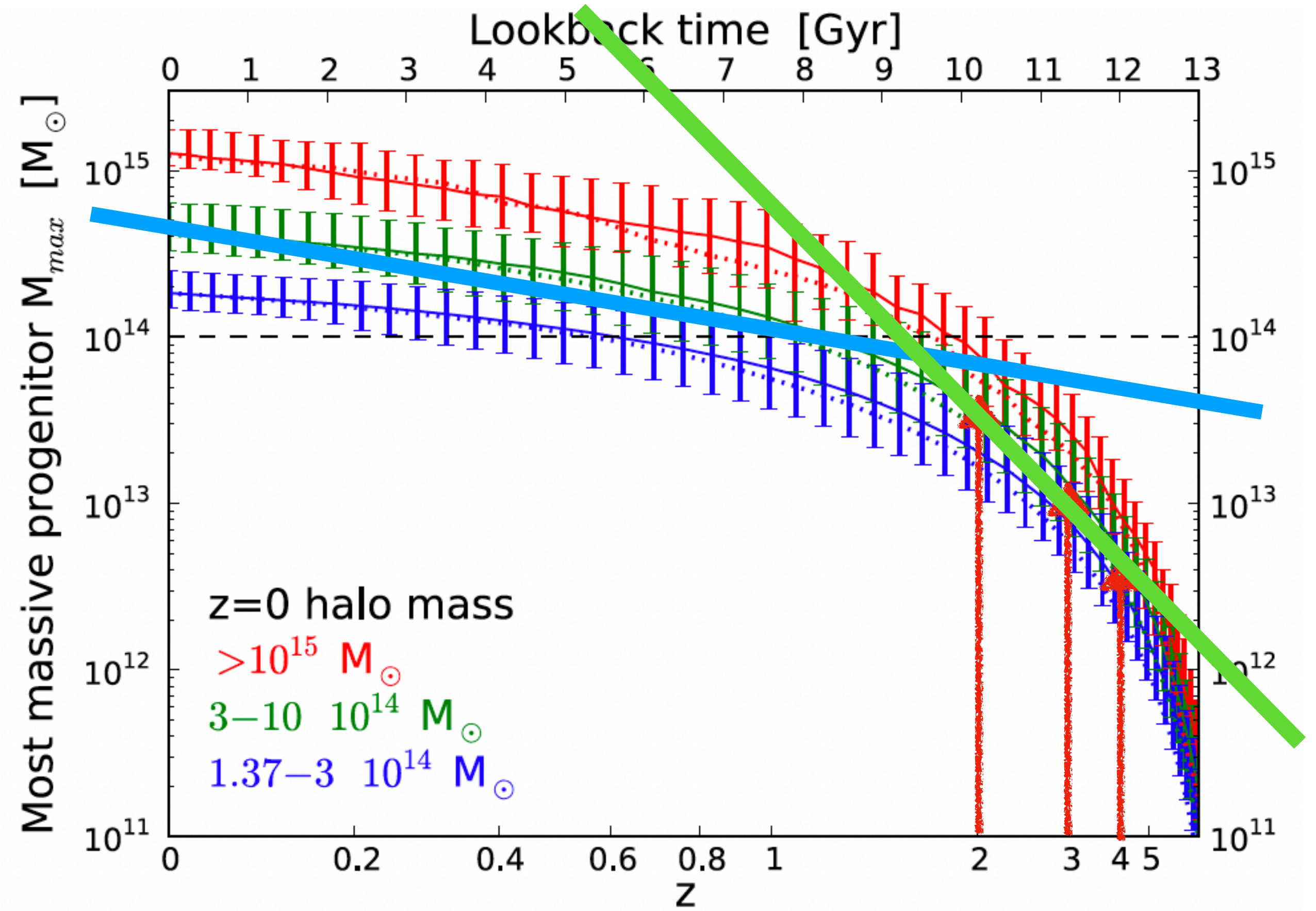
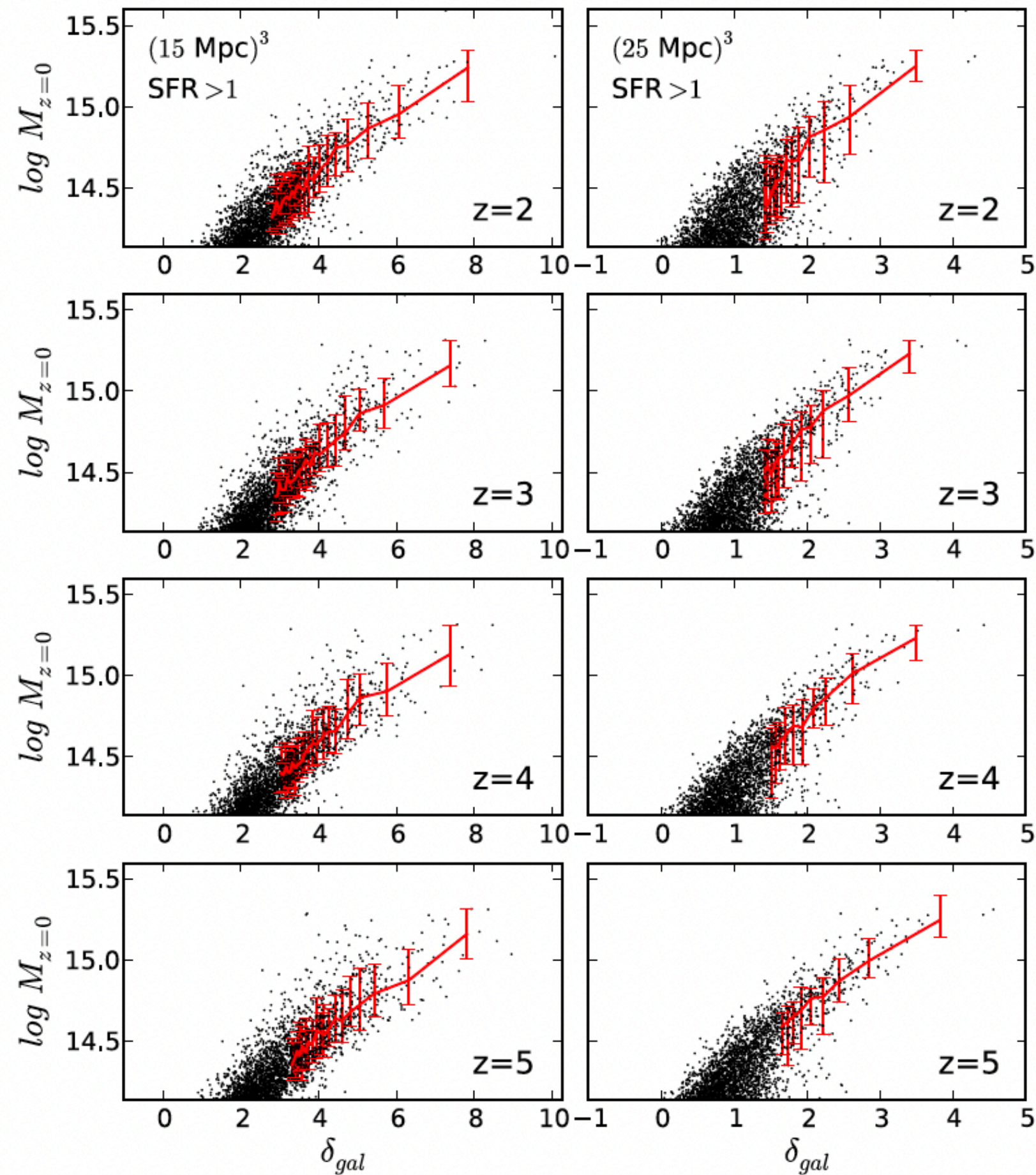
Chiang, Overzier & Gebhardt 2013

How to define and identify protoclusters



Chiang, Overzier & Gebhardt 2013

How to define and identify protoclusters



Chiang, Overzier & Gebhardt 2013

Protoclusters (overdensities at $z > 2$, $\Delta \ll 200$) are ideal laboratories to study galaxy properties in dense environments, and environmental dependence of galaxy formation and evolution in the early universe. Galaxy evolution in dense environment at high- z is expected to be accelerated.

Protoclusters magnify details of the assembly processes:

Infalling of galaxies from the cosmic web (or simply increase in the environ density)

Triggering of star formation

Interactions between galaxies

Coevolution of galaxies and their SMBH

Formation of the BCG

First stages of gravitational heating of the proto-ICM

Feedback and enrichment of the proto-ICM

Build up of the ICL

(see review by Overzier 2016 ARAA)

X-ray observables in protoclusters and high-z clusters

i) X-ray emitting AGN

**ii) thermal emission from shocked or heated
diffuse intra cluster medium**

**iii) non thermal diffuse emission due to IC from
relativistic electron.**

**iv) population of HMXB in starbursting
galaxies.**

The Spiderweb Galaxy

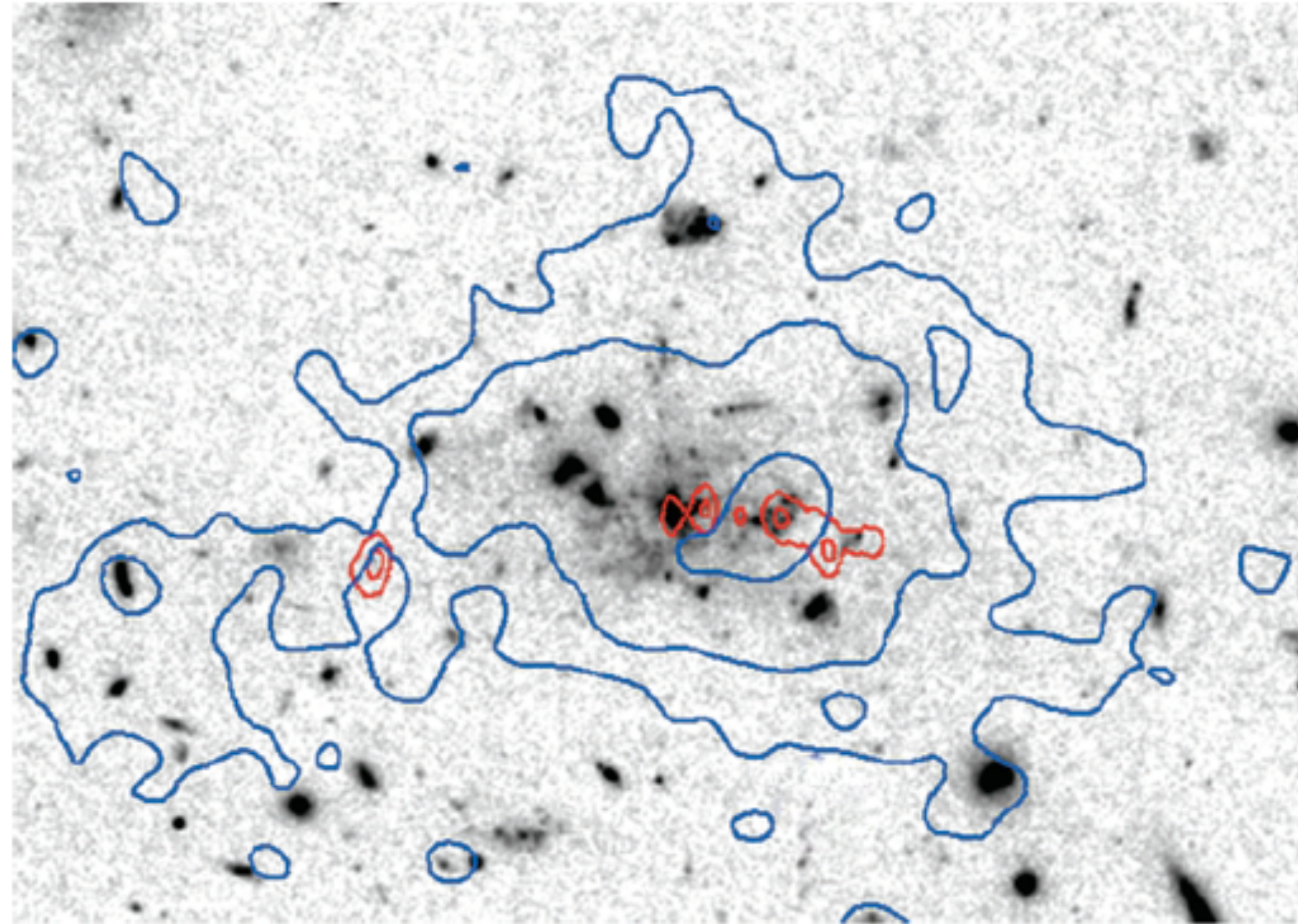
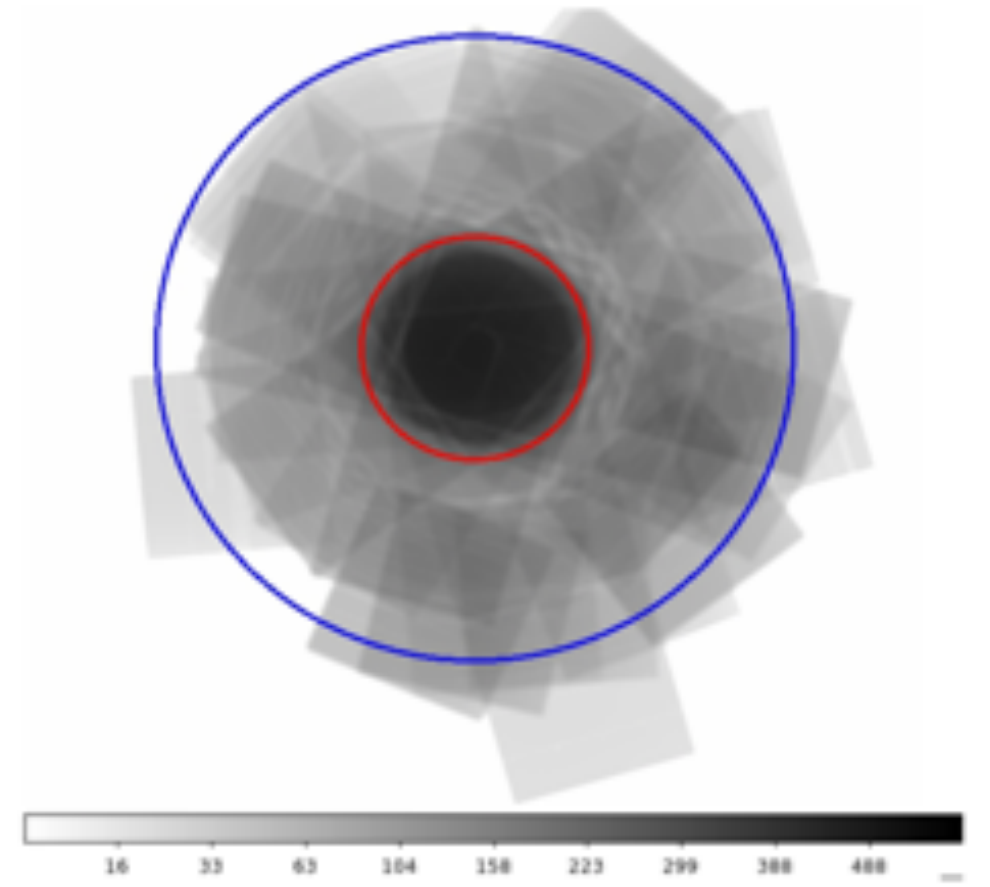


FIG. 2.— VLT $\text{Ly}\alpha$ contours (*blue*, resolution $\sim 1''$ FWHM) delineating the gaseous nebula and the VLA 8 GHz contours (*red*, resolution $\sim 0''.3$) delineating the nonthermal radio emission are superimposed on the composite ($g_{475} + I_{814}$) ACS image. The image shows a $33'' \times 23''$ region rotated 10° from north. The gaseous nebula extends for >200 kpc and is comparable in size with the envelopes of cD galaxies in the local universe.

Miley et al. 2006



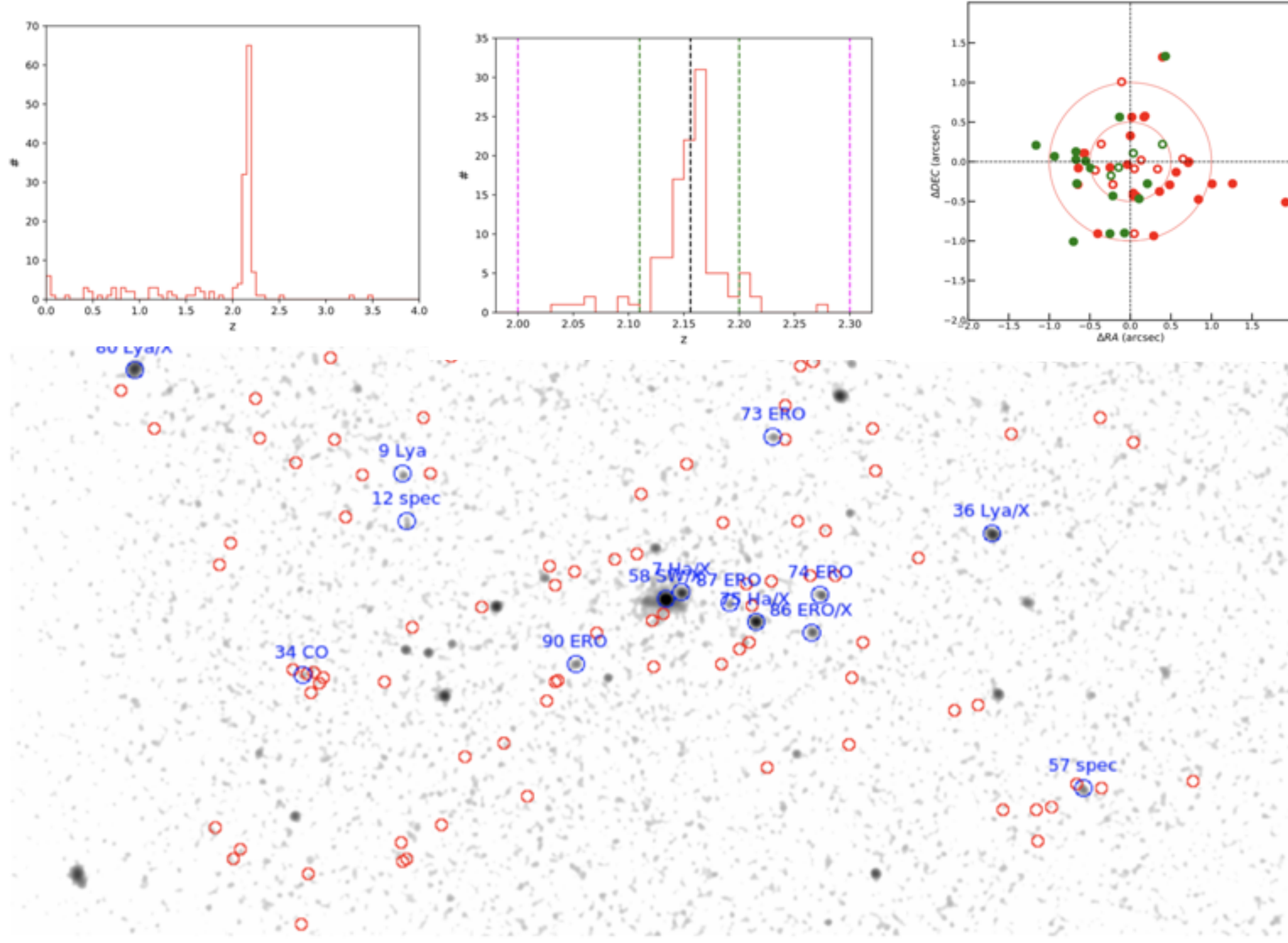
715 ks with Chandra ACIS-S

At $z \sim 2.156$ - 5 arcmin ~ 2.5 Mpc

PT et al. 2022, A&A, 662, 54

AXIS - Galaxies SWG - September 2022

Identification of X-ray emitting members



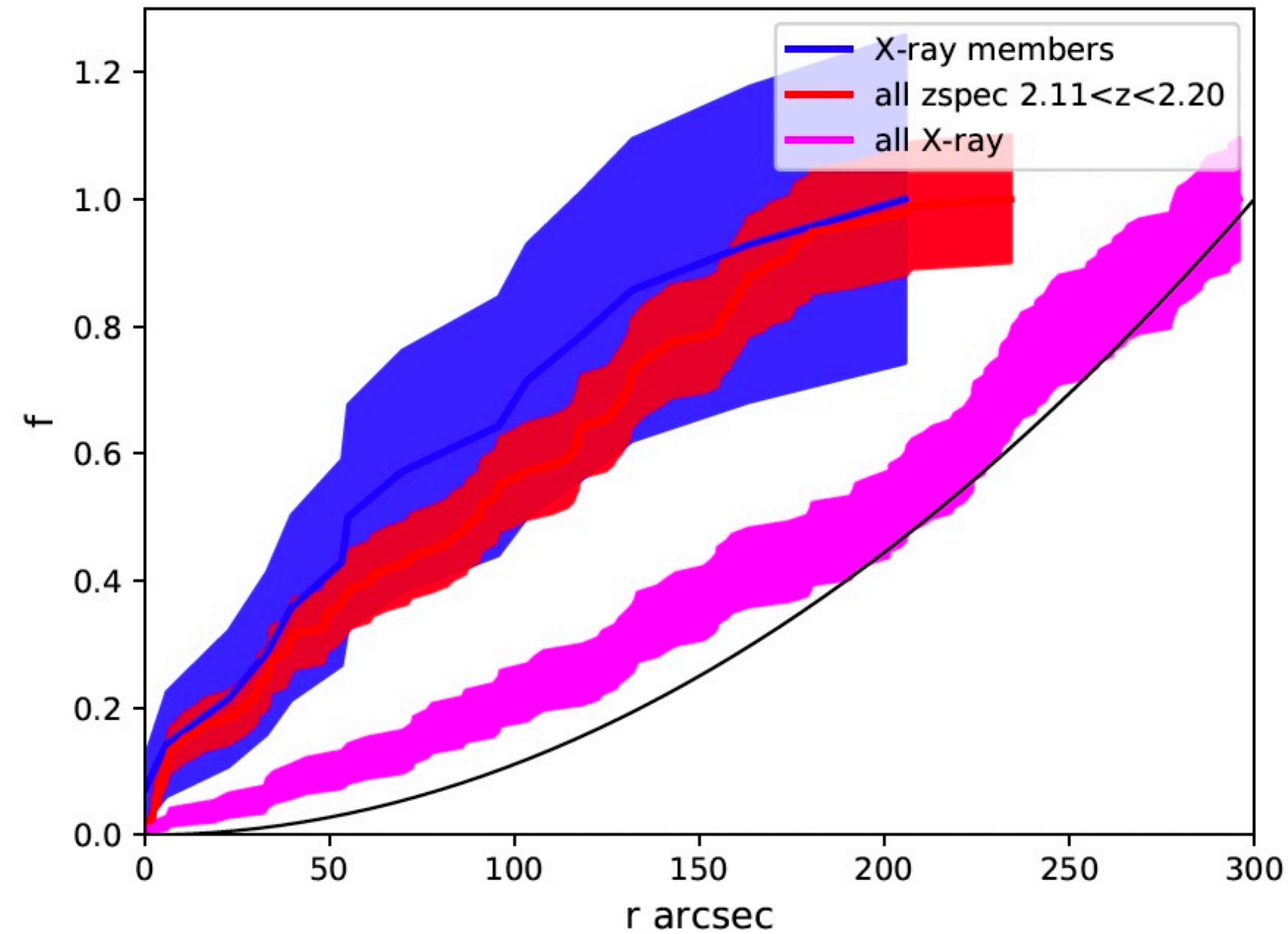
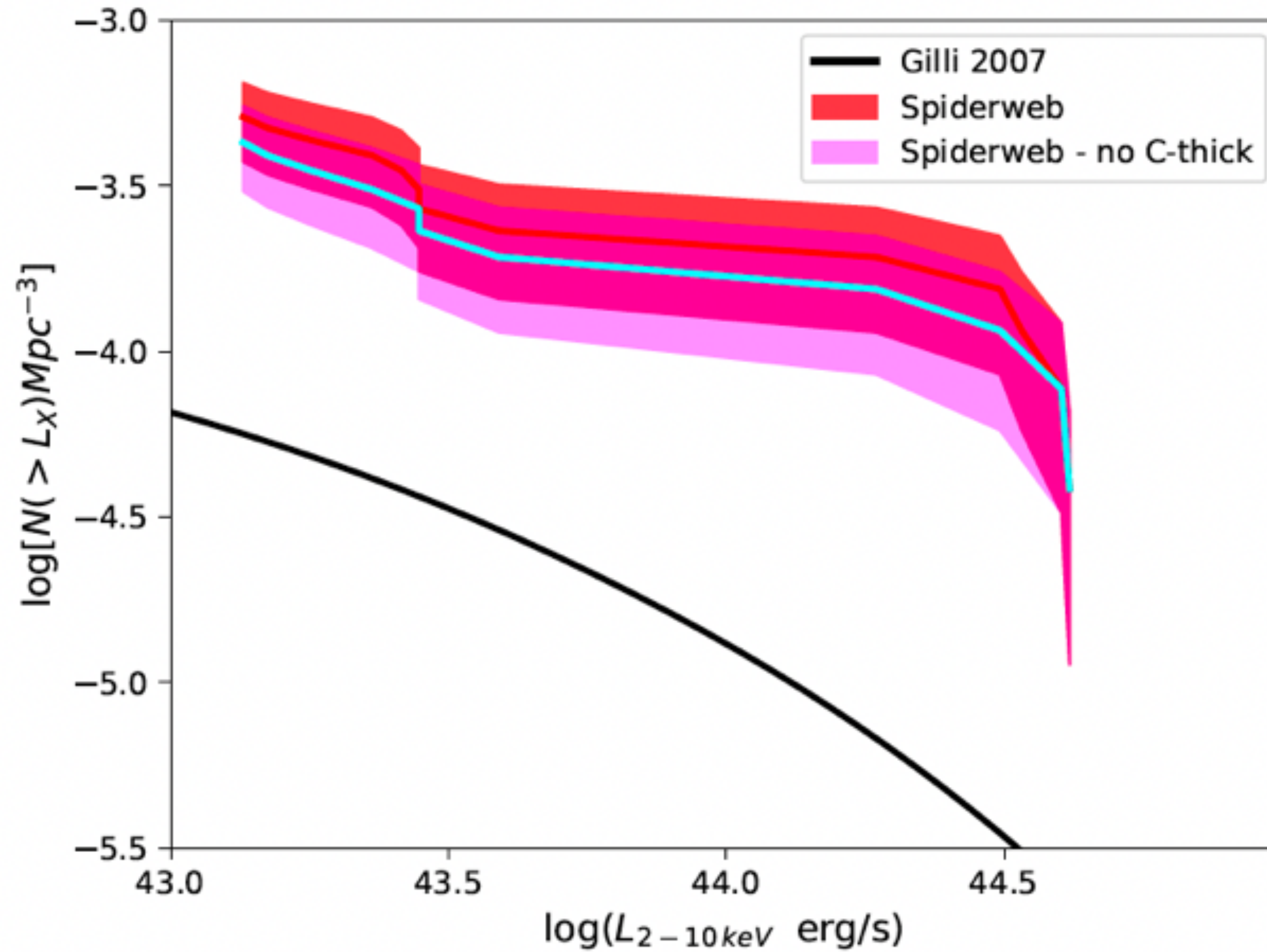
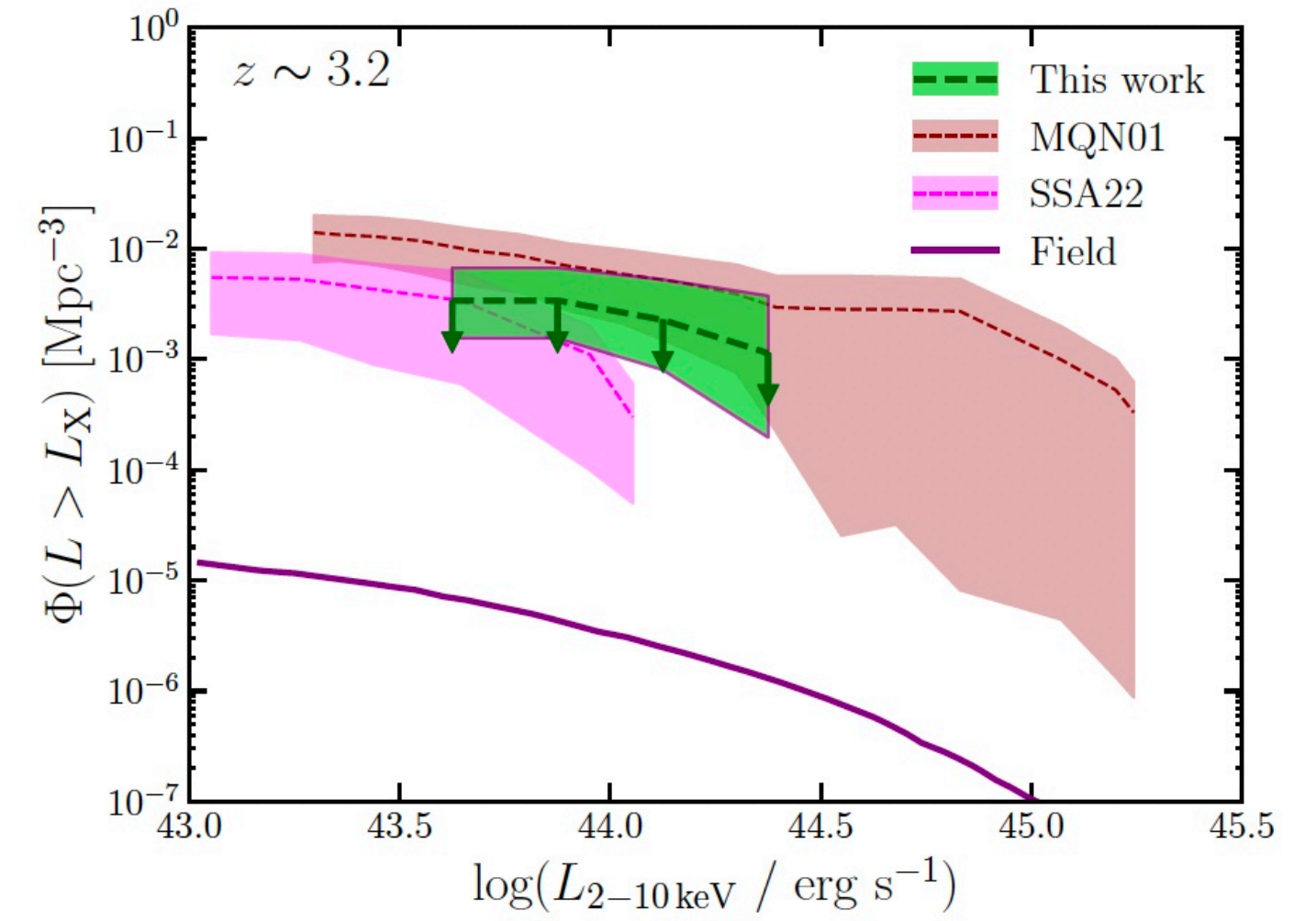
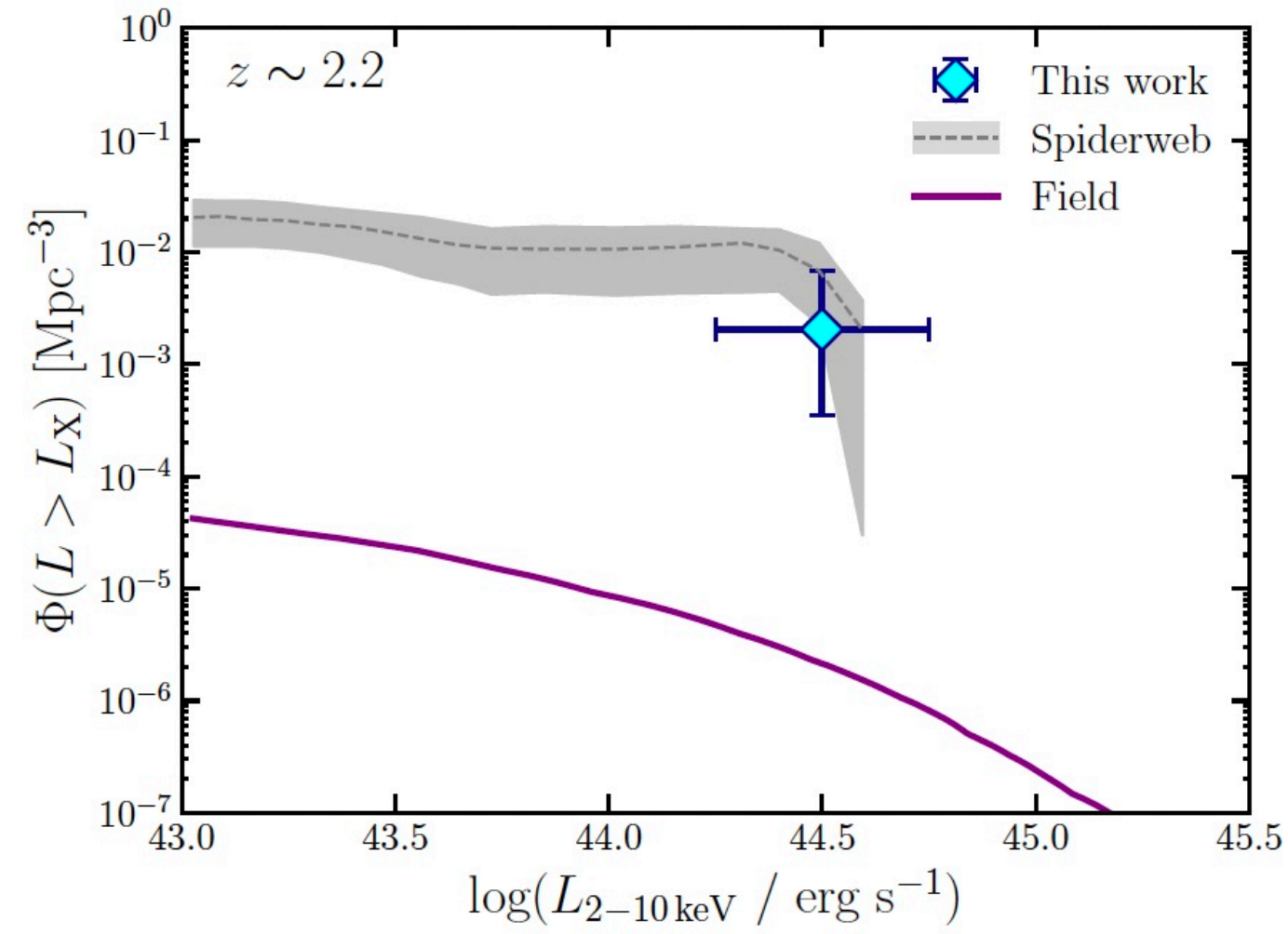
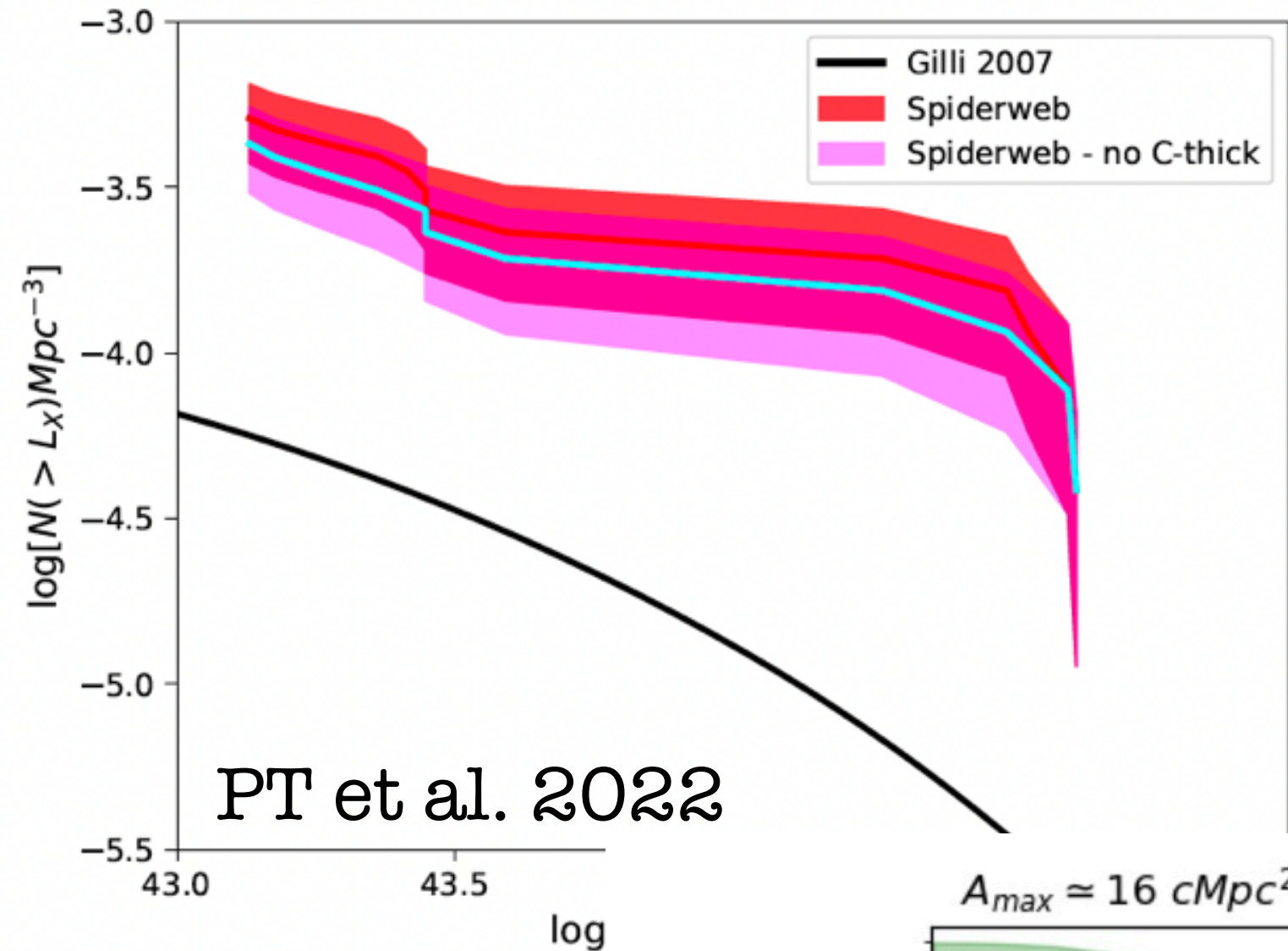


Fig. 9. Fraction of sources within a given radius from the Spiderweb Galaxy. X-ray cluster members (shown in blue) have the same distribution as all the spectroscopically confirmed protocluster members in the $2.11 < z < 2.20$ range (shown in red). On the other hand, the distribution of all the X-ray sources (dominated by the field) is clearly less

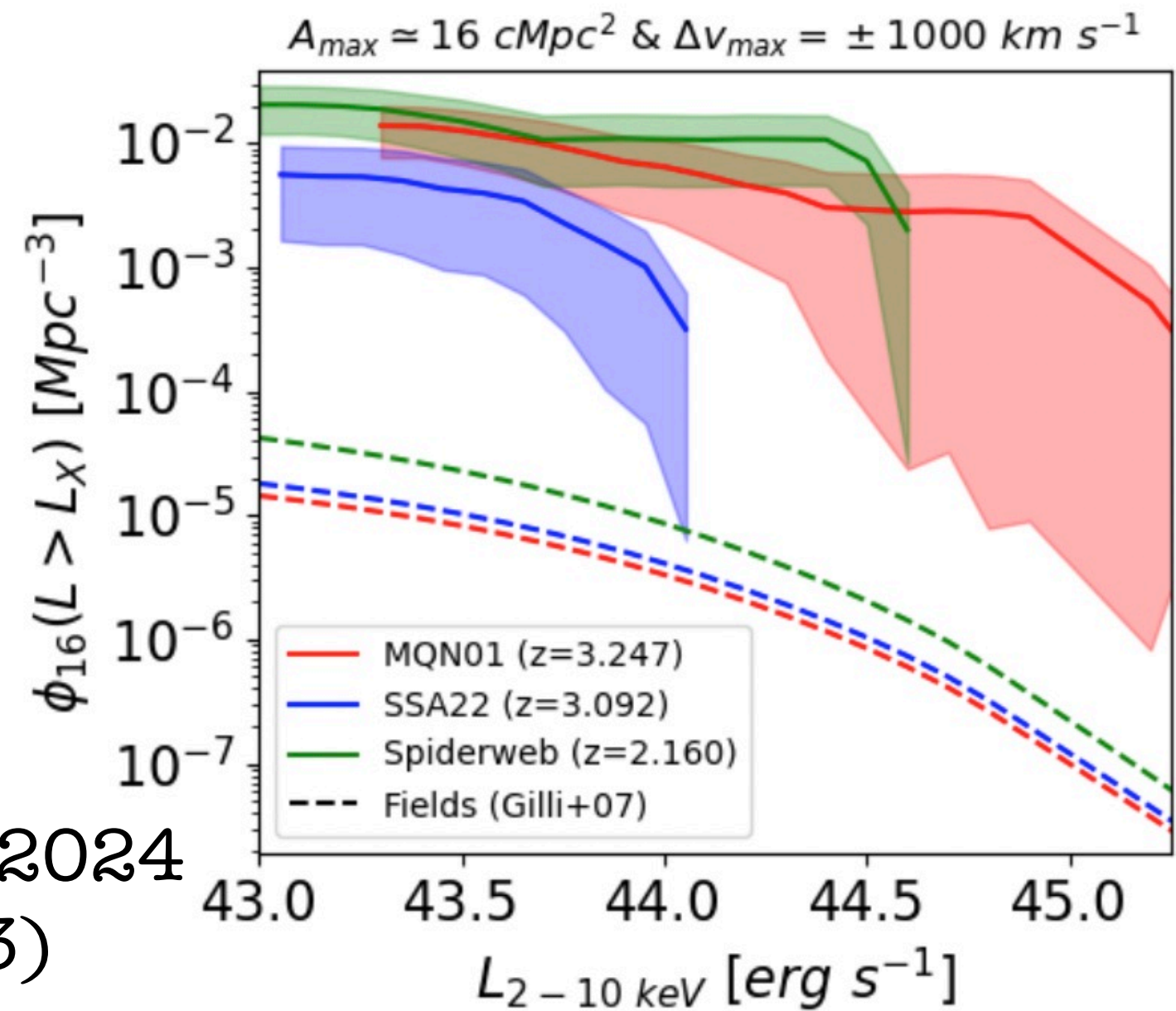
Strong excess (Spiderweb Galaxy is excluded)



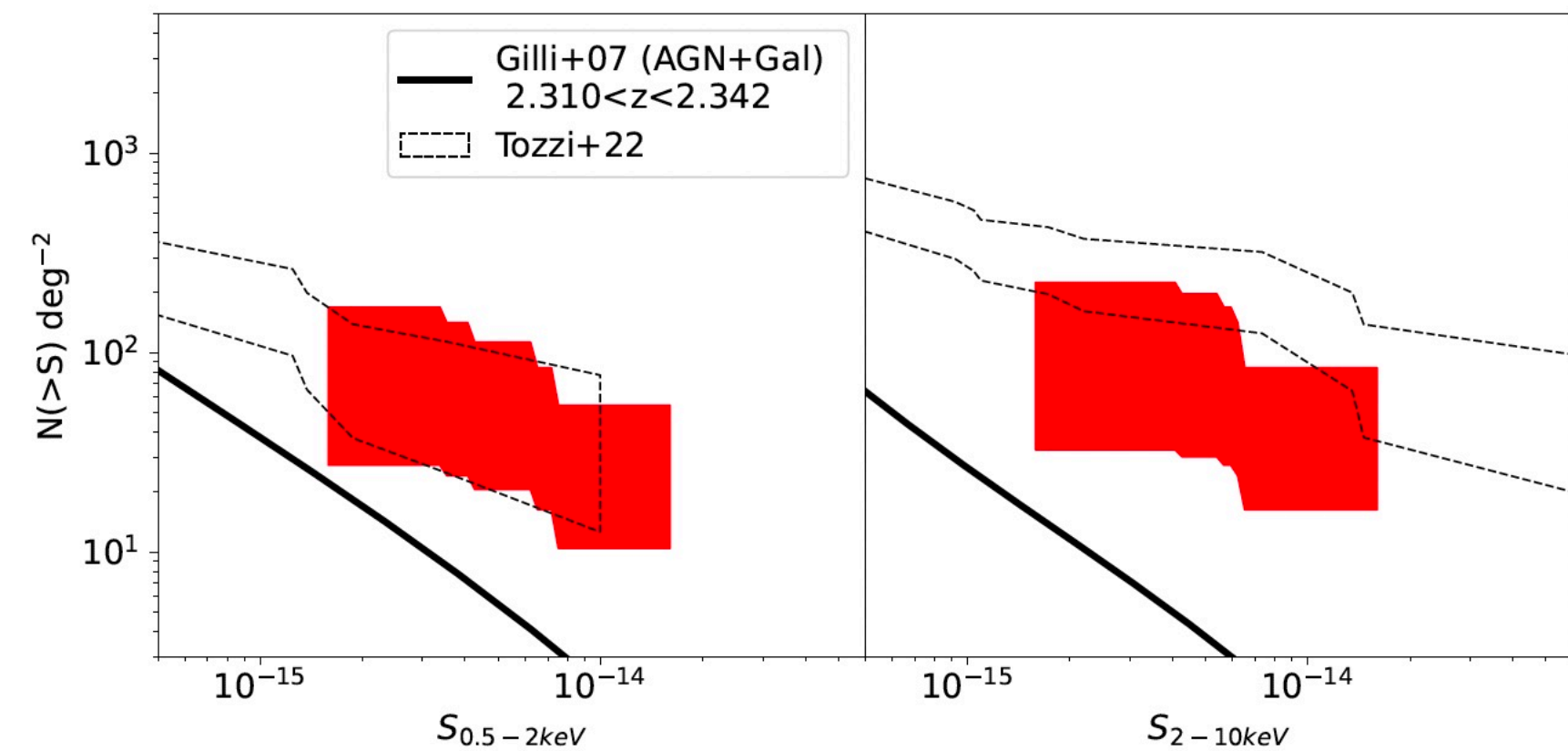
Strong excess (Spiderweb Galaxy is excluded)



Vito et al. 2024
Traina et al. 2025



Travascio et al. 2024
(MQN01 $z \sim 3$)



Wu et al. 2025 (BOSS1441)

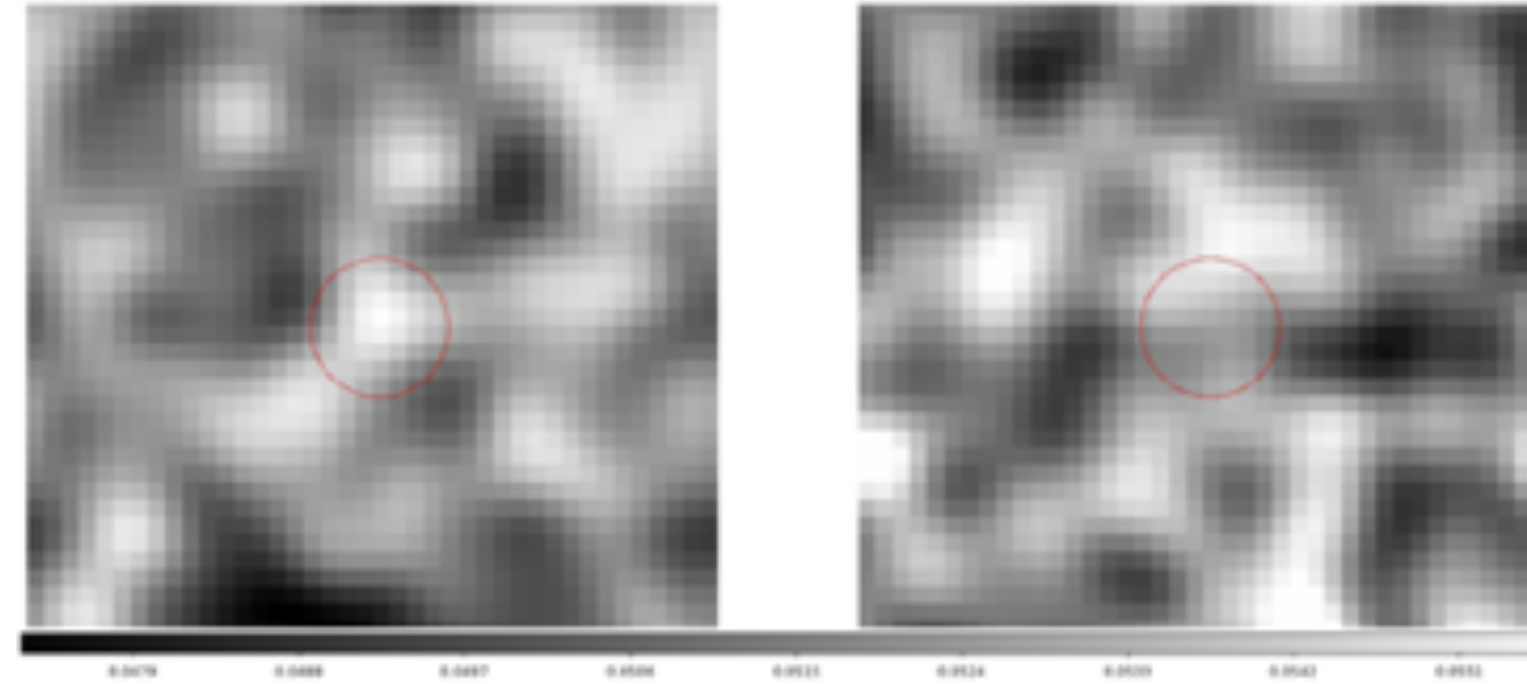


Fig. 17. Left panel: stacked image of the 82 spectroscopically confirmed protocluster members in the soft band. The size of the cutout is 20×20 arcsec, while the red circle shows the 2 arcsec radius region used to perform aperture photometry on the stacked image. Right panel: same as in the left panel in the hard band.

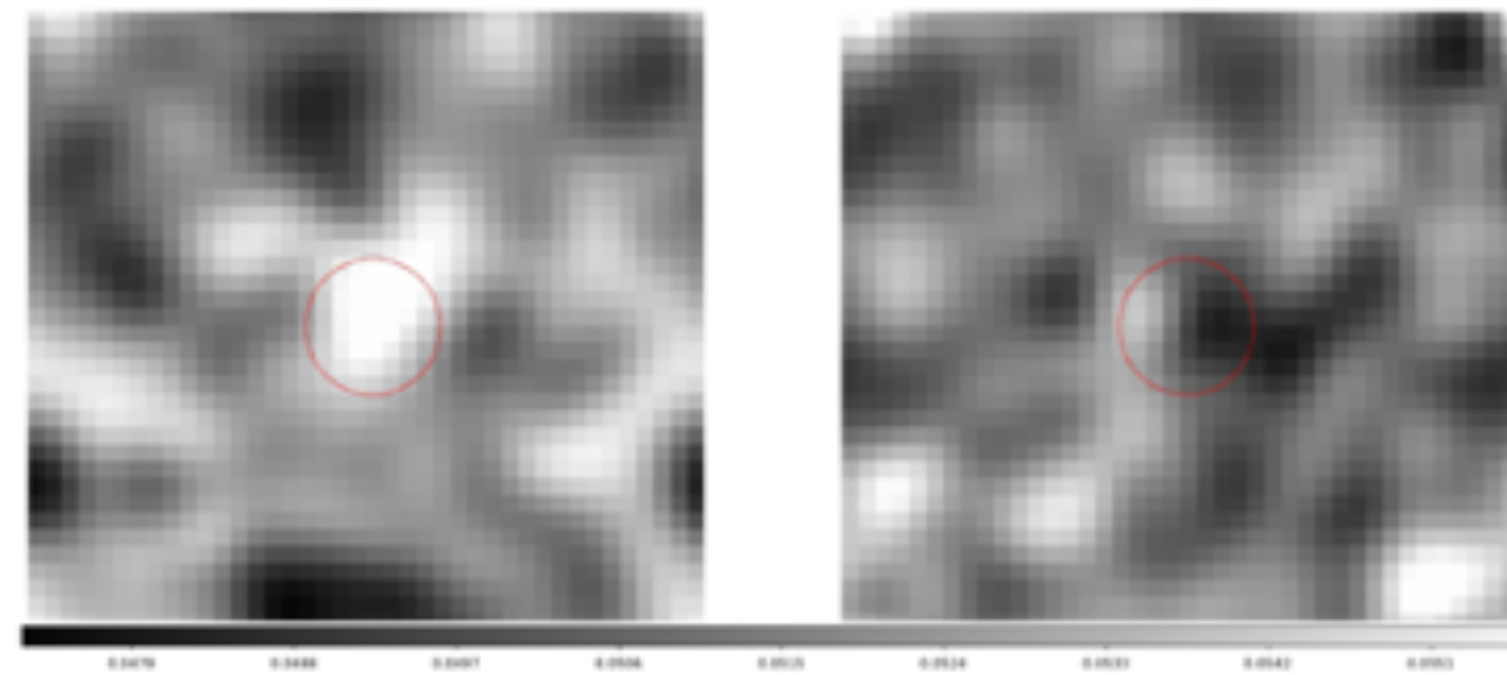
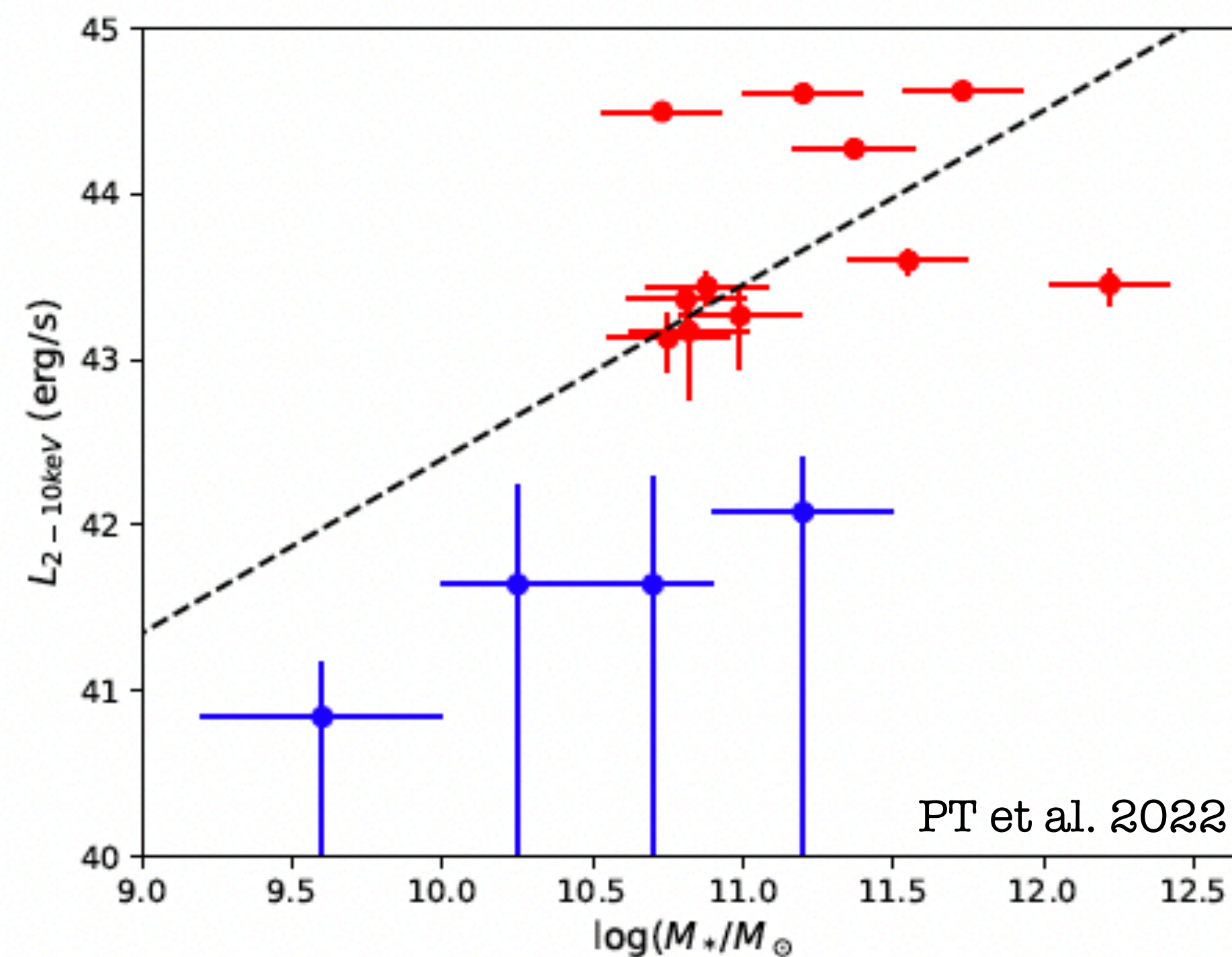
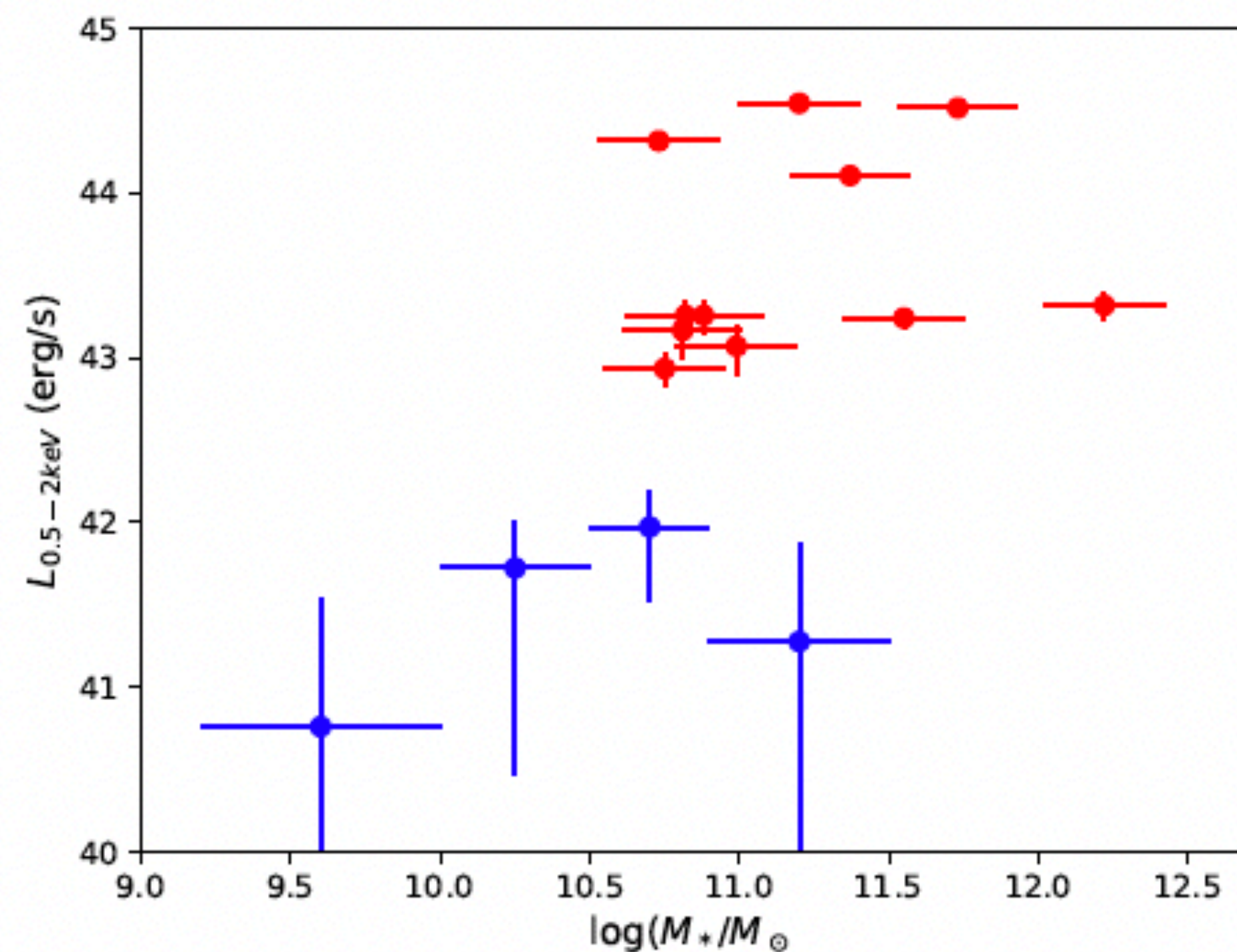


Fig. 18. Left panel: stacked image of the 81 color or narrow-band selected protocluster member candidates in the soft band. The red circle shows the 2 arcsec radius region used to perform aperture photometry on the stacked image. Right panel: same as in the left panel in the hard band.

No low-LX hidden in other members or member candidates

Possible cumulative signal from SF galaxies?



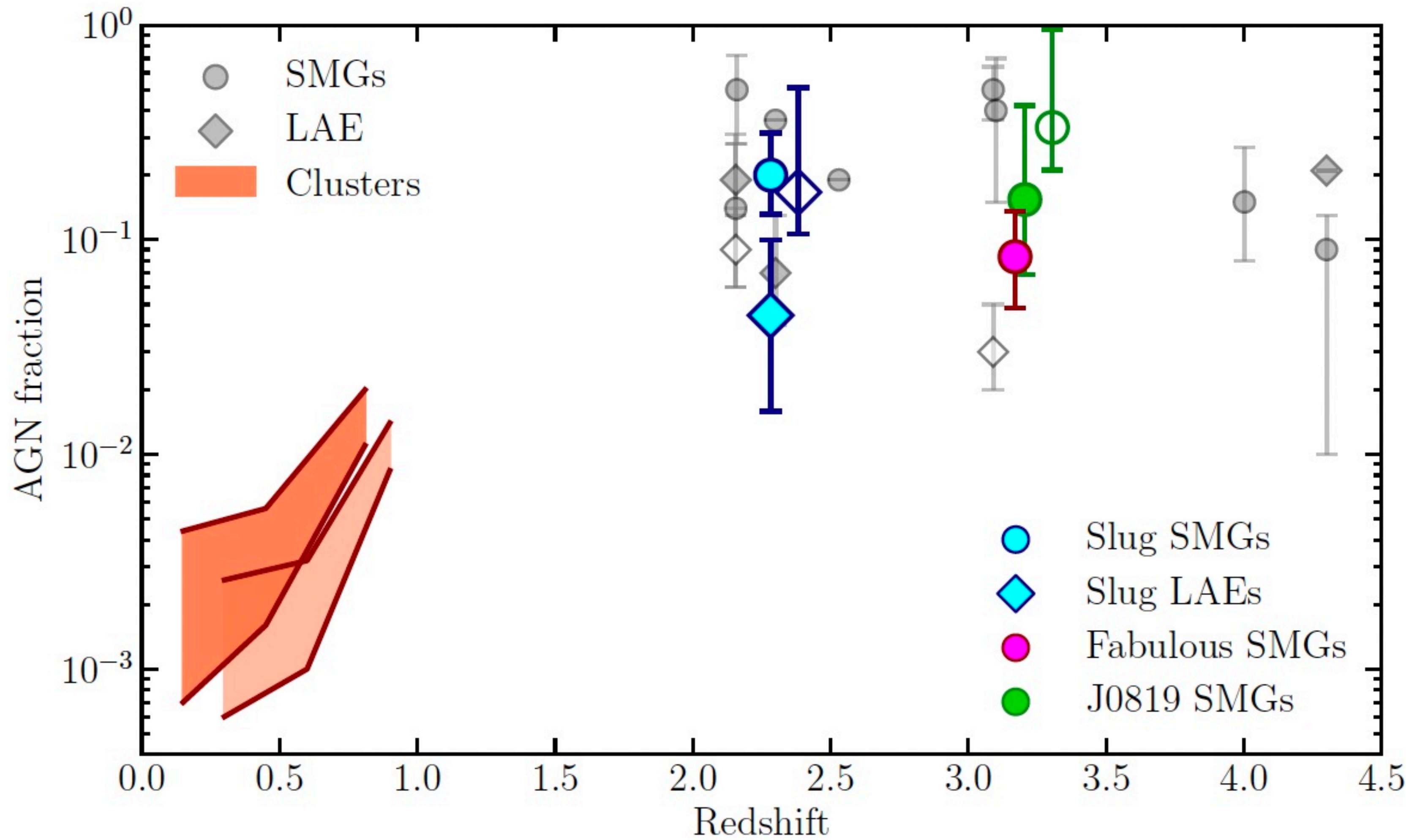
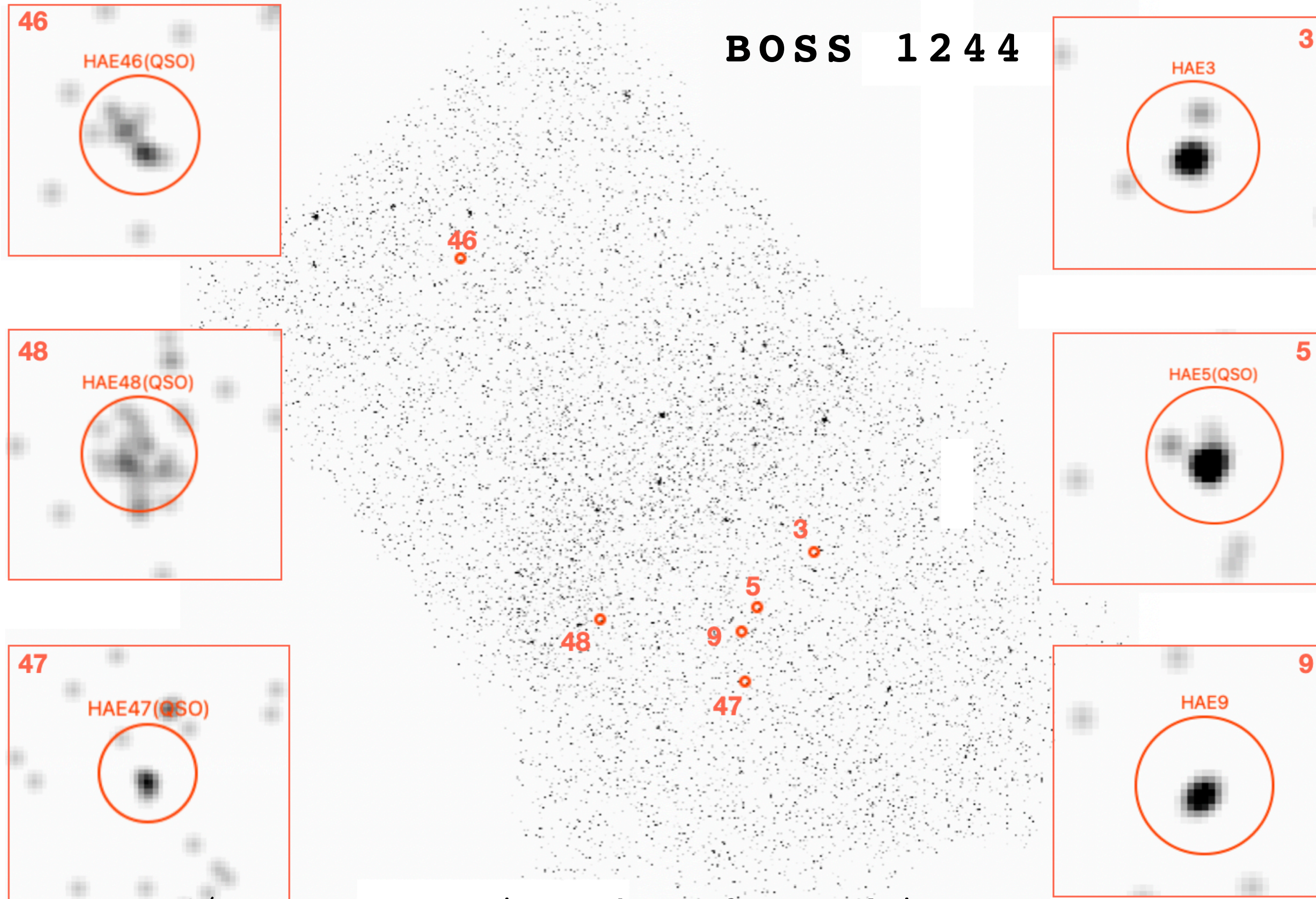


Fig. 3. Fractions of X-ray selected AGN with respect to different population of galaxies (i.e., SMGs, LAEs) in the Slug, Fabulous and J0819 protoclusters, compared to other protoclusters (Lehmer et al. 2009; Digby-North et al. 2010; Smail et al. 2014; Chen et al. 2016; Macuga et al. 2019; Umehata et al. 2019; Vito et al. 2020; Polletta et al. 2021; Tozzi et al. 2022b; Monson et al. 2023; Pérez-Martínez et al. 2023; Vito et al. 2024; Travascio et al. 2025) and the X-ray AGN fractions in local clusters (Martini et al. 2006; Bufanda et al. 2017). Empty blue and green points are the fractions computed for spectroscopically confirmed members (see Table 5).

Vito et al. 2024
Traina et al. 2025



BOSS 1244

**Lepore, M., et al.
2025 in preparation**

• 6/51 spectroscopic members detected in X-ray

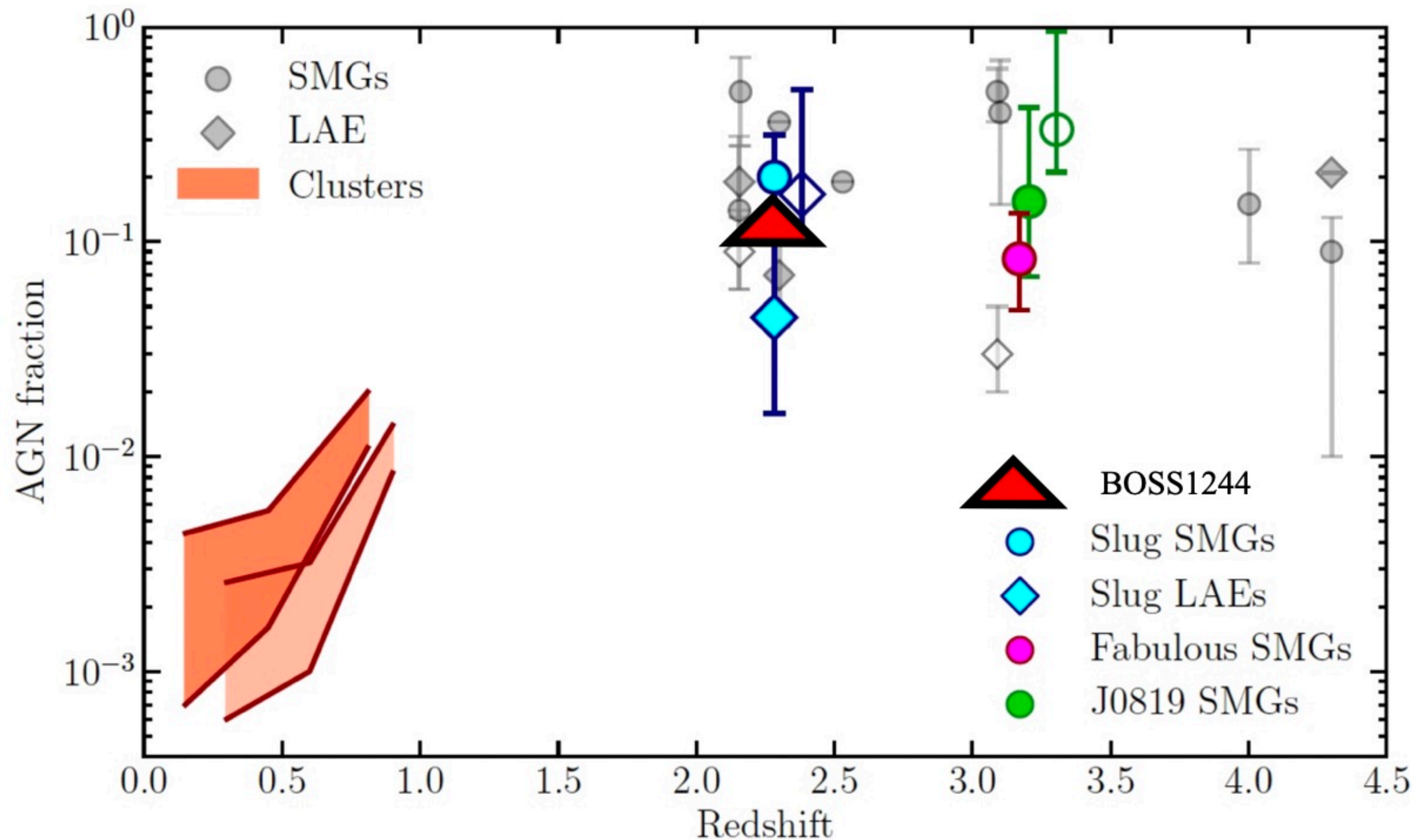


Fig. 3. Fractions of X-ray selected AGN with respect to different population of galaxies (i.e., SMGs, LAEs) in the Slug, Fabulous and J0819 protoclusters, compared to other protoclusters (Lehmer et al. 2009; Digby-North et al. 2010; Smail et al. 2014; Chen et al. 2016; Macuga et al. 2019; Umehata et al. 2019; Vito et al. 2020; Polletta et al. 2021; Tozzi et al. 2022b; Monson et al. 2023; Pérez-Martínez et al. 2023; Vito et al. 2024; Travascio et al. 2025) and the X-ray AGN fractions in local clusters (Martini et al. 2006; Bufanda et al. 2017). Empty blue and green points are the fractions computed for spectroscopically confirmed members (see Table 5).

Vito et al. 2024
Traina et al. 2025

- The f_{AGN} is $\sim 13\%$ of the spec confirmed members in the mass range $\log(M_*/M_\odot) > 10.5$
- Synergy with NIR, MIR (JWST) and submm (ALMA) data for SF and cold gas
- Martinez-Perez et al. 2025, Shimakawa et al. 2025

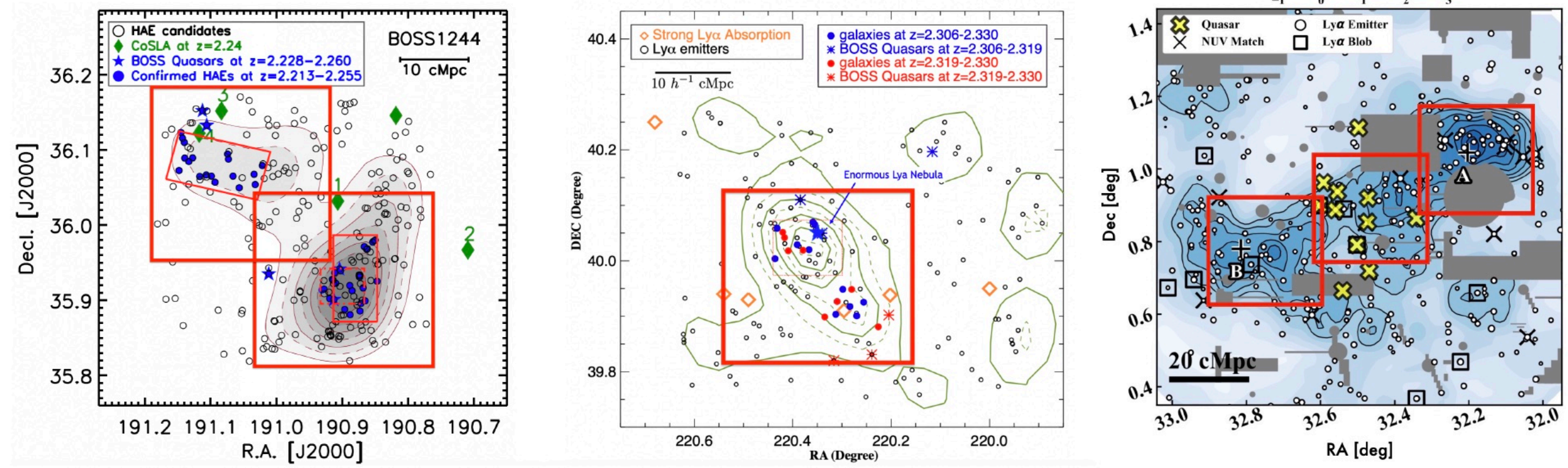
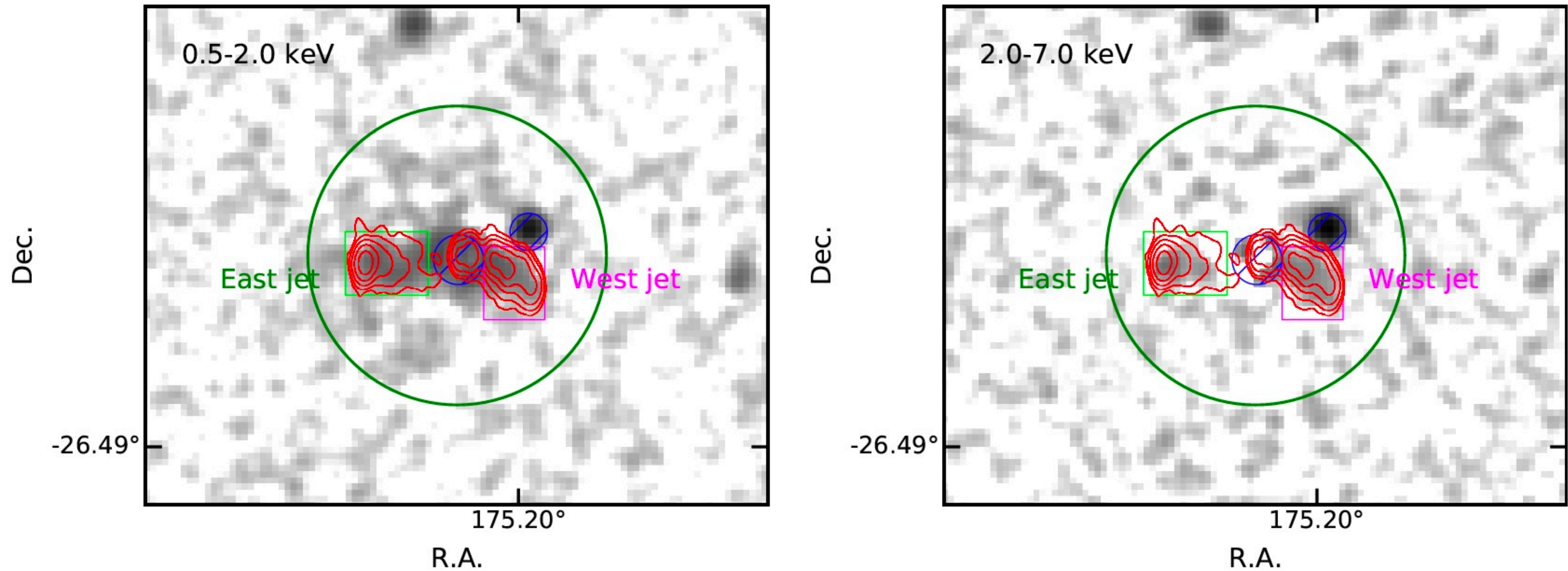


Figure 2: Left: BOSS1244 field adapted from [12]. The thin red boxes show the regions of the spectroscopic survey, while the black and blue circles are HAE candidates and HAE spectroscopically confirmed members, respectively. The blue stars are BOSS AGNs. Center: BOSS1441 field, adapted from [11]. The orange diamonds represent Ly α absorption systems and the red asterisks represent BOSS QSOs. Right: BOSS0210 LAE overdensity map, adapted from [15]. Circles and yellow crosses represent the LAE candidates and the BOSS QSOs, respectively. The red thick boxes show the ACIS-I FoVs of this proposal.

Table 1: List of *Chandra* pointings. (1): object ID; (2): Right ascension; (3): Declination; (4) redshift; (5): Galactic hydrogen column density; (6): galaxy overdensity¹; (7): Proposed time (ks); (8): Archival time (ks); (9): GTO time (ks). *RA* and *Dec* refer to the ACIS-I FoV center as shown in Fig.2.

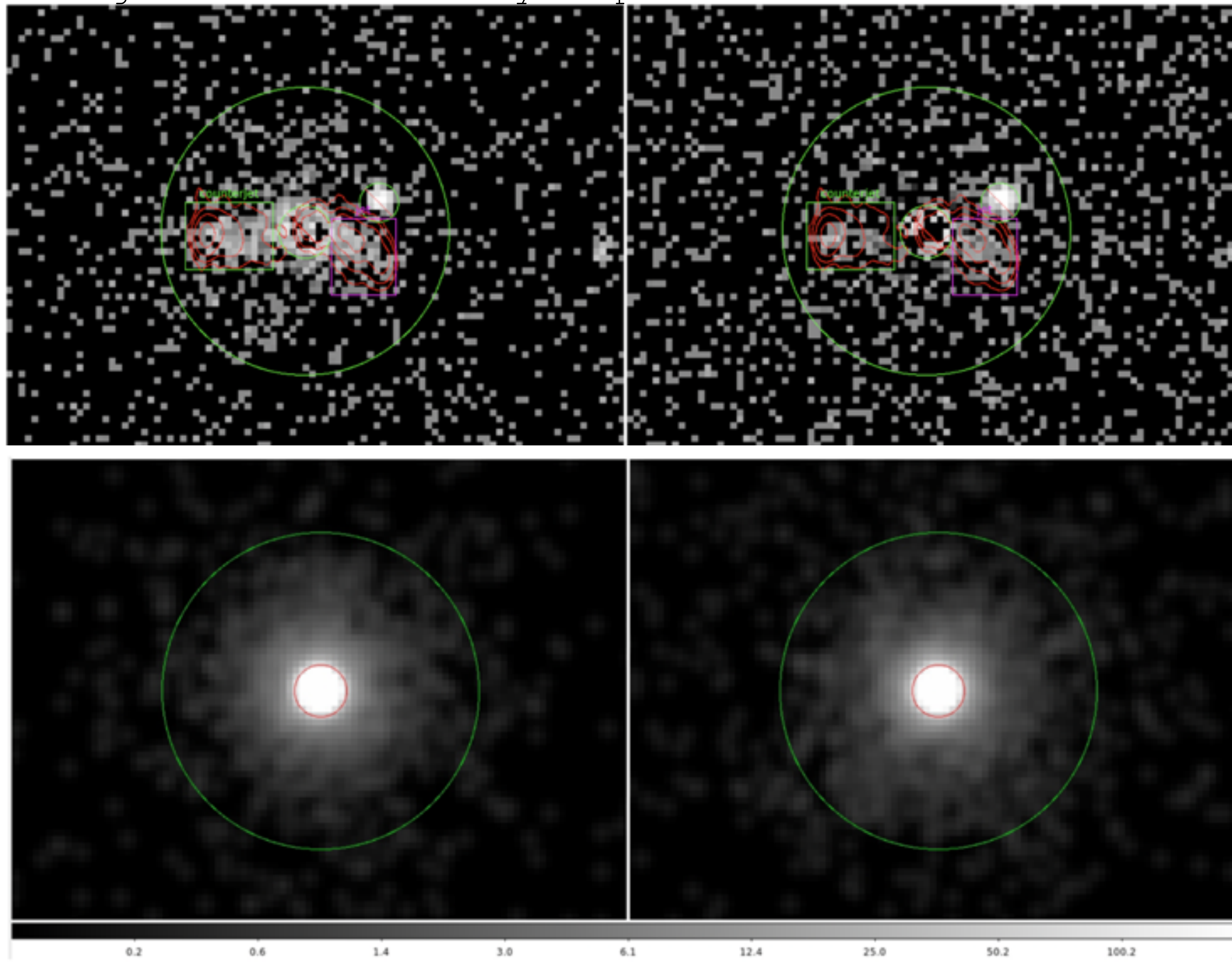
| ID | RA | Dec | redshift | N_{HGal} $10^{20}/cm^2$ | δ_g | t_{exp} prop | t_{exp} arch | t_{exp} GTO |
|------------|------------|-------------|-------------------|------------------------------|----------------|-------------------|-------------------|------------------|
| (1) | (2) | (3) | (4) | (5) | (6) | (7) | (8) | (9) |
| 1244NE | 12:44:19.2 | +36:04:48.0 | 2.246 ± 0.001 | 1.33 | 10.9 ± 2.5 | 140 | 30 | – |
| 1244SW | 12:43:31.2 | +35:55:12.0 | 2.230 ± 0.002 | 1.27 | 22.9 ± 4.9 | – | 30 | 120 ² |
| 1441 | 14:41:24.0 | +40:00:00.0 | 2.32 ± 0.02 | 1.07 | 10.8 ± 2.6 | 110 | 45 ³ | – |
| 0210E | 02:08:48.0 | +01:00:00.0 | 2.177 ± 0.023 | 2.93 | – | 170 | – | – |
| 0210C | 02:09:48.0 | +00:54:00.0 | 2.177 ± 0.023 | 2.93 | – | – | – | 150 ⁴ |
| 0210W | 02:11:00.0 | +00:46:48.0 | 2.177 ± 0.023 | 2.93 | – | 170 | – | – |
| Total time | | | | | | 590 | 105 | 270 |

¹ Overdensity of LAEs for BOSS1441 and overdensity of HAEs for BOSS1244



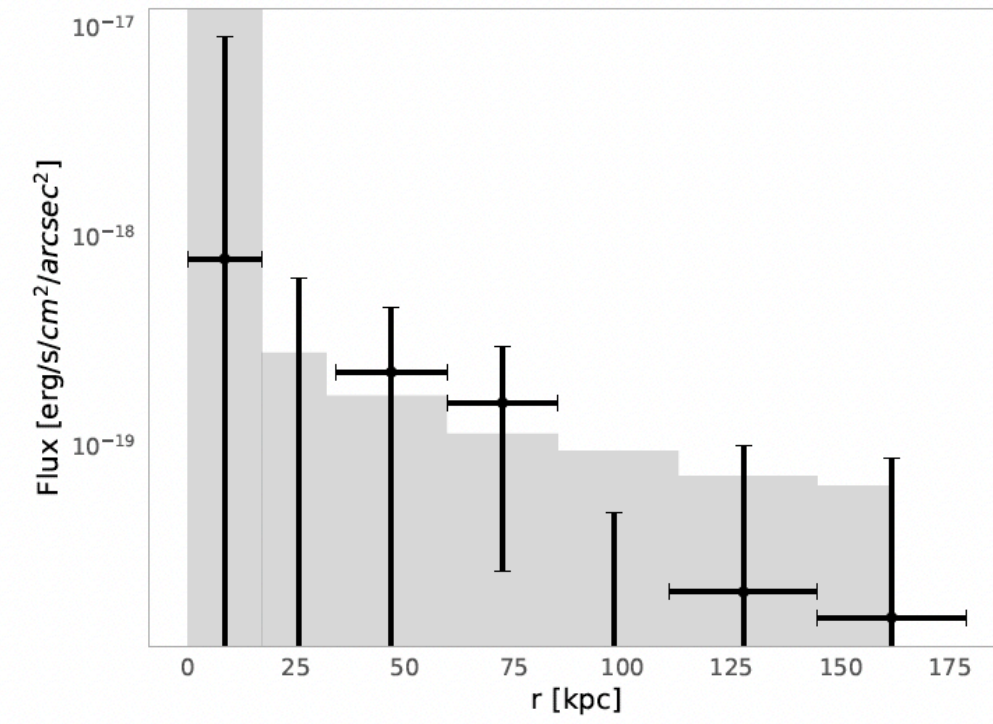
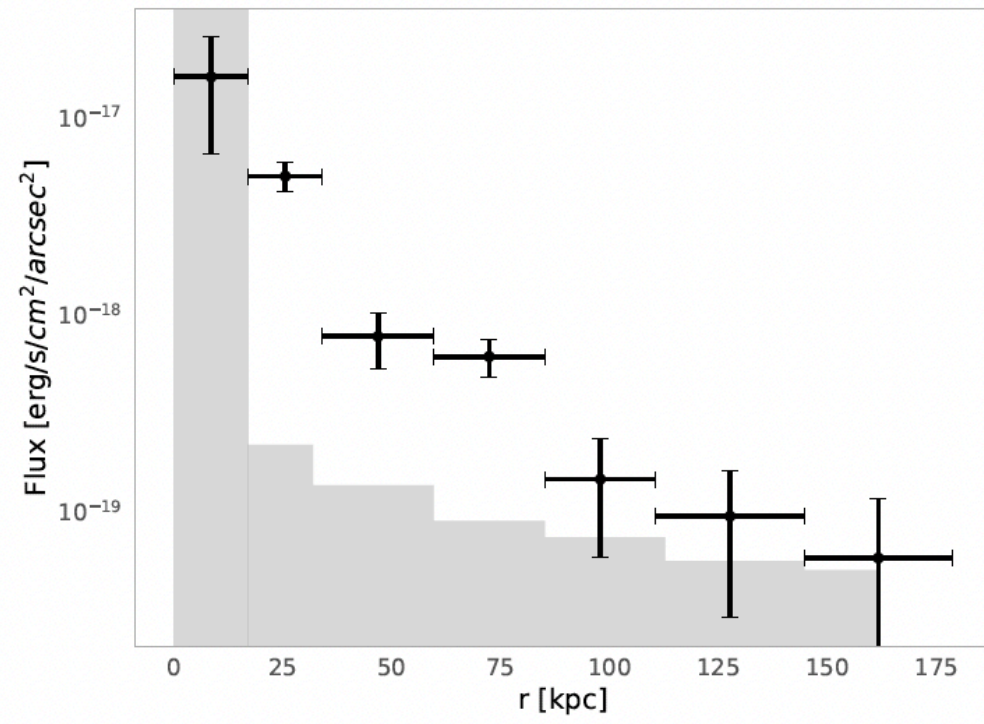
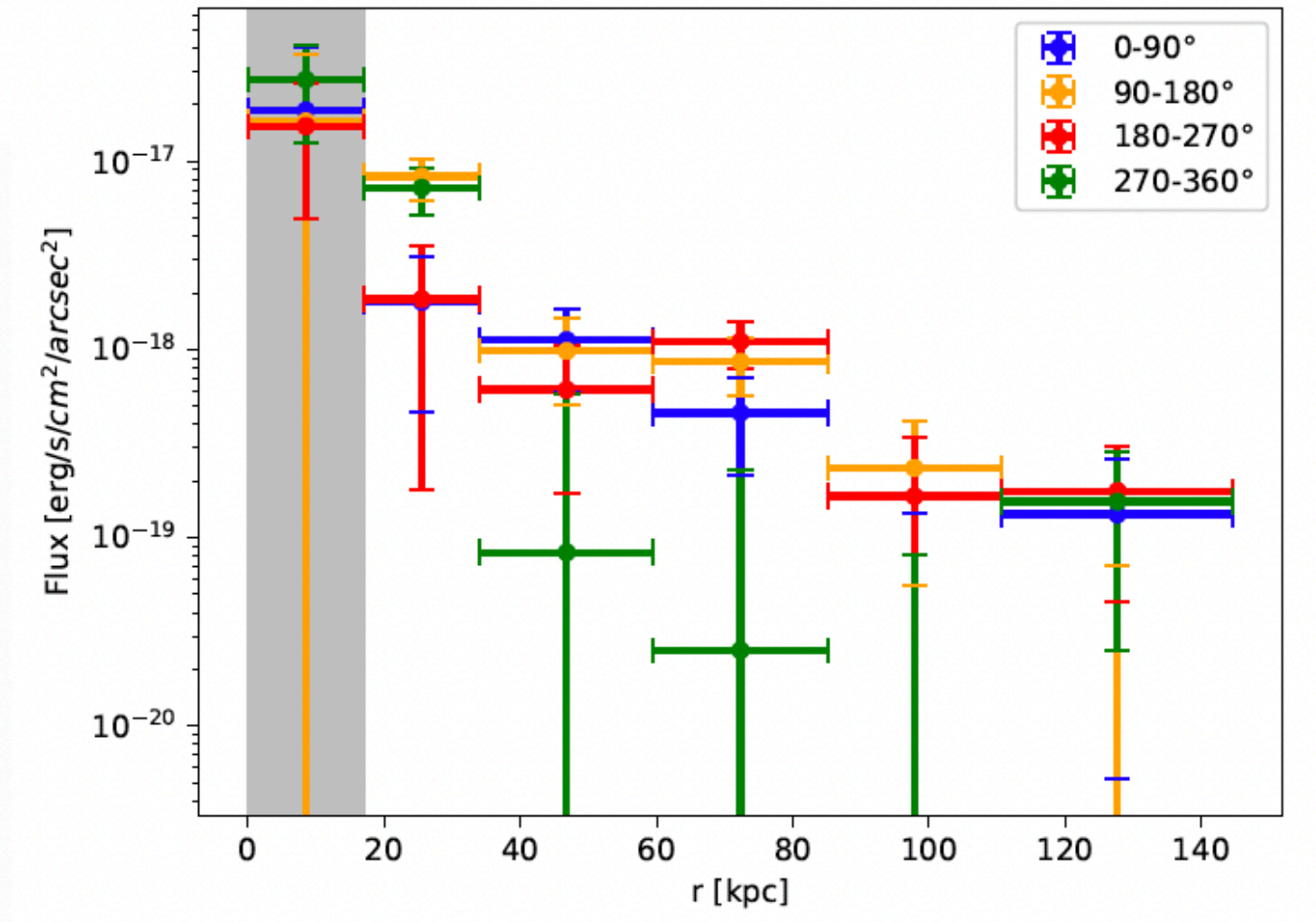
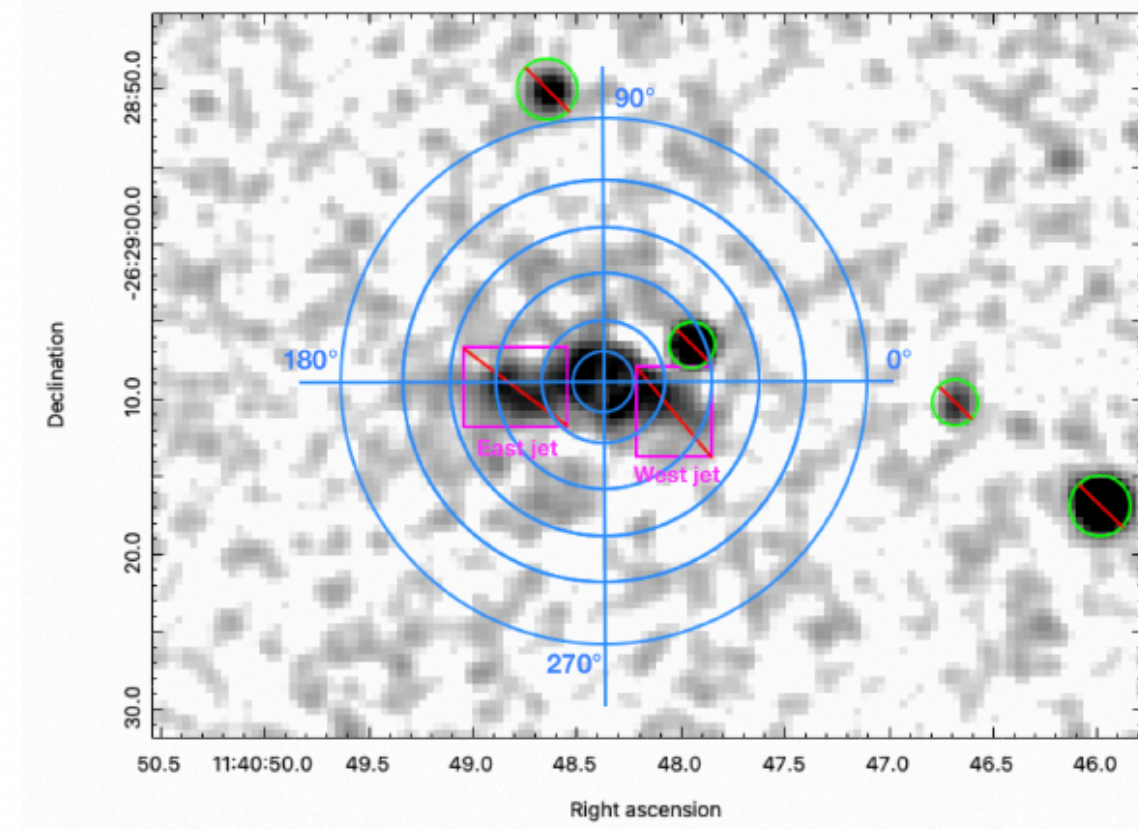
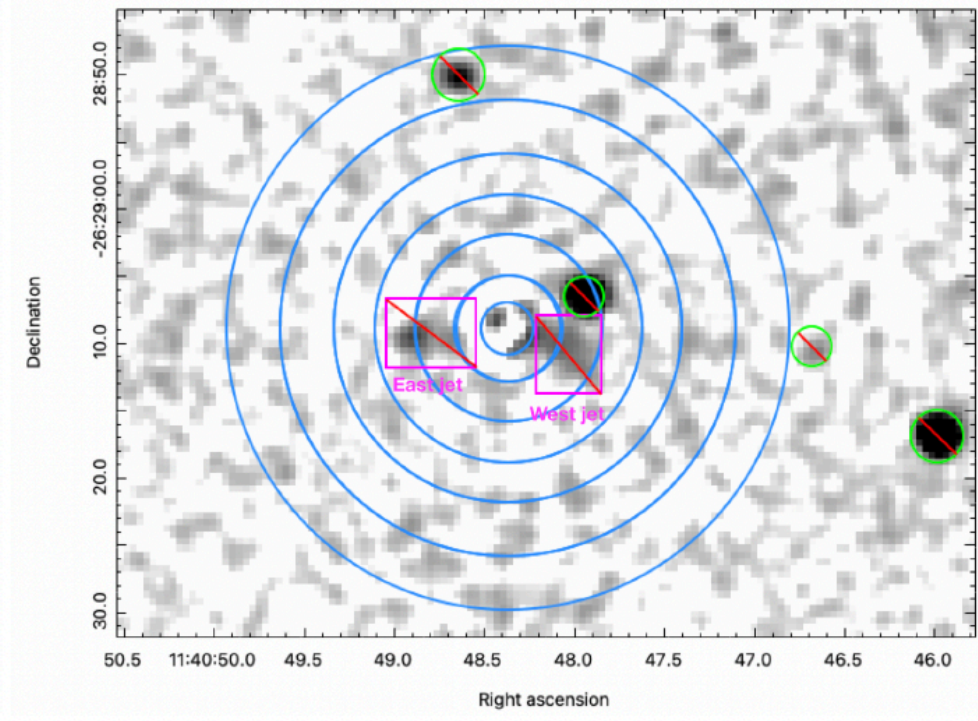
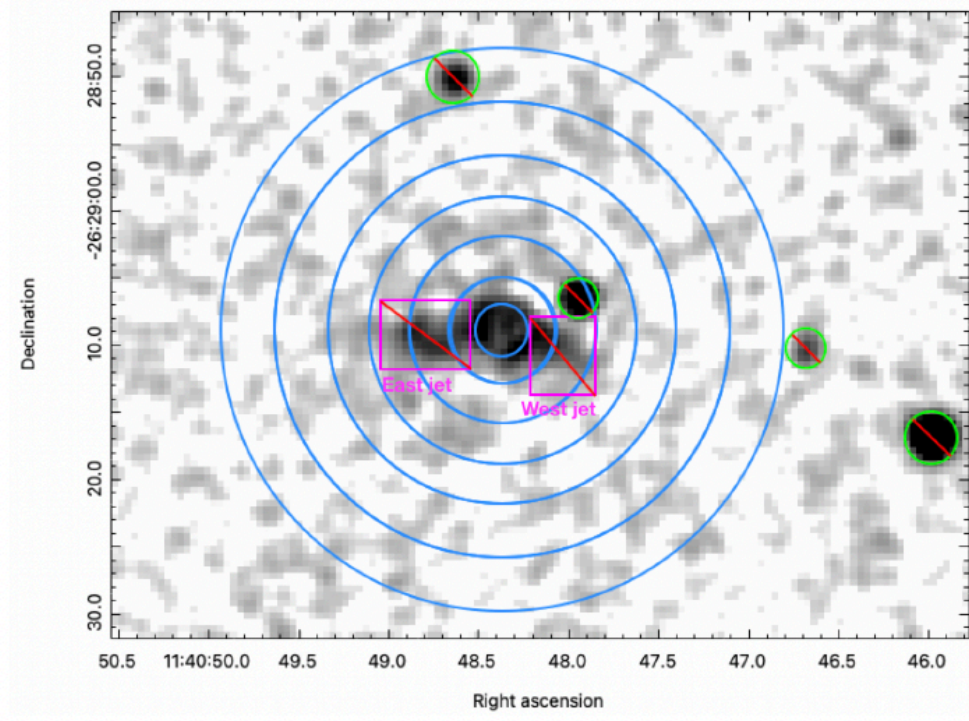
- Diffuse emission in the soft (left) and hard (right) band in the Spiderweb. Red contours are 10 GHz JVLA contours (Carilli et al. 2022)

PSF wings subtraction: a key step to measure the diffuse emission



IFPU Focus Week: the emergence of the cosmic web - September 2025

Lepore et al. 2024



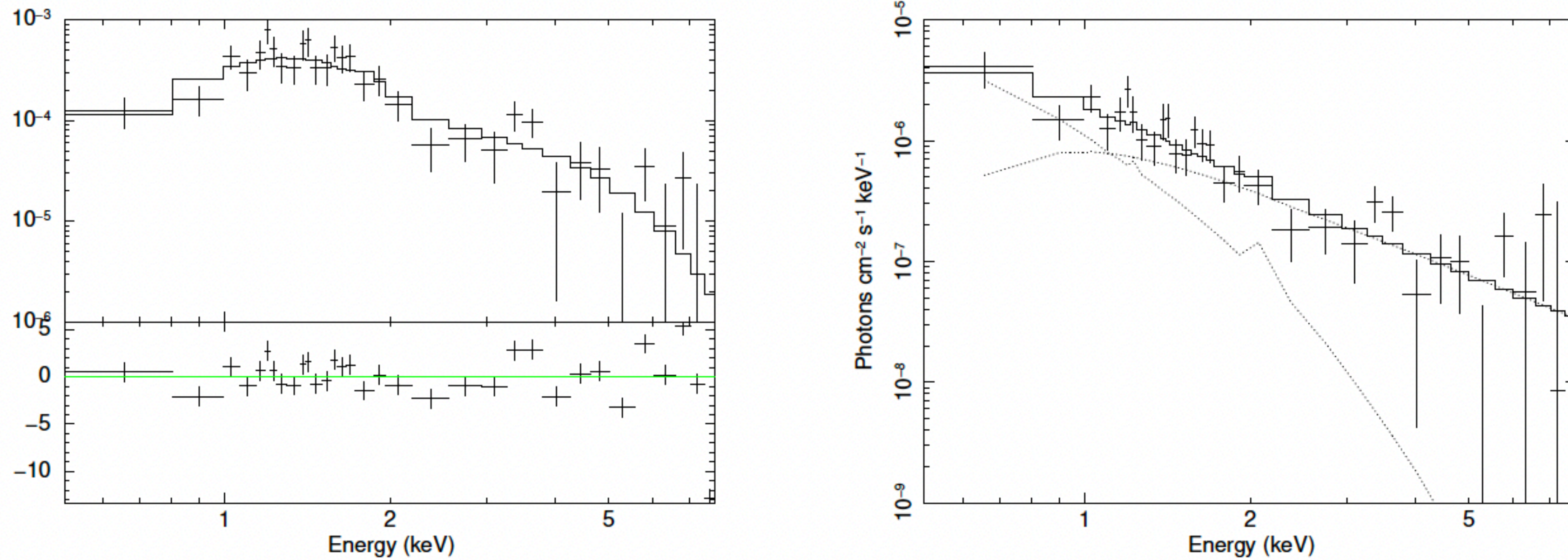


Fig. 14. *Left:* spectrum (folded with the instrument spectral response) of the isotropic diffuse emission (after removing the central, AGN-dominated region, and the jet regions) fitted with a thermal meka1 model plus the AGN contamination. *Right:* unfolded spectrum with the two model components shown with dotted lines. The AGN contamination (absorbed power law) is dominant at energies >1.5 keV, while the thermal component is dominant below 1 keV.

PT et al. 2022

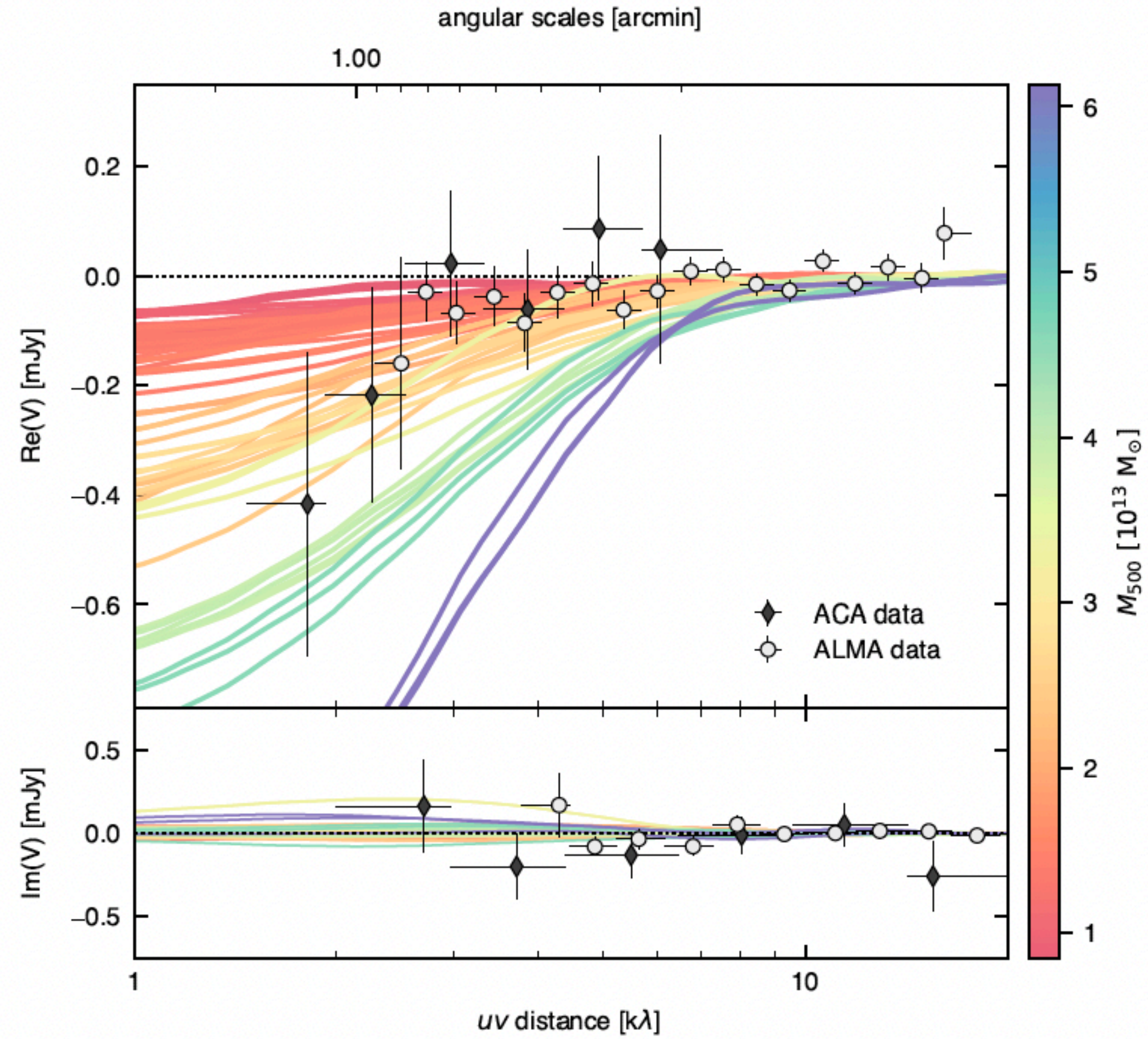
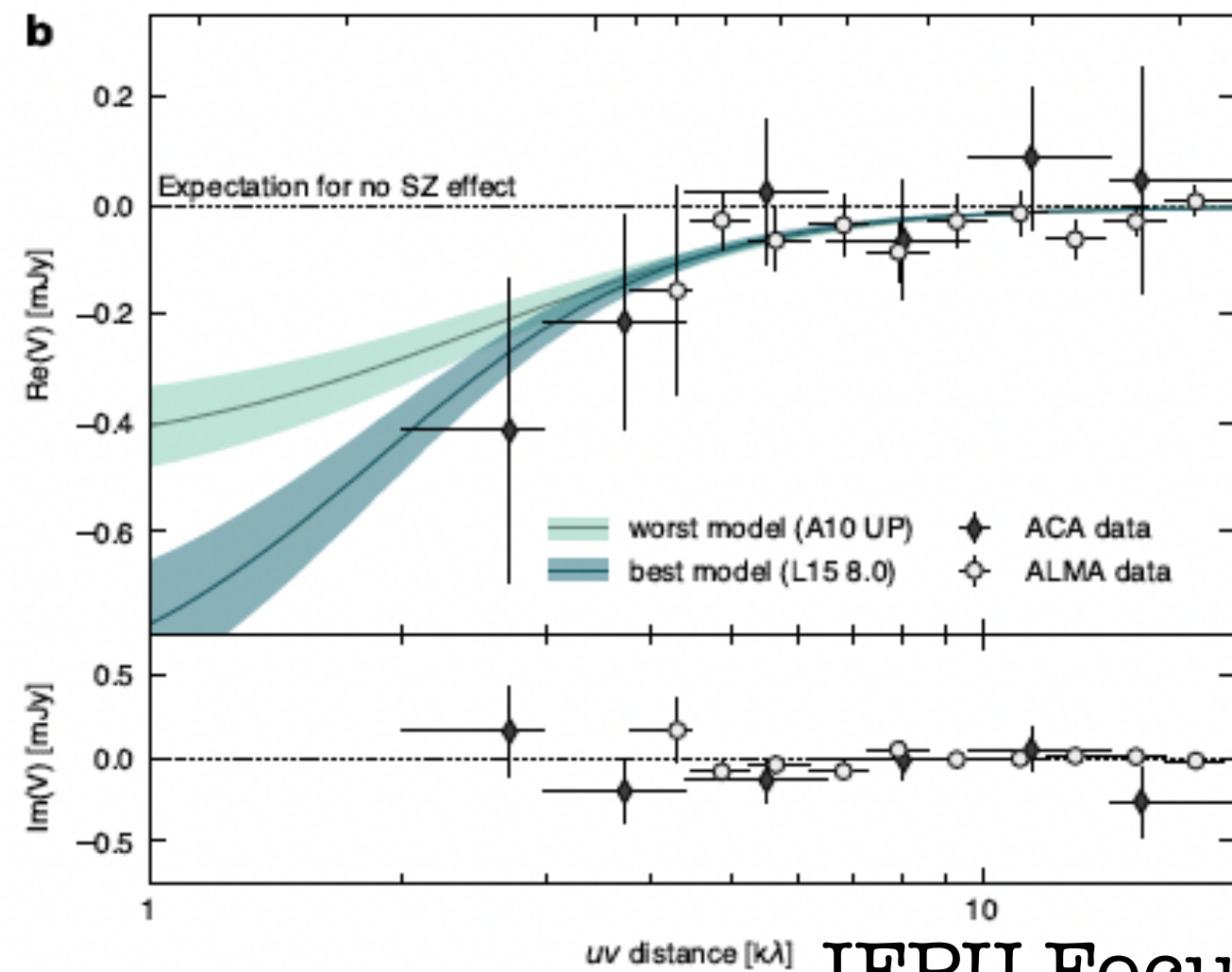
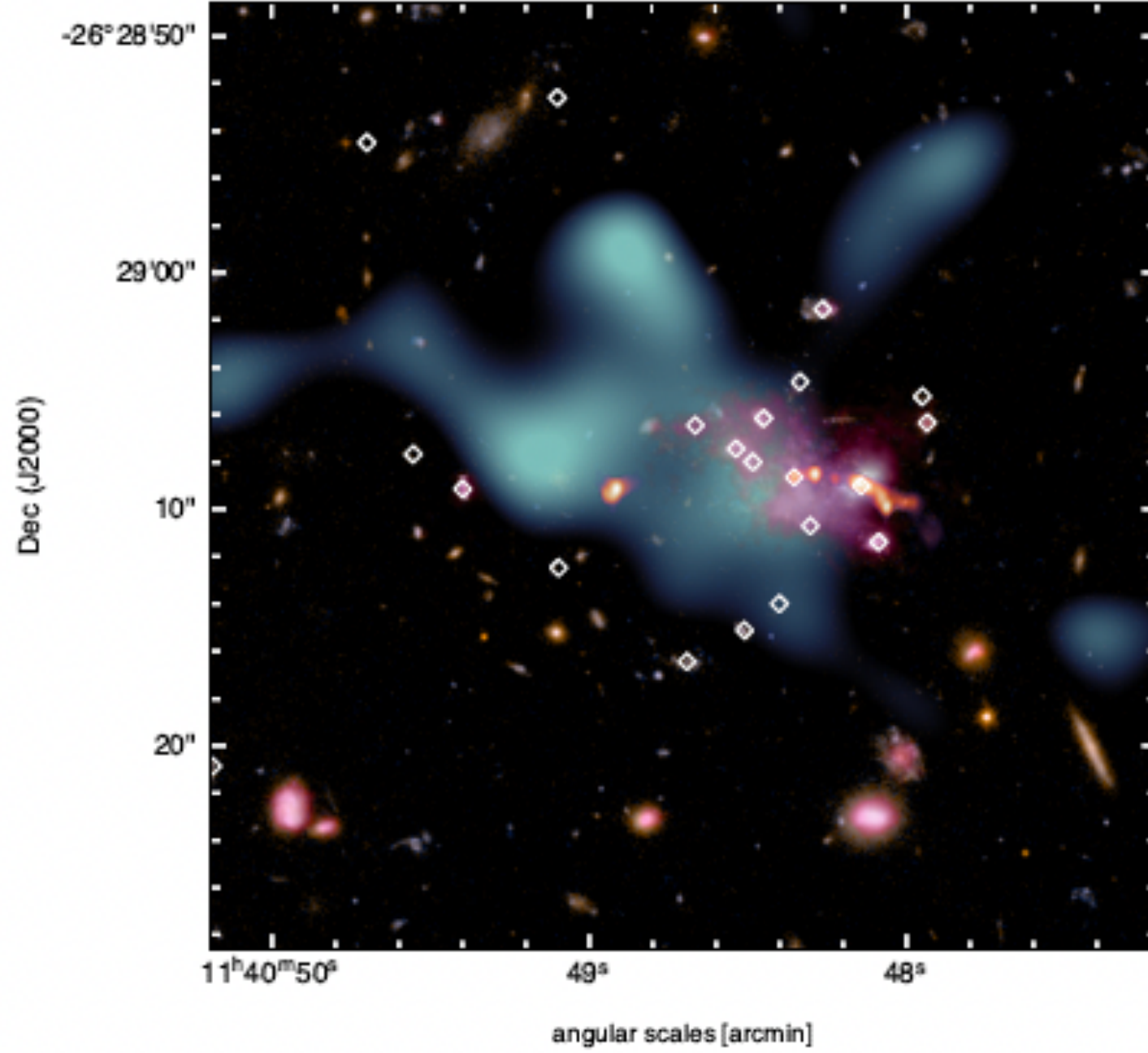
$$kT = 2.0^{+0.7}_{-0.4} \text{ keV}$$

$$M_{\text{ICM}} = 1.67^{+0.17}_{-0.17} 10^{12} M_{\odot}$$

$$M_{\text{tot}}(<100 \text{ kpc}) = 1.5^{+0.5}_{-0.3} 10^{13} M_{\odot}$$

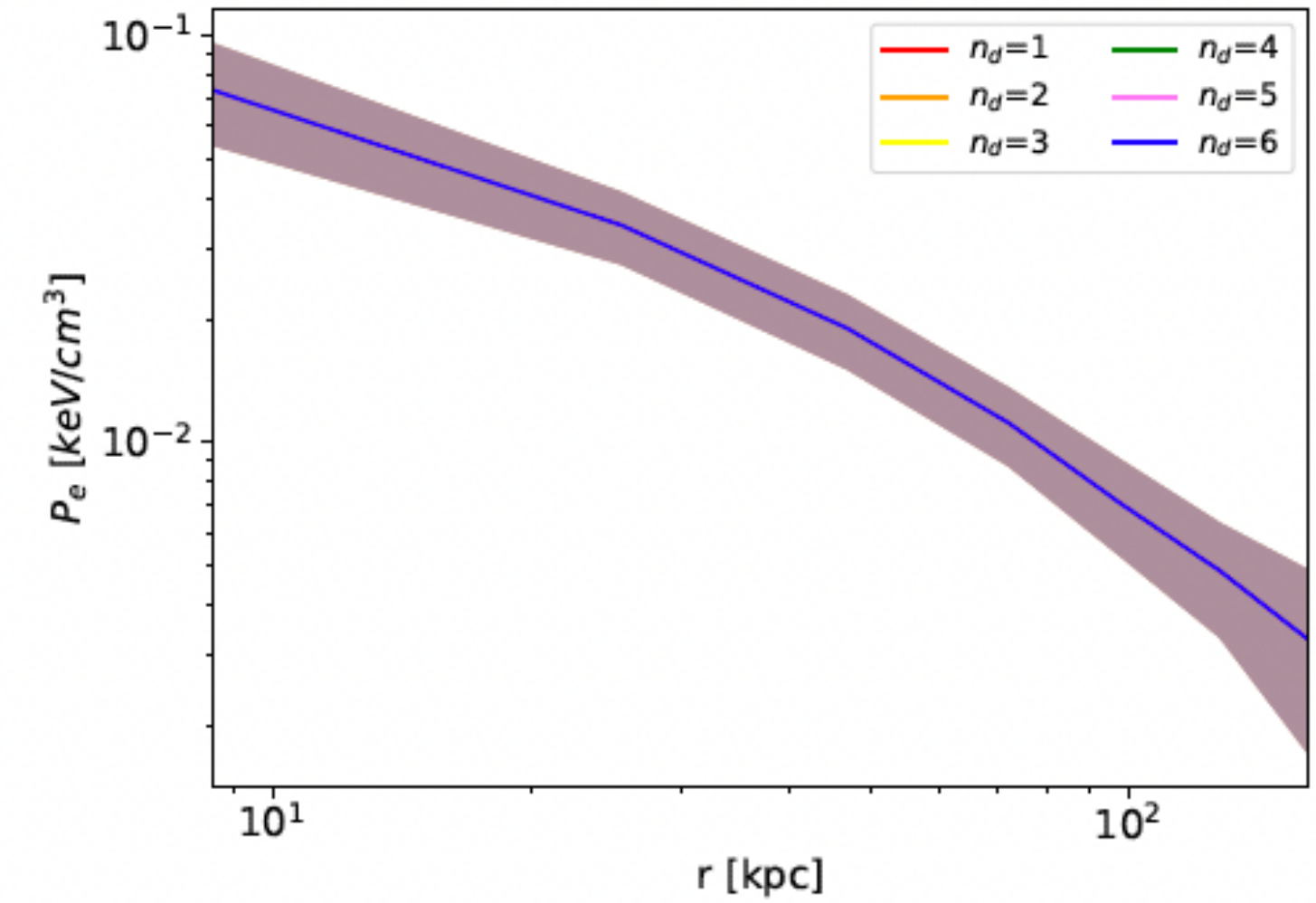
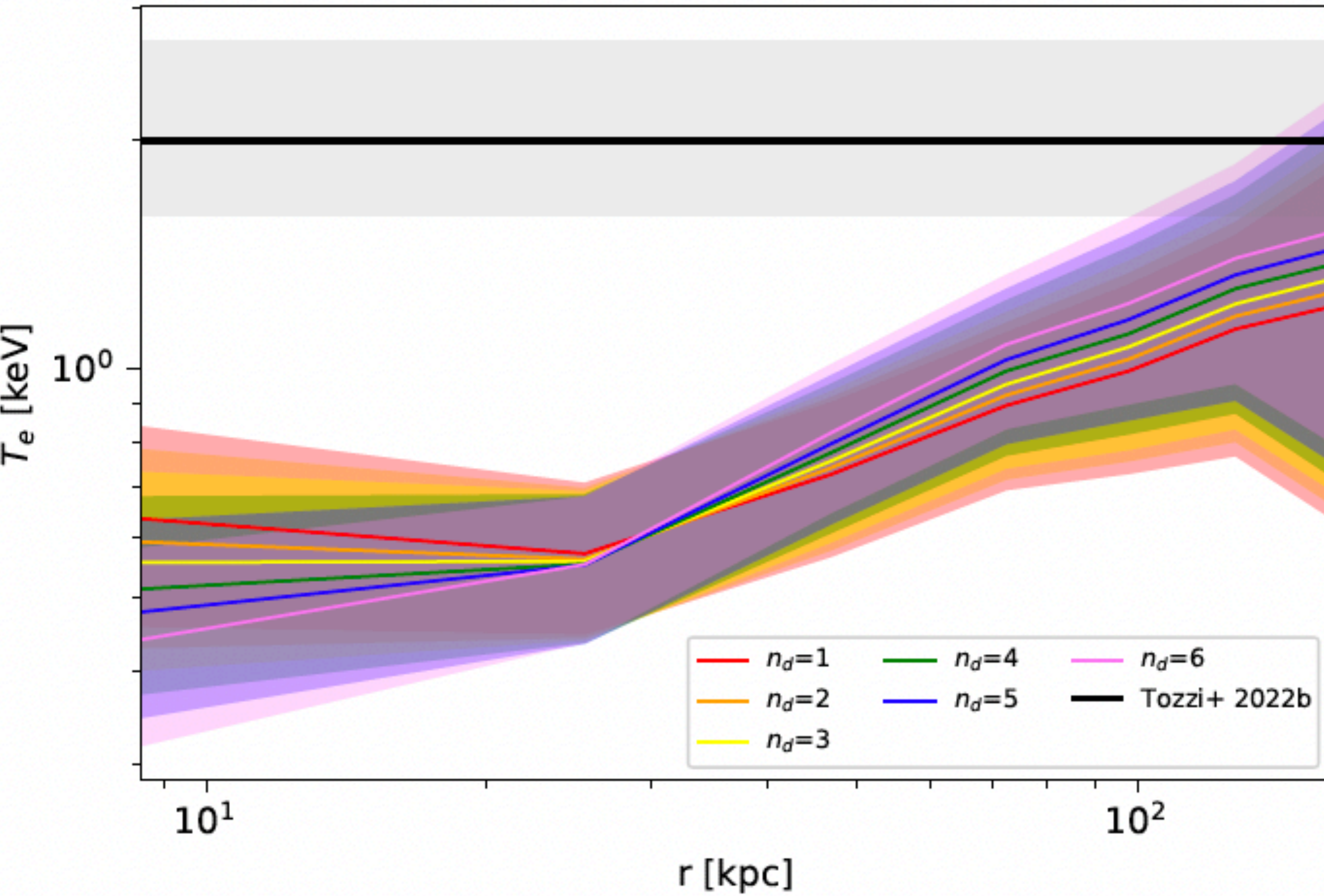
$$M_{500} = 3.0^{+1.1}_{-1.1} 10^{13} M_{\odot}$$

Consistent with the low-mass case simulation of Saro et al. (2009)



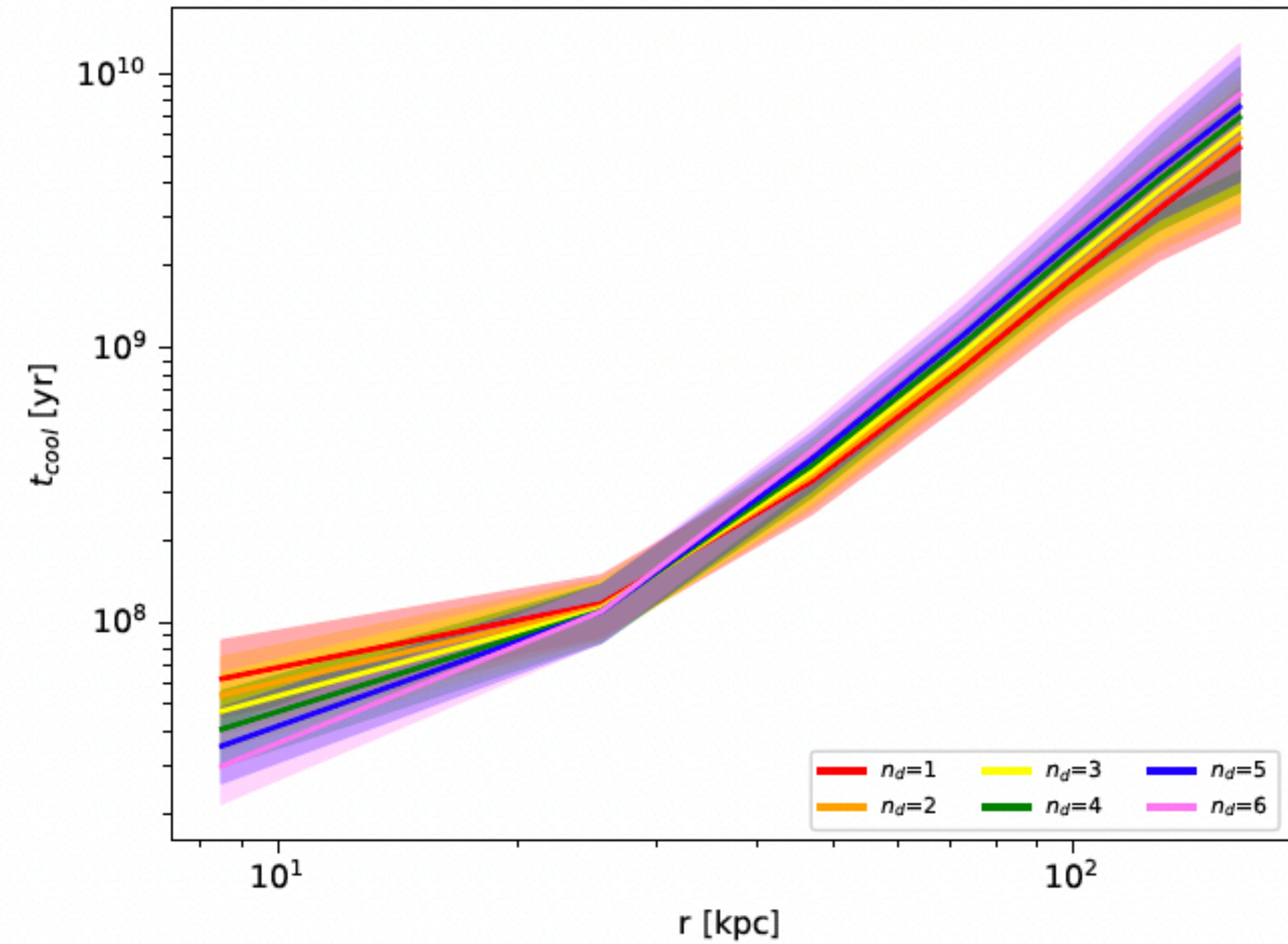
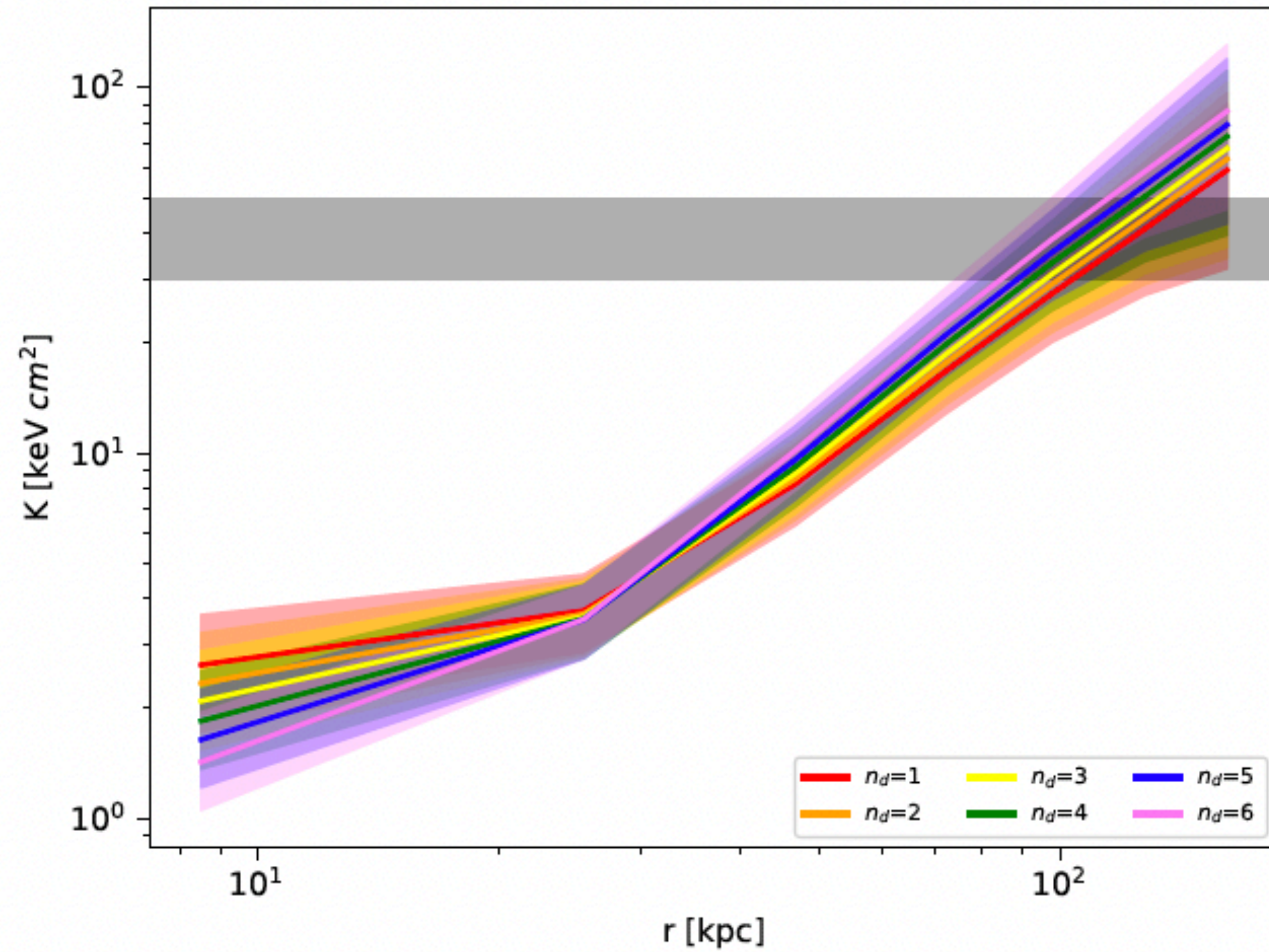
Di Mascolo et al. 2023

Temperature gradient in the ICM



Lepore et al. 2023

Cool core (cooling flow?) in the Spiderweb



~ adiabatic cooling flow of 250–1000 M/yr (optimal value 760 M/yr)

SFR values:

1390±150 M/yr (Seymour et al. 2012)

1150±580 M/yr (Rawlings et al. 2013)

Lepore et al. 2023

Table 2. Best-fit values for the reference spectral analysis of the diffuse emission.

| Region | kT (mekal) keV | F_S $\text{erg s}^{-1} \text{cm}^{-2}$ | F_H $\text{erg s}^{-1} \text{cm}^{-2}$ | $L_{0.5-2 \text{ keV}}$ erg s^{-1} | $L_{2-10 \text{ keV}}$ erg s^{-1} |
|------------------|------------------------|---|---|--|---|
| Isotropic Region | $1.98^{+0.70}_{-0.43}$ | $(2.5 \pm 0.6) \times 10^{-15}$ | $(2.4 \pm 0.9) \times 10^{-16}$ | $(7.7 \pm 1.8) \times 10^{43}$ | $(7.3 \pm 1.7) \times 10^{43}$ |
| West jet | 1.90 ± 0.20 | $(1.32 \pm 0.21) \times 10^{-15}$ | $(1.78 \pm 0.28) \times 10^{-15}$ | $(4.1 \pm 0.7) \times 10^{43}$ | $(5.5 \pm 0.9) \times 10^{43}$ |
| East jet | 2.51 ± 0.21 | $(1.89 \pm 0.25) \times 10^{-15}$ | $(1.02 \pm 0.13) \times 10^{-15}$ | $(1.18 \pm 0.15) \times 10^{44}$ | $(6.4 \pm 0.8) \times 10^{43}$ |

Notes. We note that in this table, flux and luminosity values of the isotropic (thermal) emission have not been corrected by the geometrical factor, but directly correspond to the best-fit values obtained from the extraction region. Error bars refer to 1σ c.l. on a single parameter.

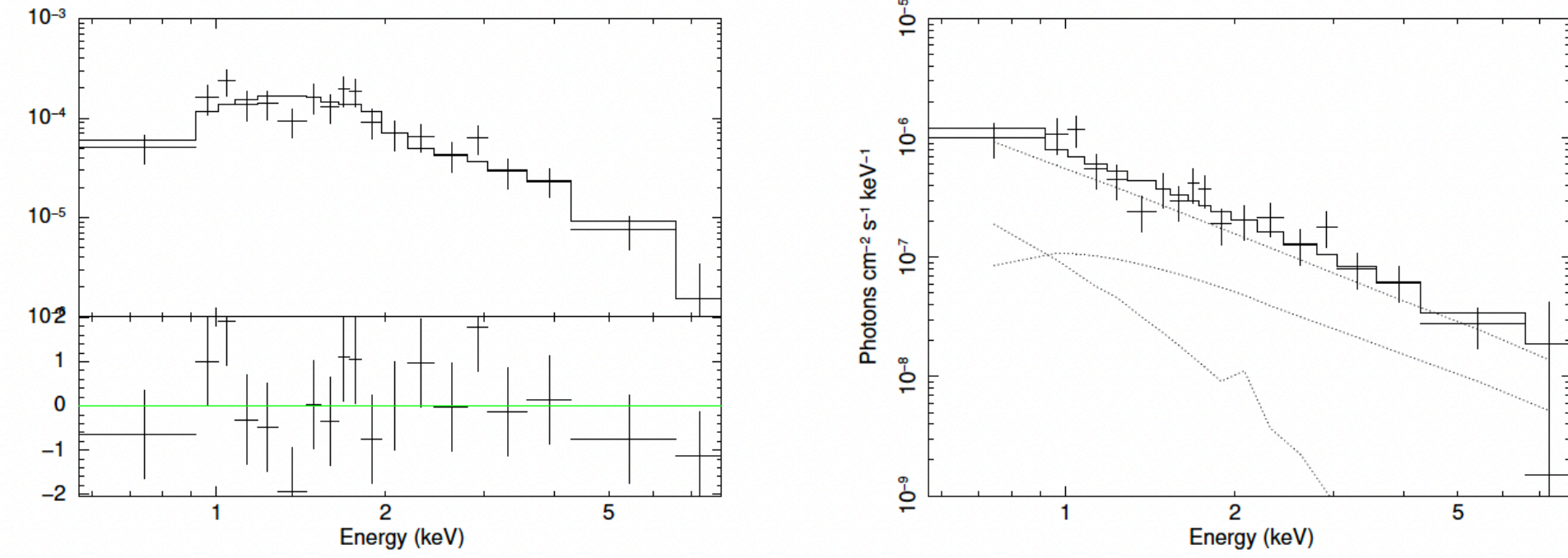


Fig. 15. *Left:* spectrum (folded with the instrument spectral response) of the emission in the west jet region (including the AGN contamination and the residual thermal emission from the ICM) fitted with a power law. *Right:* unfolded spectrum with the three components in the model shown with dotted lines. The lowest dotted line corresponds to the thermal emission from the overlapping ICM, while the line in the middle accounts for the AGN wings contamination. The IC from the relativistic population in the west jet is shown by the unabsorbed power law that is dominating at any energy.

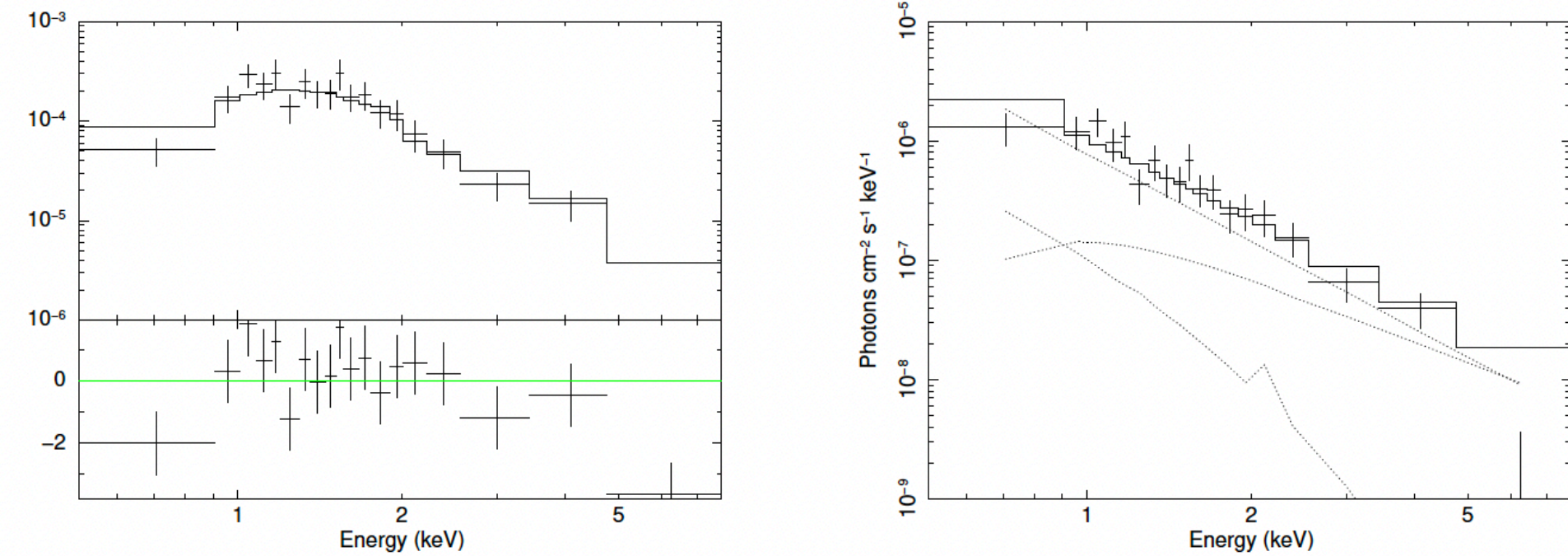


Fig. 16. *Left:* spectrum (folded with the instrument spectral response) of the emission in the east jet region (including the AGN contamination and the residual thermal emission from the ICM) fitted with a power law. *Right:* unfolded spectrum with the three components in the model shown with dotted lines. The lowest dotted line corresponds to the thermal emission from the overlapping ICM, while the line in the middle accounts for the AGN wings contamination. The IC from the relativistic population in the east jet is shown by the unabsorbed power law that is dominating at any energy.

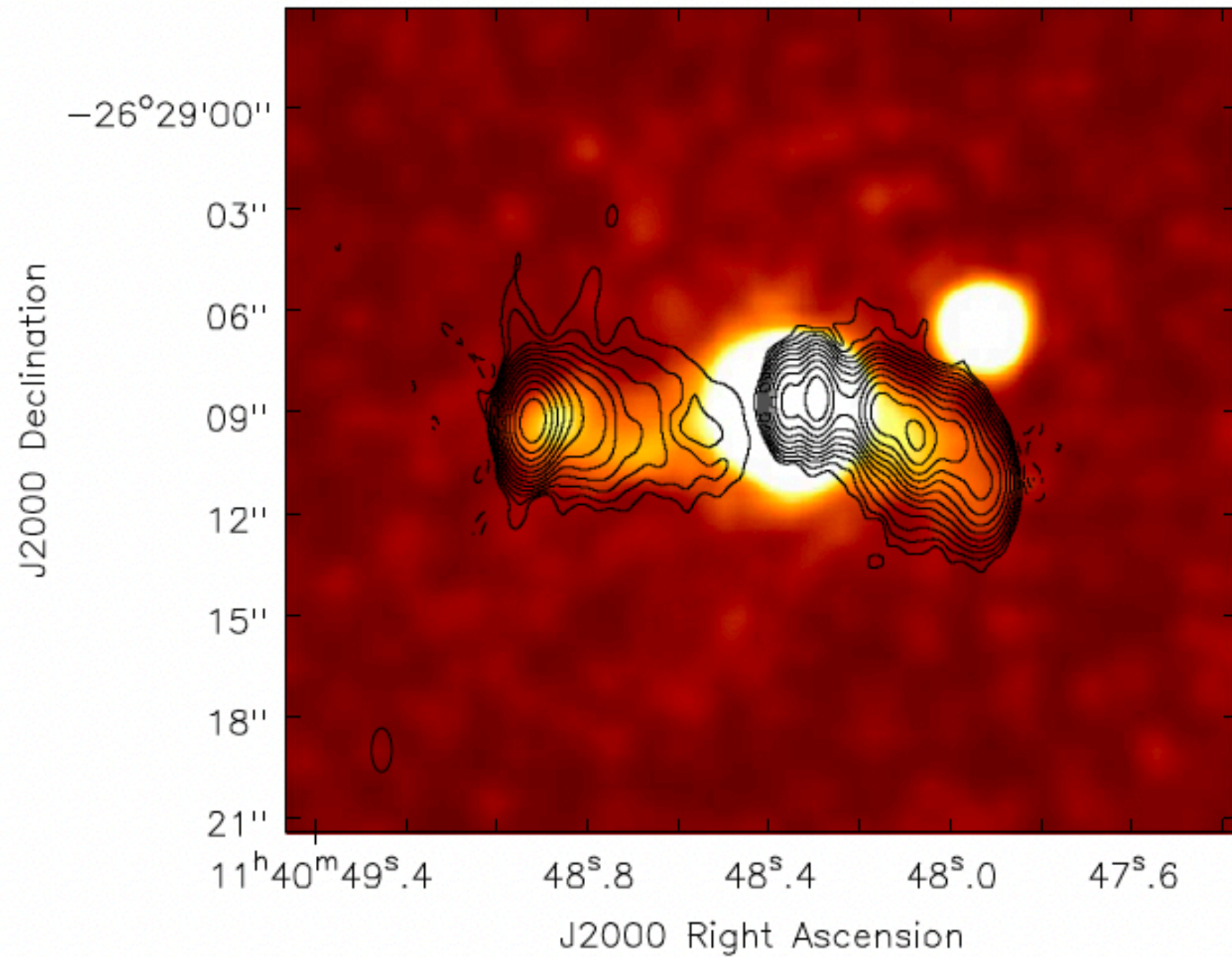


Figure 2. Contour image of the 2 GHz to 4 GHz VLA image of the Spiderweb galaxy, at a resolution of $1''.3 \times 0''.6$, major axis north–south. The contour levels are a geometric progression in a factor of two, starting at $20 \mu\text{Jy beam}^{-1}$. Negative contours are dashed. The color scale is the same Chandra Observatory total X-ray emission (0.5–7 keV) as shown in Figure 1.

Carilli et al. 2022
Anderson et al. 2022

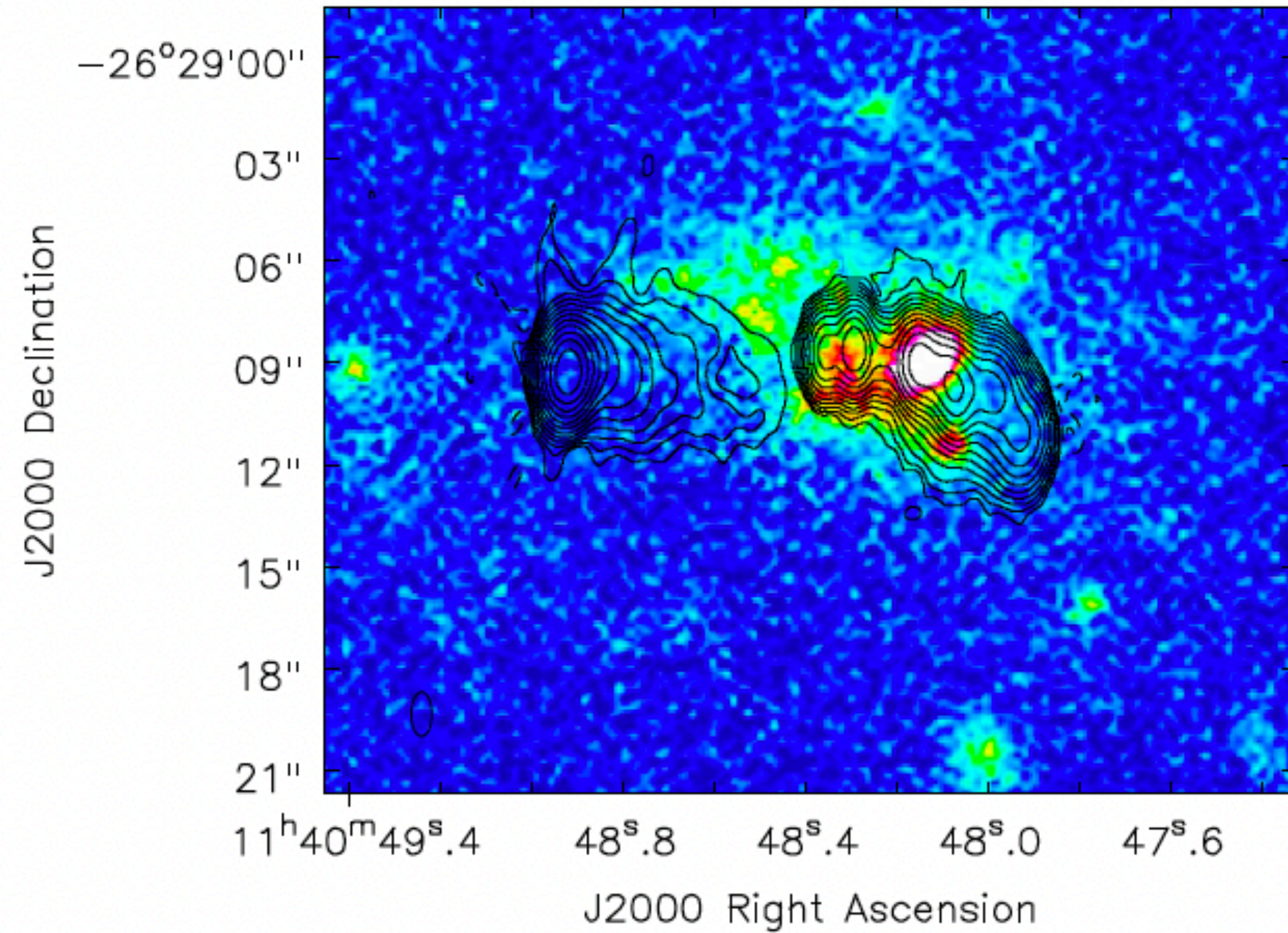


Figure 3. Same contour image as in Figure 1. The color image is the ESO narrowband filter image, roughly centered on the $\text{Ly}\alpha$ emission line from the Spiderweb galaxy at $z = 2.16$ (M. Nonino et al. 2022, in preparation).

AXIS answers the big questions posed by the Astro2020 Decadal Survey

AXIS Deep Extragalactic Survey

The AXIS Science Pillars

Astro 2020 asks...

...AXIS answers

Why X-rays?

Why AXIS?

Pillar 1: "What seeds supermassive black holes and how do they grow?"

AXIS determines the origin of massive black holes
X-rays identify clean census of black holes in distant JWST galaxies
AXIS' PSF and large area enable imaging of distant, faint sources

Pillar 2: "How do gas, metals, and dust flow into, through, and out of galaxies?"

AXIS shows how supernovae and AGN transform galaxies
X-rays uniquely probe the million-degree gas that drives gas flows
High contrast imaging separates diffuse gas and bright sources

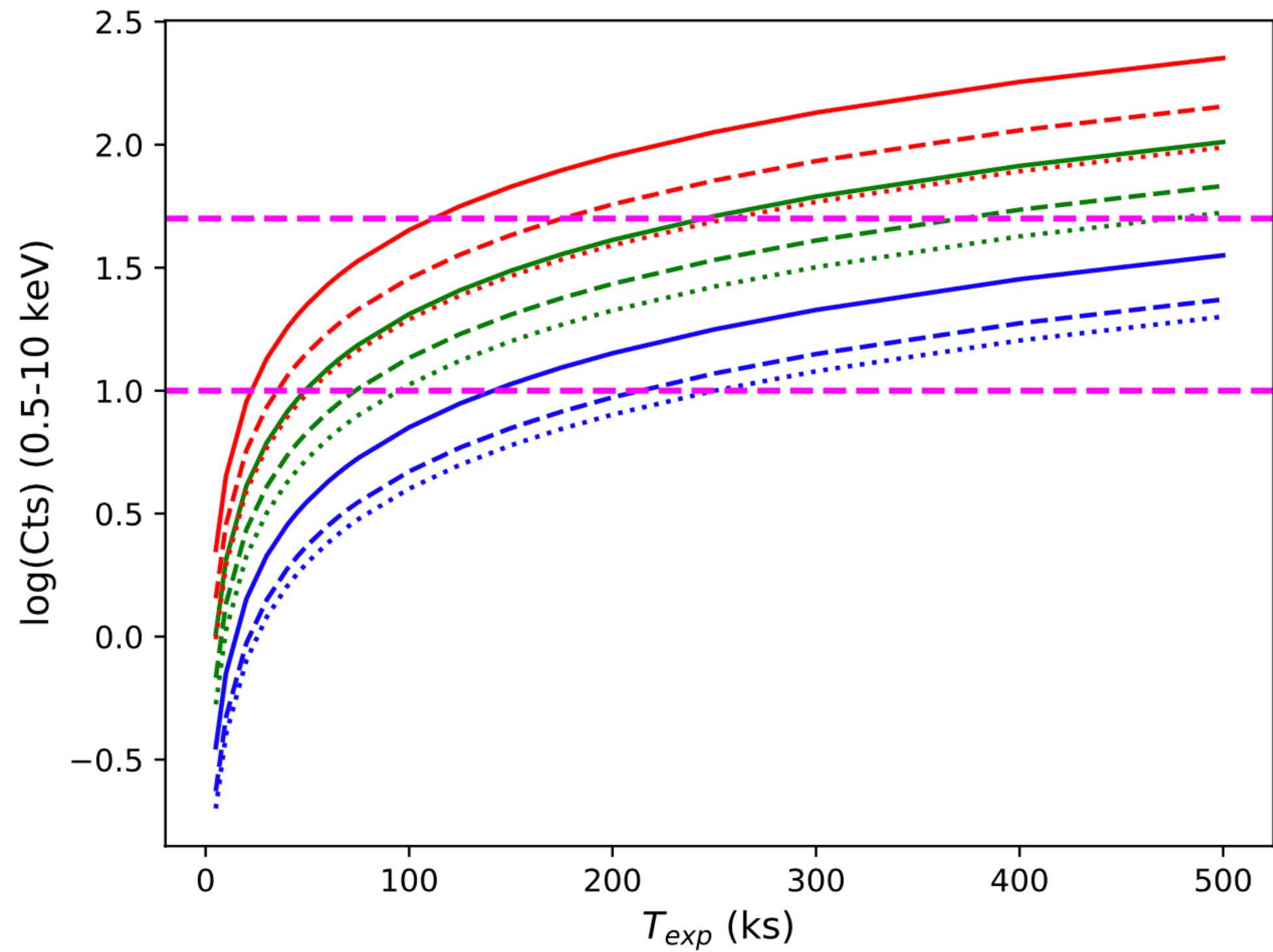
Pillar 3: "What powers the diversity of explosive phenomena across the electromagnetic spectrum?"

AXIS discovers explosive transients both near and distant
X-rays uniquely encode information on transient progenitors
AXIS enables transient alerts, TDAMM surveys and fast followup

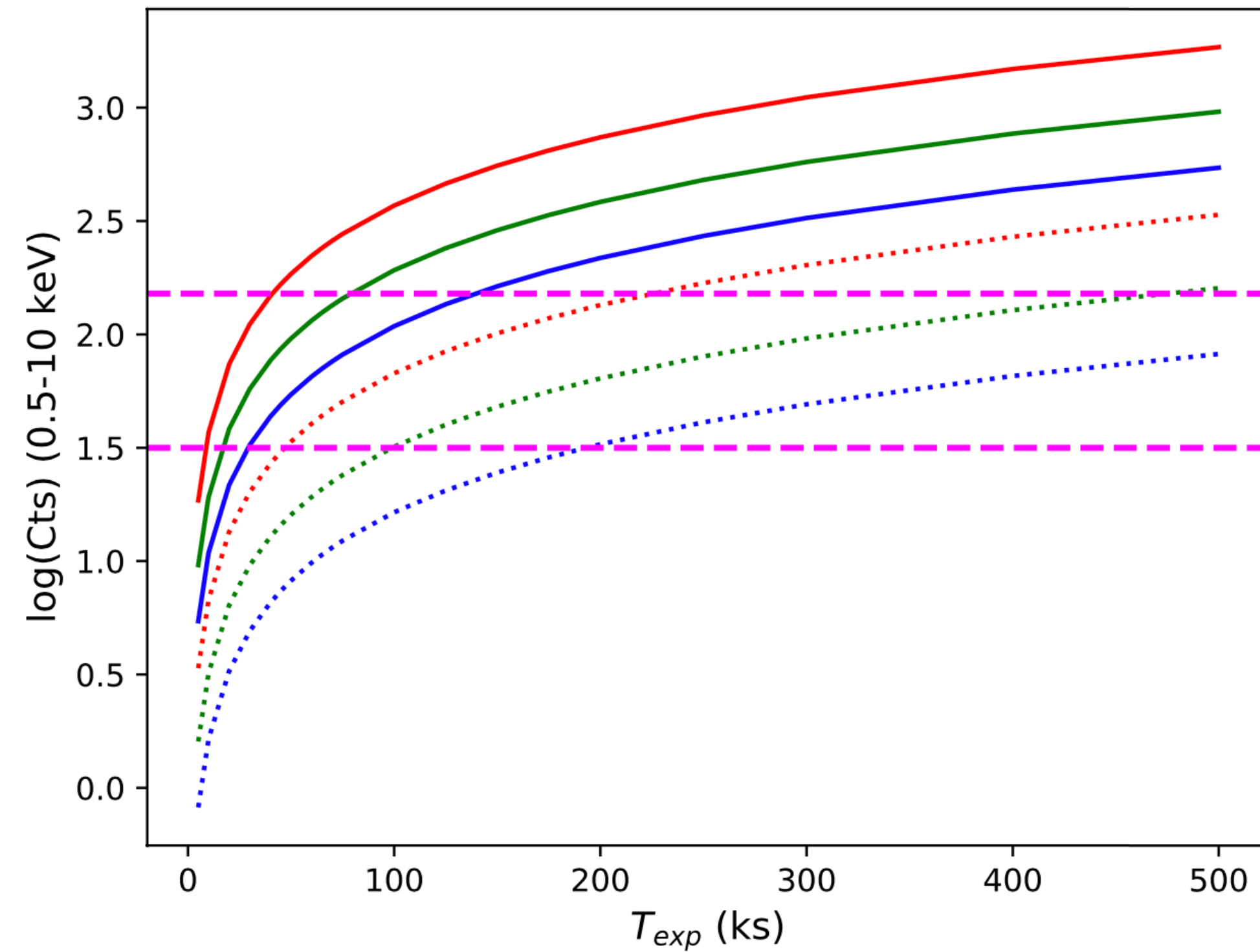
The Extragalactic Surveys will find >20,000 AGN over cosmic time, >50x more than the Chandra Deep Field.

The Galactic Plane Survey will discover >1M new sources in crowded fields, 10x deeper and 5x wider than current best X-ray surveys.

Detection of AGN with AXIS



Detection of proto-ICM with AXIS



AXIS GO Science Book, Ed. H. Russel & L. Lopez
See also <https://axis.umd.edu/>

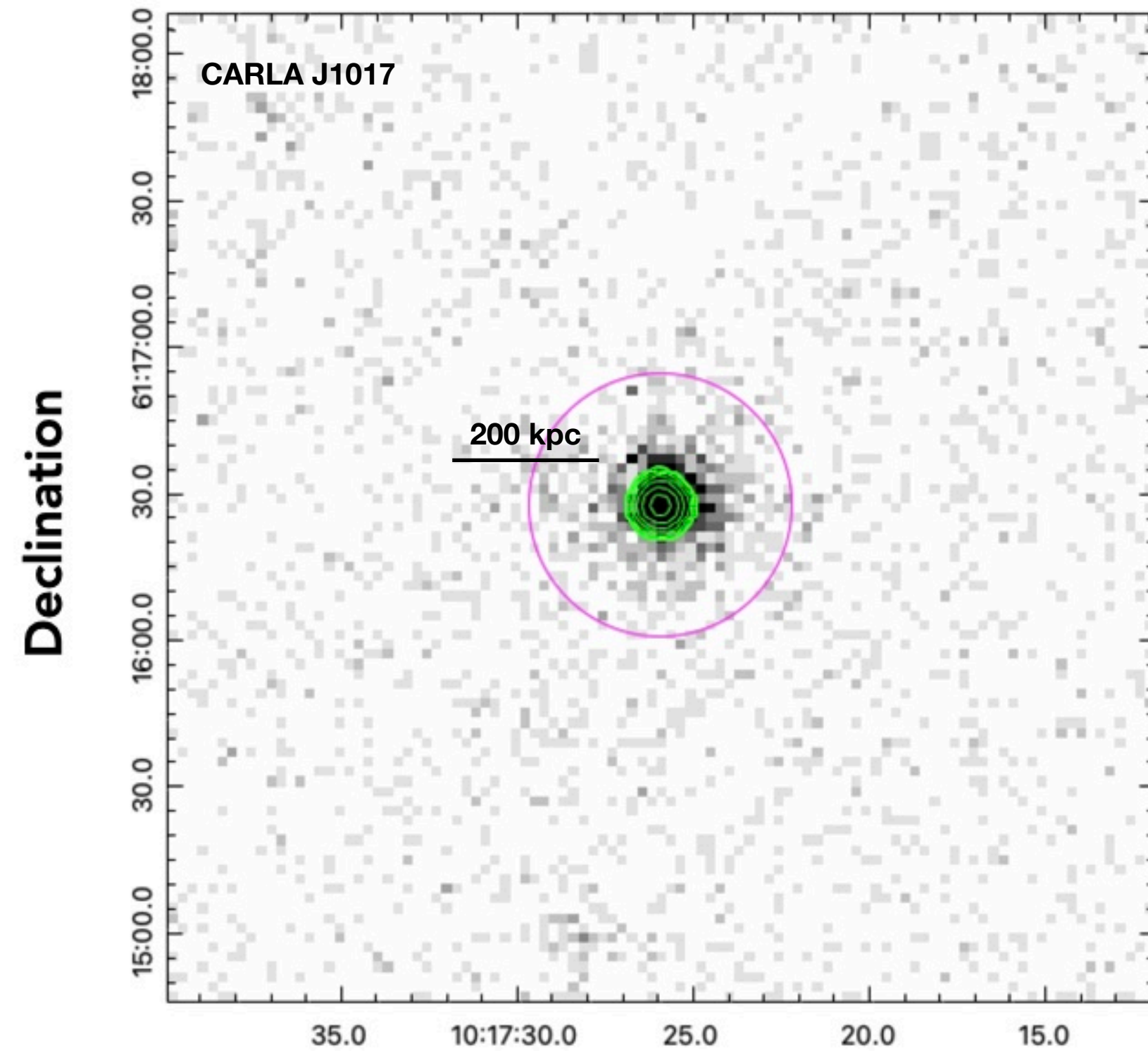
A small protocluster program with AXIS (1.16 Ms)

Table 3. Test sample of protoclusters suitable for this science case. (1): Object ID; (2): Right ascension; (3): Declination; (4) Redshift; (5): Galactic hydrogen column density in units of 10^{20} cm^{-2} ; (6): Galaxy overdensity; (7) Reference to the discovery paper; (8), (9): Exposure time in ks for AXIS observations for AGN and ICM.

| Protoclusters with radio beacon | | | | | | | | |
|---------------------------------------|-------------|-------------|------|------------|------------------|-------|---------------|---------------|
| ID | RA | Dec | z | N_{HGal} | δ_g | Ref. | t_{exp} AGN | t_{exp} ICM |
| MRC0156-252 | 29:38:21.9 | -24:59:32.1 | 2.02 | 1.10 | 17.8 ± 2.4^a | [141] | 130 | 40 |
| USS1707+105 | 17:10:06.5 | 10:31:06.2 | 2.35 | 6.18 | 12 ± 2^b | [177] | 200 | 100 |
| MRC2104-242 | 21:06:58.2 | -24:05:11.3 | 2.49 | 4.16 | 14.0 ± 2.1^a | [141] | 200 | 100 |
| Protoclusters without dominant galaxy | | | | | | | | |
| ID | RA | Dec | z | N_{HGal} | δ_g | Ref. | t_{exp} AGN | t_{exp} ICM |
| BOSS1244 | 12:43:31.2 | +35:55:12.0 | 2.23 | 1.27 | 22.9 ± 4.9^c | [361] | 180 | 80 |
| HS1700+643 | 17:00:55.00 | +64:11:26.7 | 2.30 | 2.11 | 6.9 ± 2.1^d | [373] | 200 | 100 |
| SSA22 | 22:17:34.0 | +00:05:01 | 3.09 | 4.23 | 7.6 ± 1.4^e | [372] | 250 | 180 |

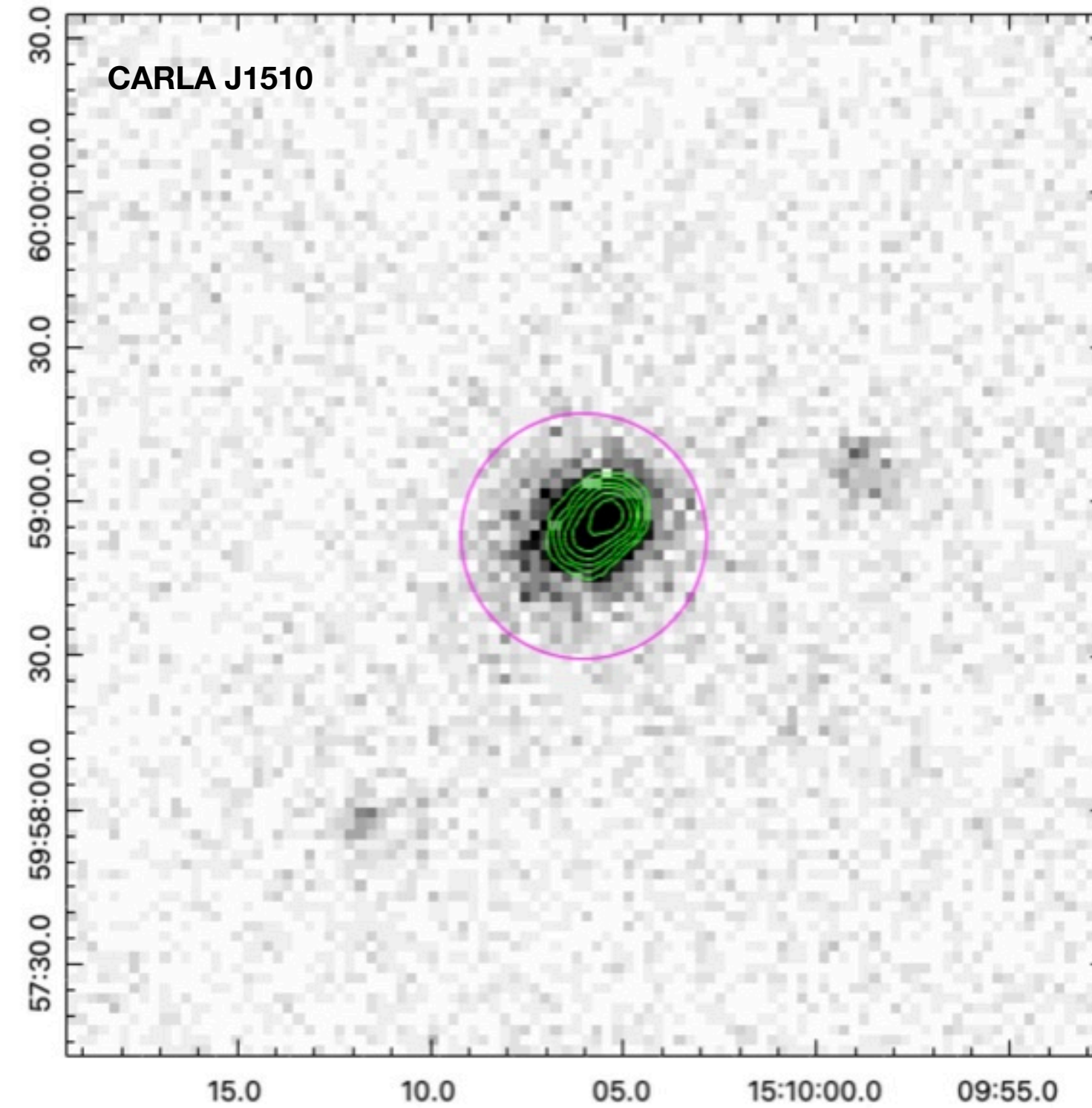
^aDensity of IRAC sources from [141], ^bDensity of H α emitters from [177], ^cDensity of H α emitters from [361],
^dDensity of IRAC sources from [373], ^eDensity of Lyman Break Galaxies from [392]

AXIS GO Science Book, Ed. H. Russel & L. Lopez
See also <https://axis.umd.edu/>



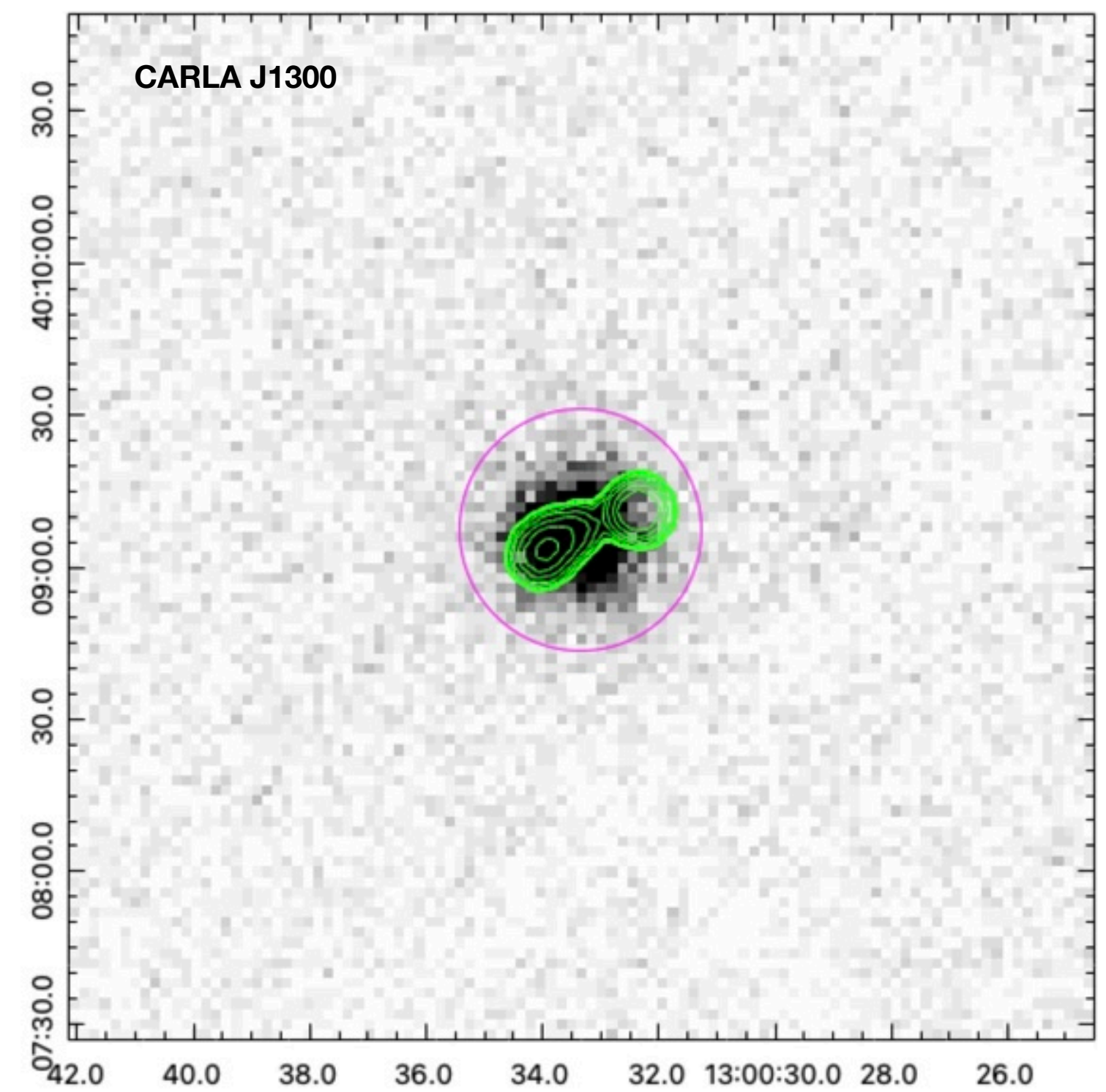
Radio-Loud QSO
 $z = 2.801$

MOS1 16 ks
 MOS2 18 ks
 pn 15 ks



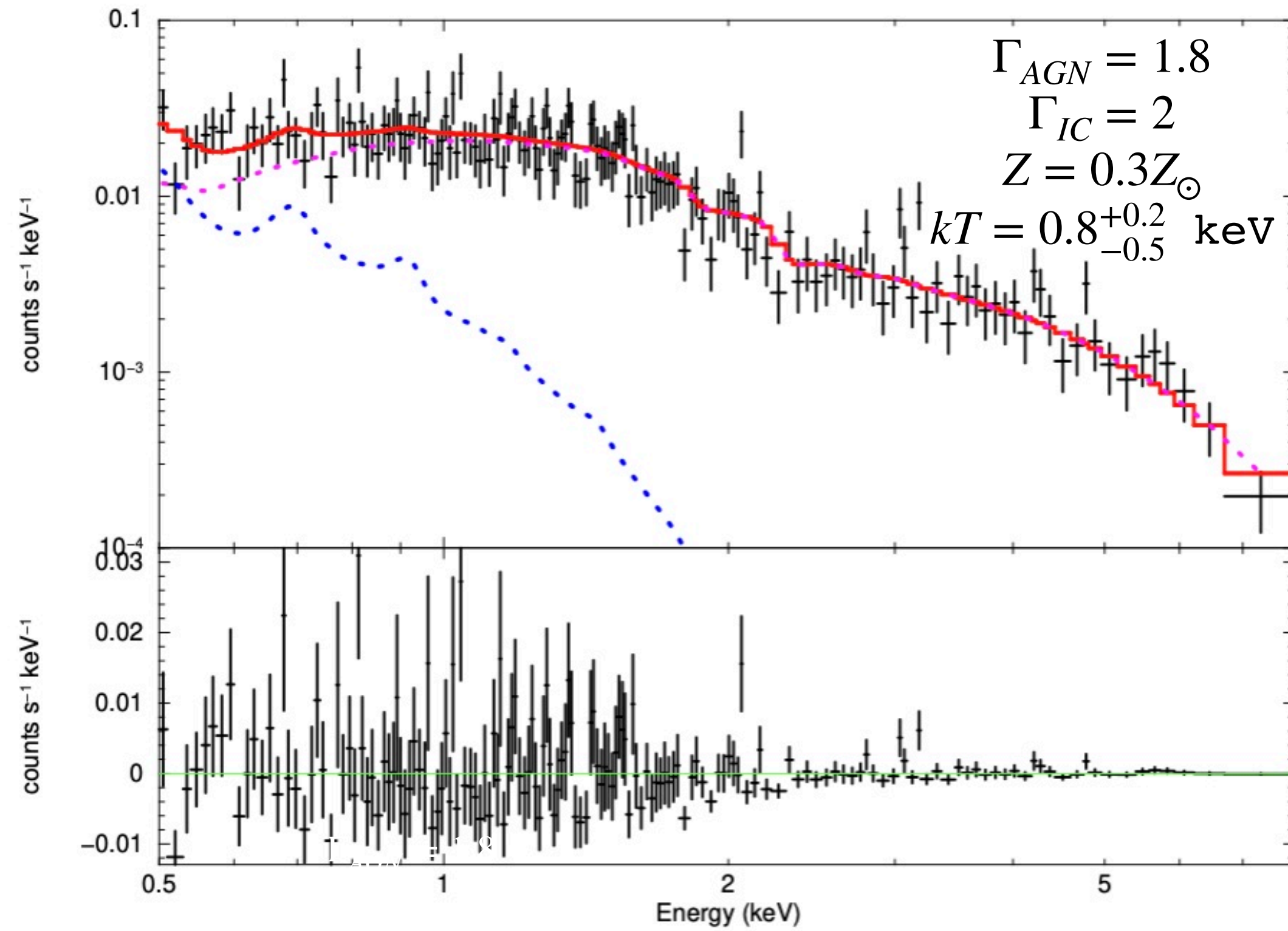
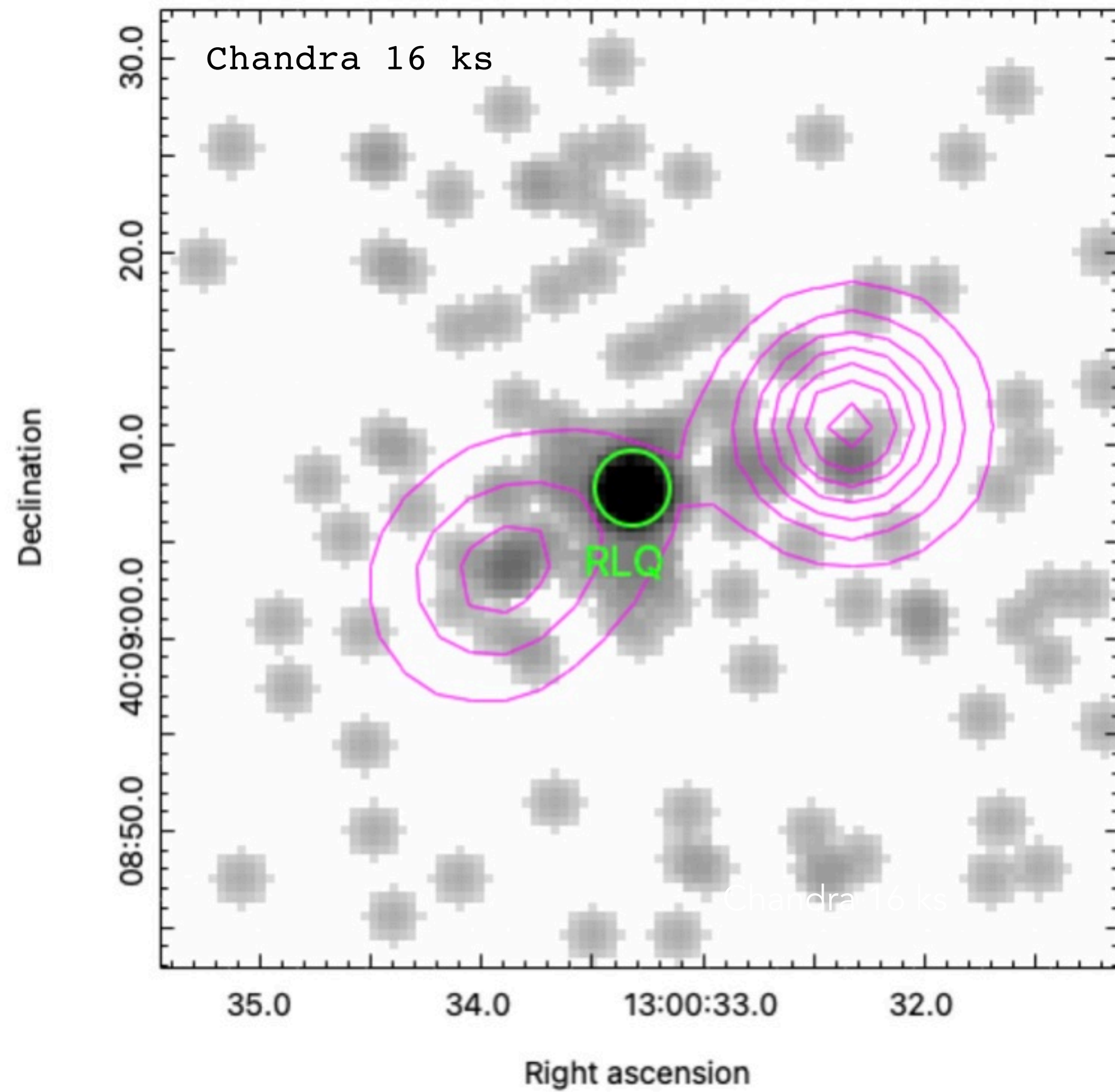
Radio-Loud QSO
 $z = 1.725$

MOS1 42 ks
 MOS2 42 ks
 pn 27 ks



Radio-Loud QSO
 $z = 1.675$

MOS1 52 ks
 MOS2 52 ks
 pn 18 ks

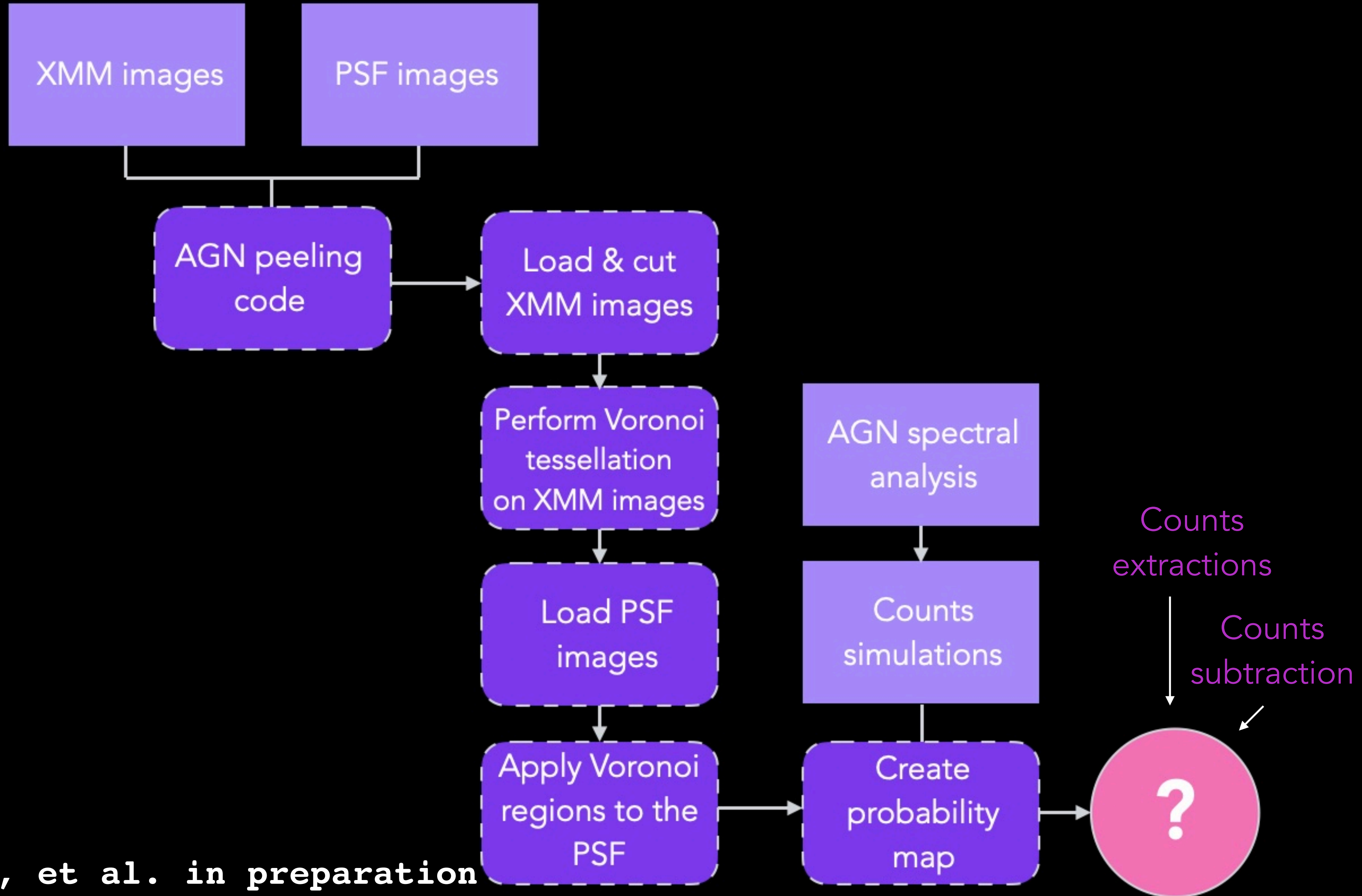


Lepore, M., et al. in preparation

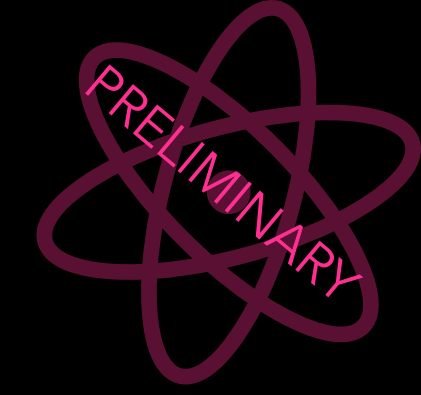
The presence of thermal emission is detected from spectral analysis only at 2σ confidence level

IFPU Focus Week: the emergence of the cosmic web - September 2025

THE CARLA SAMPLE: AGN PEELING CODE

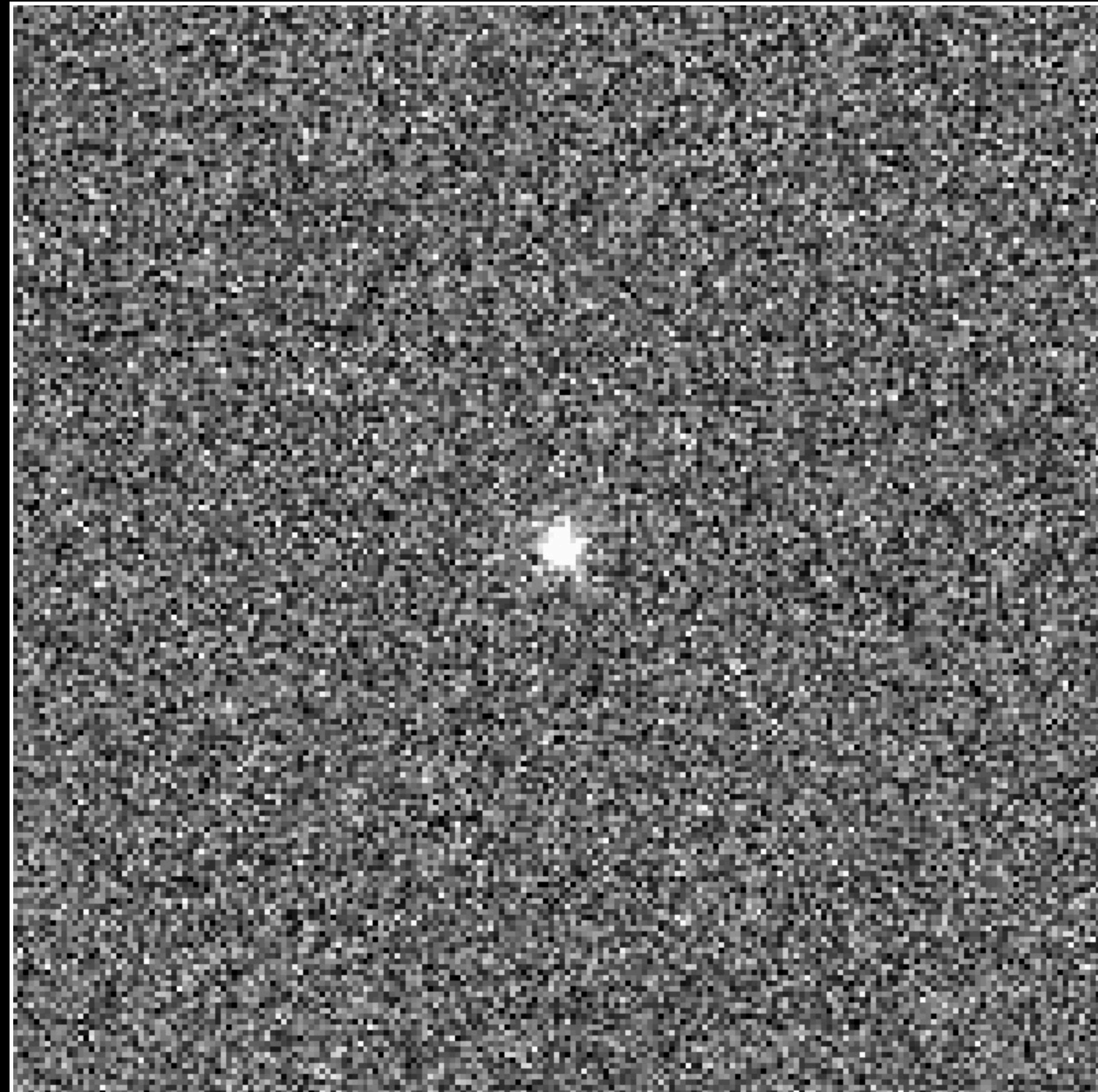


THE CARLA SAMPLE: AGN PEELING

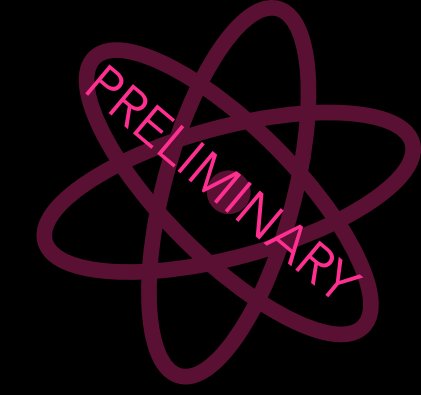


Cluster AGN Removal for ICM Tracing and analysis
Lepore et al., in prep

AGN + background simulated image

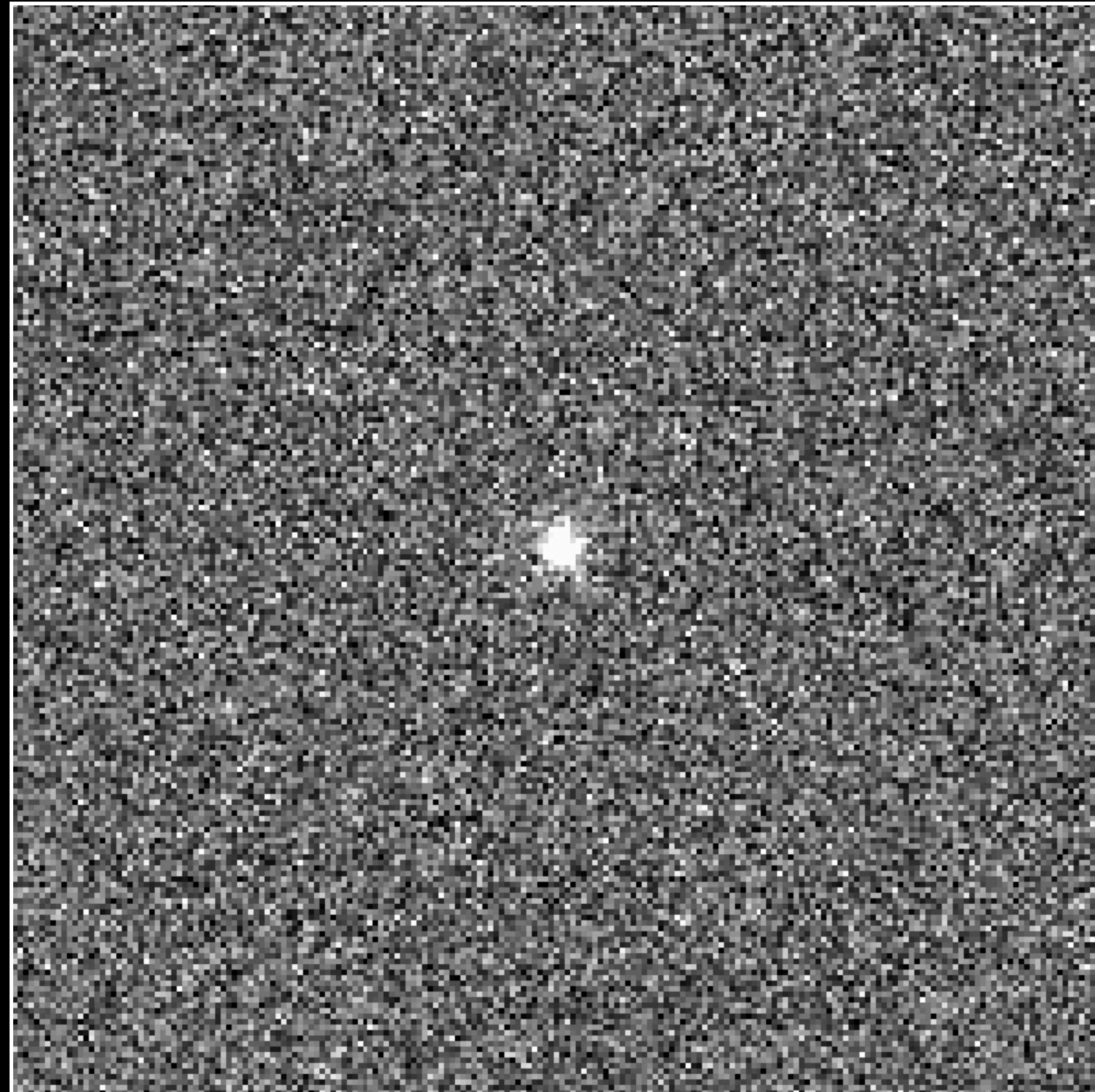


THE CARLA SAMPLE: AGN PEELING

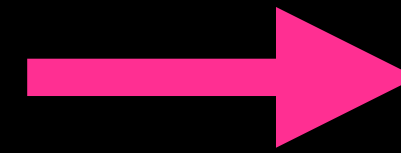


Cluster AGN Removal for ICM Tracing and anaYsis

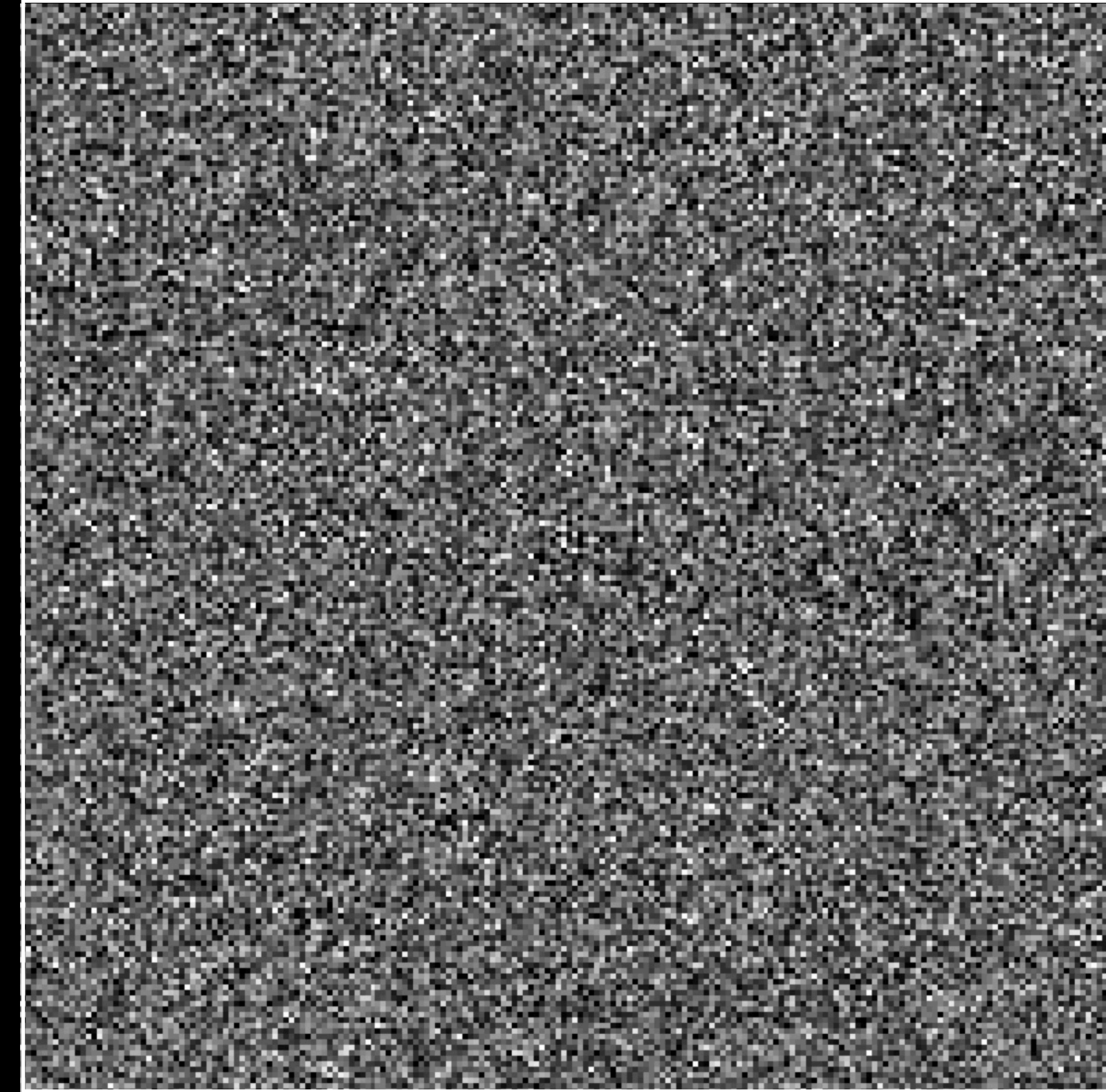
AGN + background simulated image



N-step subtraction



Output: AGN-subtracted residual

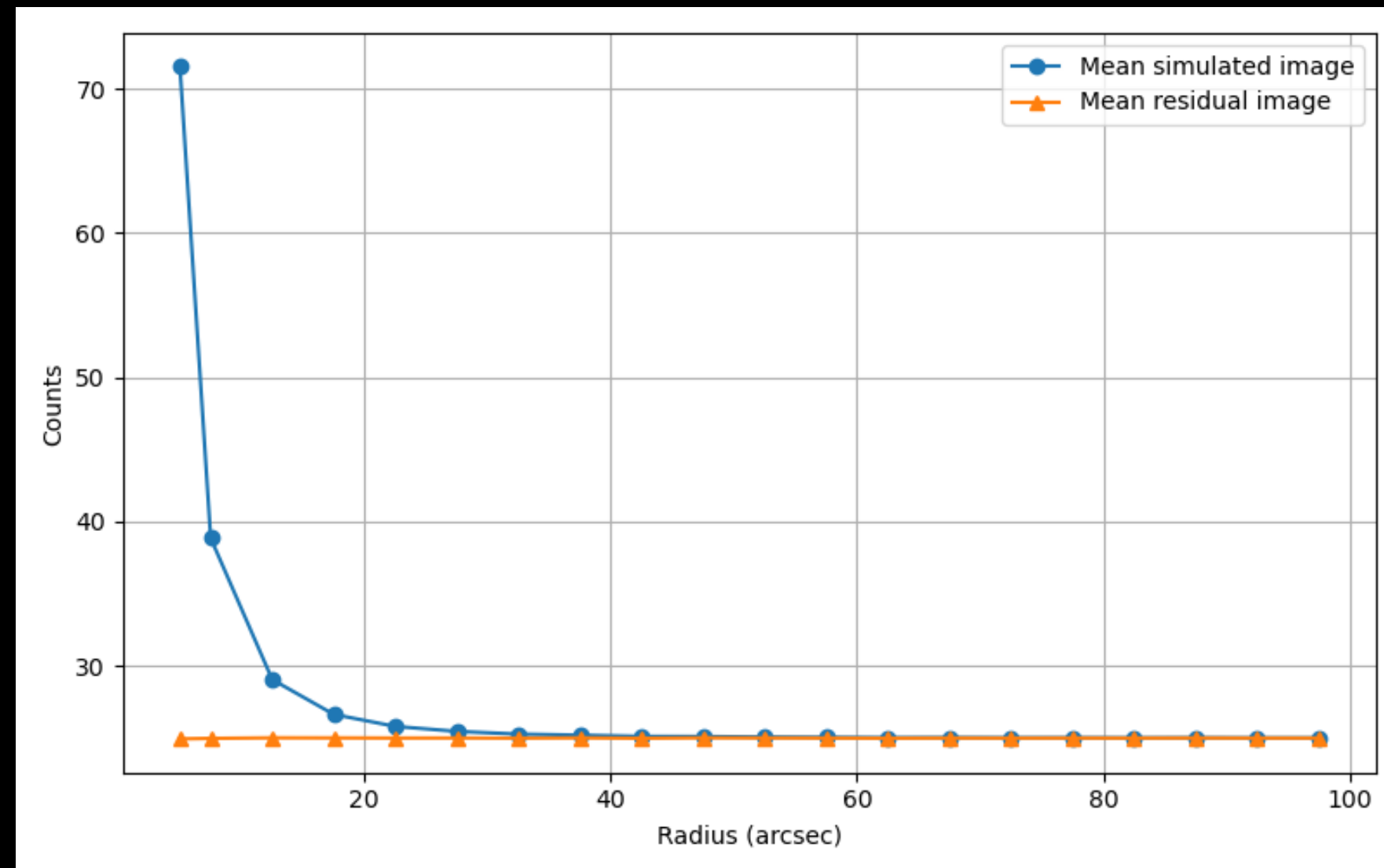


Simulated X-ray AGN removal using Voronoi-based PSF
sampling and N-step probabilistic subtraction

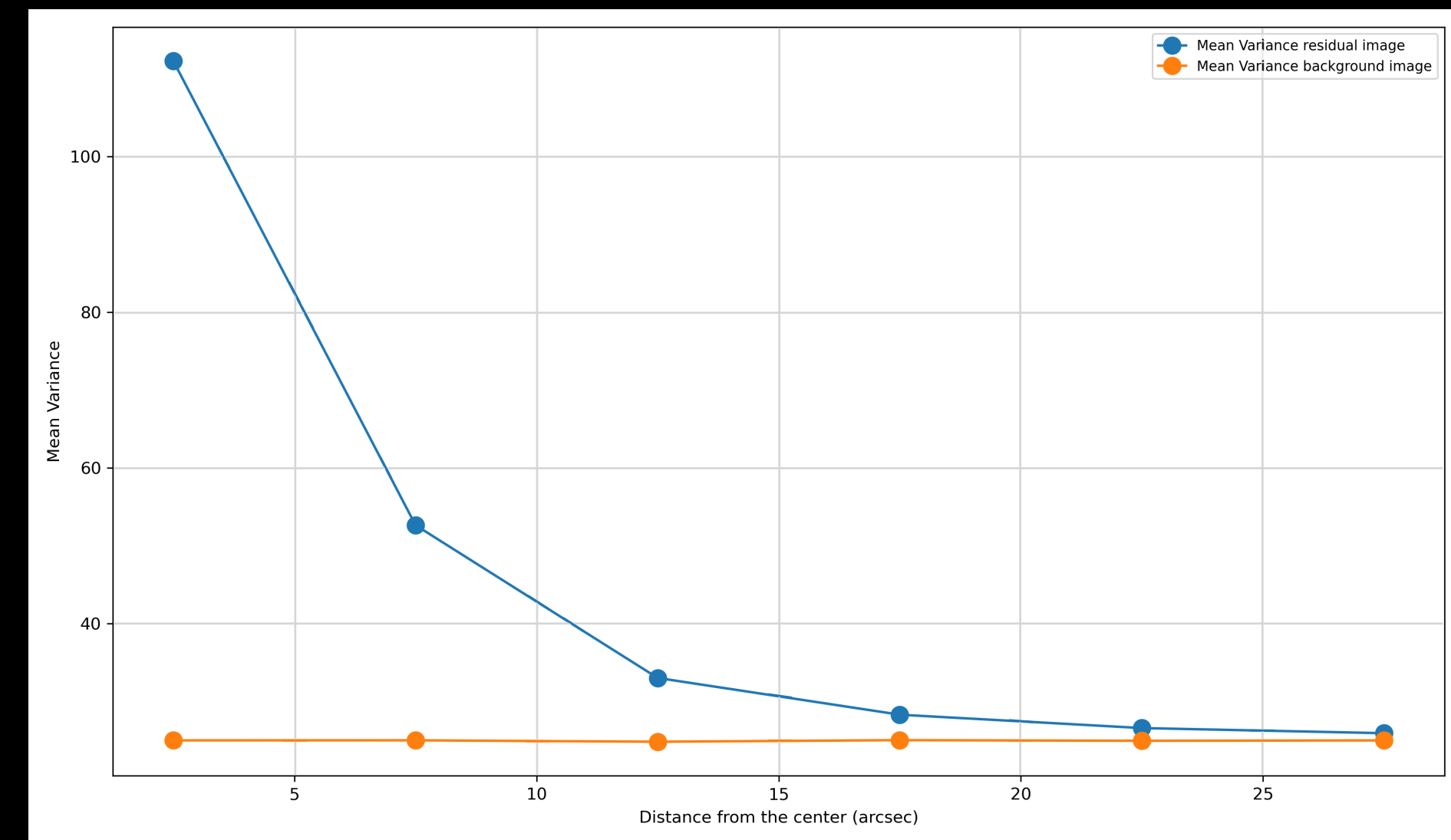
Lepore, M., et al. in preparation

THE CARLA SAMPLE: CLARITY

Cluster AGN Removal for ICM Tracing and analysis



Photometry in 20'' from the center



Mean Variance

Simulated X-ray AGN removal using Voronoi-based PSF
sampling and N-step probabilistic subtraction

Conclusions

X-ray are key to explore several energetic phenomena during the transition from protoclusters to clusters ($2 < z < 3$):

Nuclear emission in member galaxies

Heating of the diffuse baryons (proto ICM) and their chemical enrichment

Possible cooling flows around strong beacons

IC emission from relativistic jets (strong synergy with radio observations)

HMXB emission associated to SF

Indirectly: feedback processes from AGN onto diffuse baryons

But protoclusters are not classic X-ray targets. Most of the "X-ray science" need ancillary data (spectroscopy, NIR imaging, Radio, etc), to begin with a clean selection based on stellar mass and large FOV.

High angular resolution and FOV are both very important (see AXIS).

However, significant results can be obtained in complex sources (Spiderweb-like) with XMM, by combining spatial and spectral information.